Title
Population and Individual Stem Cell Dynamics in the Olfactory Epithelium

Author
Gadye, Levi Benjamin

Publication Date
2016

Peer reviewed|Thesis/dissertation

Population and Individual Stem Cell Dynamics in the Olfactory Epithelium

By

Levi Benjamin Gadye

A dissertation submitted in partial satisfaction of the

requirements for the degree of

Doctor of Philosophy

in

Neuroscience

in the

Graduate Division

of the

University of California, Berkeley

Committee in charge:

Professor John Ngai, Chair

Professor Gian Garriga

Professor Iswar Hariharan

Professor David Schaffer

Fall 2016

Abstract

Population and Individual Stem Cell Dynamics in the Olfactory Epithelium

Levi Benjamin Gadye

Doctor of Philosophy in Neuroscience

University of California, Berkeley

Professor John Ngai, Chair

Unlike the majority of the nervous system, the olfactory epithelium (OE) continuously produces new neurons throughout adulthood. Under homeostatic conditions, OE neurogenesis is fueled by the ongoing divisions of globose basal cells (GBCs), but following severe injury that destroys all mature cell types, the normally quiescent horizontal basal cells (HBCs) regenerate the entire tissue, including GBCs, neurons, and sustentacular cells. Moreover, conditional knockout (cKO) of the transcription factor, p63, induces HBCs to differentiate at steady-state (Fletcher et al. 2011). However, the cellular and transcriptional dynamics underlying HBC self-renewal and differentiation remain poorly characterized. To maintain tissue homeostasis, an appropriate balance of stem cell self-renewal and differentiation is achieved via invariantly asymmetric divisions in invertebrates (Doe and Bowerman 2001), and a mixture of symmetric and asymmetric divisions during vertebrate development (Lechler and Fuchs 2005; Morrison et al. 1995). While regulators of these types of mitoses are conserved in adult tissues, adult stem cell divisions are often modulated by the surrounding tissue, a phenomenon known as population asymmetry (Simons and Clevers 2011). Lineage tracing of stem cells can provide insights into population asymmetry in adult tissues (Ritsma et al. 2015; Bonaguidi et al. 2011), and single-cell RNA sequencing has recently emerged as a powerful tool for probing the transcriptional changes that occur in cycling and regenerating tissues (Trapnell et al. 2014; Shin et al. 2015). This dissertation explores mechanisms of HBC self-renewal and differentiation at steady-state and during regeneration using lineage tracing and single-cell RNA-seq. The following was determined: (1) Symmetric HBC divisions are balanced by population asymmetry, independent of spindle orientation and cell polarity biases in dividing HBCs, producing activated HBCs; (2) At steady-state, p63cKO HBCs differentiate directly into sustentacular cells without dividing, and give rise to proliferative neural progenitors that generate numerous neurons; (3) During regeneration, all HBCs are recruited into an activated state and enter the cell cycle prior to renewing or differentiating; and (4) The sustentacular lineage develops prior to the neuronal lineage and via fewer changes in transcriptional state. These results provide novel insights into the dynamics that regulate HBC renewal and differentiation, as well as avenues for further exploration of OE stem cell subtypes, and provide a methodological model for investigating adult stem cells in other tissues.

Table of Contents

List of Figures

Acknowledgements

To my wife - for conspiring with me academically, artistically, argumentatively, and athletically
To my mother - for teaching me to be humble, compassionate, curious, and voraciously literate
To my father - who else to thank for my chutzpah?
To my brothers - for lifetimes of laughter and worldly inspiration
To my grandparents - for inspiring me to find joy in the ongoing pursuit of knowledge
To my friends - for too many shenanigans and the willingness to call me out
To LP and the Sustentaculars - the dream lives on
To Michael Sanchez and Samuel Israel - my scientific brothers in arms
To Diya Das - for snark, snack alerts, and endless computational savvy
To Russell Fletcher - for invaluable mentorship, encouragement, and generosity of wisdom
To John Ngai - for taking me on, teaching me the true meaning of skepticism, challenging me to stick with my science, and seeing me through to the end.

Thank you all.

See you in the comments.

Chapter 1:
Population asymmetry and the olfactory epithelium

Introduction

Adult stem cells are fundamental to the resilience of long-lived animals, providing many tissues with newborn cells as older cells are lost due to aging or injury. The stem cell of a given tissue has historically been defined as a resident cell type that divides relatively rarely, self-renews, and demonstrates the capacity to produce differentiated daughter cells (Siminovitch, McCulloch, and Till 1963). First characterized in the hematopoietic system (Till and McCulloch 1961), adult stem cells exhibiting these traits have since been described in both highly-cycling tissues, like epidermis (C. S. Potten 1974) and intestine (Cheng and Leblond 1974), as well as in slower-cycling tissues, like brain (Altman and Das 1965). Across the many tissues that harbor adult stem cells, these hallmarks of stem cell character are typically present, though the mechanisms underlying their self-renewal and differentiation can vary.

Simultaneous self-renewal and differentiation of adult stem cells can be accomplished via asymmetric divisions, which produce daughter cells with differential fates from single parental cells (Horvitz and Herskowitz 1992). In some contexts, particularly early in development, stem cells only divide asymmetrically, a strategy known as invariant asymmetry (Inaba and Yamashita 2012; Li 2013). Under this paradigm, the brunt of differentiated cell production is left to short-lived progenitor or transit-amplifying cells, which replicate only a few times before terminally maturing into the proper number of differentiated cells. Symmetric divisions, which generate progeny of equivalent stem or differentiated fates, can rapidly expand or deplete the stem cell pool, but a combination of renewing and differentiating symmetric divisions can still result in cellular diversity. This strategy is known as population asymmetry (Simons and Clevers 2011). Studies across a diversity of cycling tissues have shown that stem cell mitoses are rarely invariant (Ritsma et al. 2015; Clayton et al. 2007; Doupé et al. 2012; Sun et al. 2014), suggesting that adult stem cell divisions may be regulated by population asymmetry, rather than invariant asymmetry, even when both asymmetric and symmetric divisions are present (Tetteh, Farin, and Clevers 2014).

The nervous system possesses relatively few adult neural stem cells, most of which are located deep inside the brain (Suh et al. 2007; Lois and Alvarez-Buylla 1993; Kempermann, Kuhn, and Gage 1998). The olfactory epithelium (OE), the peripheral neuroepithelium responsible for the sense of smell, presents a unique opportunity for the study of mammalian adult neural stem cells *in vivo*: olfactory sensory neurons are replaced every 30-60 days by newborn neurons arising from a lineage of immature precursors and multipotent progenitors (Mackay-Sim and Kittel 1991). Moreover, like epidermis but unlike the brain and much of the nervous system, the OE

quickly regenerates following severe injury, due to differentiation of a normally quiescent stem cell, the horizontal basal cell (HBC) (Leung, Coulombe, and Reed 2007; Iwai et al. 2008). Our lab has shown that HBC self-renewal is controlled by the transcription factor p63 (Fletcher et al. 2011), which also plays a critical role in regulating basal stem cell self-renewal in the epidermis and lung (Lechler and Fuchs 2005; Zuo et al. 2014). Conditional knockout of p63 (p63-cKO releases HBCs from quiescence at steady-state, allowing for the study of HBC differentiation in the absence of injury. Thus, the OE provides a tractable system in which to study the renewal and differentiation of an adult neural stem cell both during regeneration and following steady-state release from quiescence. This dissertation explores the cellular, clonal, and transcriptional dynamics that underlie HBC renewal and differentiation following injury or conditional knockout of p63.

1.1 Adult neurogenesis and regeneration in the olfactory epithelium

The olfactory epithelium (OE) is the peripheral, pseudostratified neuroepithelium responsible for the sense of smell. Olfactory sensory neurons (OSNs) extend dendrites into the nasal lumen for detection of volatile odorants and project axons to the olfactory bulb. Individual OSNs are replaced in an ongoing process by immature neurons generated by the divisions of basal stem cells (Graziadei and Graziadei, 1979). One such stem cell, the globose basal cell (GBC), supports steady-state homeostasis by dividing daily, and can also regenerate OSNs following severing of the olfactory nerve (Caggiano, Kauer, and Hunter 1994). The HBC lies between the GBC layer and the basement membrane and rarely divides under steady-state conditions; however, upon ablation of all other cell types, the HBC population rapidly enters the cell cycle and regenerates all cell types of the OE (Fig. 1.1) (Leung et al., 2007).

Because of its relative quiescence and its ability to self-renew and differentiate, the HBC is thought to be an adult tissue stem cell of the OE. The HBC expresses skin-specific stem cell markers, and its progeny express factors known to regulate neuronal specification in the brain, allowing for facile identification of all cell types using immunohistochemistry (Carter et al., 2004). Like epidermal progenitors, and unlike all other cells of the OE, HBCs express the cytokeratins Keratin5 and Keratin14 (Holbrook, Szumowski, and Schwob 1995); they display extracellular matrix (ECM) receptors on the cell membrane, such as ICAM1 and various integrins; and they modulate their mitoses in response to injury (Leung, Coulombe, and Reed 2007). Our lab and others recently showed that the transcription factor p63 is highly expressed in the ICAM+ HBC population (Fletcher et al. 2011; Packard et al. 2011). Intriguingly, conditional loss of p63 in HBCs causes a defect in HBC self-renewal and maintenance of steady-state quiescence (Fletcher et al., 2011). This is similar to the phenotype of p63 loss-of-function in developing skin, in which stem cells fail to engage in a normal program of self-renewal and differentiation, leading to defects in epidermal stratification (Romano et al. 2012). Moreover, the

transcription factor Sox2, a well-known regulator of stem cell function and adult neurogenesis (Sarkar and Hochedlinger 2013), plays a specific role in the OE, where it is expressed by HBCs, GBCs, and sustentacular cells. Sox2 is not required for HBC self-renewal, nor the production of neurons from GBCs, but is necessary for proper neurogenesis following severe injury (Sanchez 2014).

While the HBC has been well-defined by its expression of canonical epithelial stem cell markers, the regulation of its mitotic behavior during regeneration, or during differentiation following p63cKO, remains poorly understood. This dissertation describes the characterization of cellular strategies of HBC self-renewal and differentiation across these two paradigms of HBC activation, and explores the transcriptional changes that underlie HBC fate determination upon exit from quiescence.

1.2 Asymmetric and symmetric division from worm to mouse

Adult stem cells are defined by their ability to self-renew rarely and nearly indefinitely, and to differentiate into at least one mature cell type. In cycling tissues, which constantly replace aging cells with newborn cells, hierarchies of longer- and shorter-lived stem cells are believed to underlie the production of transit-amplifying cells that multiply only a handful of times before maturing into an abundance of differentiated cells, a conceptual framework originating in the seminal work of Till and McCullough on hematopoiesis (Till and McCulloch 1961). Their early experiments demonstrated that individual bone marrow cells could both self-renew and give rise to at least four differentiated blood cell types each (Weissman 2011), albeit under transplantation conditions, laying the groundwork for understanding stem cells according to strict hierarchies of increasingly fate-committed progenitors.

The mechanisms controlling stem cell renewal and differentiation have been most precisely characterized through the study of invertebrate stem cell mitosis (Doe and Bowerman 2001). In the *C. elegans* zygote, fly neuroblast, and fly germline, invariant asymmetry ensures the maintenance of stemness in one daughter cell while the other daughter cell differentiates. In a handful of vertebrate tissues, such as developing neocortex and epidermis, conserved cell polarity and spindle orientation factors also promote asymmetric divisions, though symmetric divisions may also occur (Kriegstein and Alvarez-Buylla 2009; Lechler and Fuchs 2005). Findings from the study of asymmetric division in adult stem cells have been more equivocal, however, and the true symmetry or asymmetry of stem cell progeny is sometimes seen as a semantic distinction in the context of population-level stem cell dynamics (Simons and Clevers 2011). Moreover, many adult tissues rely on stochasticity in stem cell mitotic programs to produce balanced proportions of renewed and differentiating progeny in the absence of invariant

asymmetry (Poulson and Lechler 2010; Snippert et al. 2010; Doupé et al. 2010; Bonaguidi et al. 2011; Klein et al. 2010).

To address whether invariant asymmetry or population asymmetry underlies HBC mitosis, it is informative to first consider examples of stem cell divisions in invertebrates, where stem cell mitosis is tightly regulated by conserved factors and mechanisms of asymmetric cell division.

Asymmetric division and invariant asymmetry in *C. elegans* and *D. melanogaster*

The regulatory mechanisms underlying asymmetric division have been most thoroughly studied in two genetically-tractable, invertebrate model organisms, the nematode worm, *C. elegans*, and the fruit fly, *D. melanogaster*. Embryos and adults of both organisms lend themselves to real-time imaging and genetic manipulation, allowing for stem cell mitoses to be directly tracked and perturbed. Crucially, the majority of genes known to regulate stem cell divisions in *C. elegans* are both conserved and functional not only in *D. melanogaster*, but also in mouse and human, implying that stem cells may share cellular strategies for self-renewal and differentiation across phyla.

The earliest divisions of the nematode embryo are controlled by polarization of various factors that are asymmetrically inherited by its daughter cells, leading to establishment of an organized animal body plan (Munro, Nance, and Priess 2004; Goldstein and Hird 1996; Kemphues et al. 1988). The first division of the *C. elegans* zygote is particularly amenable to direct observation using differential image contrast (DIC) imaging, which allows for the sperm and egg pronuclei to be followed as the zygote reorganizes its cytosolic cargo in preparation for an asymmetric division (Gönczy and Rose 2005).

Polarization of the *C. elegans* zygote is first established by the position of a donated centrosome, provided by a single spermatozoon (Albertson and Thomson 1993; Cowan and Hyman 2004); this centrosome defines the posterior axis of the zygote. Subsequently, the subcellular actomyosin network is rearranged towards the anterior pole while the maternal pronucleus migrates to meet the paternal pronucleus at the posterior pole. This dynamic movement of the cytoskeleton promotes the segregation of various Par proteins (Par3, Par6) and aPKC to the anterior pole (Cuenca et al. 2003), which help drive regulators of spindle orientation, as well as fate-determinants, to either the anterior or posterior pole. Lastly, the spindle lines up with the anterior-posterior axis and shifts posteriorly. The zygote then divides asymmetrically, producing an anterior, larger AB cell, and a posterior, smaller P cell. Mutation of many of the aforementioned factors leads to aberrations in cellular polarization, spindle orientation, and/or fate determinant inheritance, leading to developmental defects and, eventually, death (Kemphues et al. 1988). Invariant asymmetry is thus necessary for proper nematode development beginning with the first zygotic division.

Many of these same factors also ensure the polarization of *D. melanogaster* embryonic neuroblasts, leading to asymmetric cell divisions that invariantly produce one differentiated daughter cell while renewing the parental stem cell. Prior to division, these neuroblasts delaminate from the ventral ectoderm, inheriting the apical polarization of the Par complex (including Par3 and Par6) and aPKC (Knoblich 2008). Apical aPKC promotes the segregation of fate determinants Numb, Pros, and Brat to the basal cortex of the dividing neuroblast via phosphorylation of Lgl (Ohshiro et al. 2000; Peng et al. 2000), and the apical protein complex then pulls the mitotic spindle into alignment with the apical-basal axis via a series of partner proteins, including Inscuteable, Pins, Mud, and Gαi (Nipper et al. 2007). Numb, Pros, and Brat are inherited by the basal daughter cell, where Numb inhibits Notch signaling and promotes differentiation into a ganglion mother cell, a type of neural precursor cell; the apical cell retains its stemness.

Both the nematode zygote and fly neuroblast establish their pre-mitotic cellular polarity intrinsically, following either fertilization or delamination from the ventral ectoderm, respectively. However, invariant asymmetry can also arise from extrinsic, asymmetric exposure of daughter cells to diffusible fate-determining signals. Adult *Drosophila* germline stem cells (GSCs) exhibit this type of extrinsically-enforced invariant asymmetry. In the ovarian germarium, site of egg production, a handful of GSCs each adhere to a cap cell via an adherens junction, and these cap cells continuously expose their partner GSCs to the BMP ligands, Dpp and Gbb (Fuller and Spradling 2007), leading to the repression of the differentiation gene, *Bam*. Following mitosis, one of two GSC daughter cells loses contact with the cap cell niche, escapes BMP-mediated repression of *Bam*, and *Bam* initiates a differentiation program that eventually produces an oocyte (Knoblich 2008). Notably, while adult GSCs normally divide asymmetrically, experimental ablation of a neighboring stem cell can induce GSCs to symmetrically self-renew, illustrating plasticity in the GSC mitotic program (Xie and Spradling 2000). Thus, invariant asymmetry can arise via paracrine signaling from components of the stem cell niche, independently of intrinsic segregation of fate determinants.

Asymmetric division in developing vertebrate tissues

Observation and characterization of asymmetric division in vertebrates has proven to be less straightforward than in invertebrates, which are more amenable to transgenic manipulation and live imaging techniques, but examples of asymmetric division in a few vertebrate tissues, particularly during development, have shed light on vertebrate programs of mitosis over the last few decades. Notably, while cell polarity, spindle orientation, and asymmetric fate determinant inheritance do influence the outcomes of mitoses in these contexts, these asymmetric divisions are not strictly invariant, perhaps to allow for more dynamic, population-level regulation of proliferation and differentiation in growing tissues.

In embryonic mouse epidermis, early basal stem cell divisions are oriented parallel to the basement membrane, coinciding with the production of renewed stem cells, while later in development, these divisions are more likely to orient perpendicular to the basement membrane, coinciding with the production of differentiating progenitors (Lechler and Fuchs 2005). These perpendicular divisions are not invariant, as 30% of divisions still occur parallel to the basement membrane, but perpendicular spindles still correlate with apical localization of the Par complex and the mouse homolog of Inscuteable, mInsc. Lineage tracing of these cells indeed shows that perpendicular spindle orientations result in asymmetric fates, while parallel spindle orientations result in symmetric, renewing fates (Poulson and Lechler 2010). Moreover, individual stem cells may divide once asymmetrically, and then once symmetrically, alternating between either division type, perhaps based on external cues (Poulson and Lechler 2010). Thus, while vertebrate epidermal divisions share some regulatory mechanisms with invertebrate invariant asymmetry, other (likely extrinsic) factors ultimately guide their outcomes.

Spindle orientation also plays a role in fate determination during cortical neurogenesis, but cortical neural stem cells, like epidermal stem cells, show flexibility in their regulation of asymmetric division. These neural progenitors, known as radial glia, tend to renew symmetrically early in development before transitioning towards primarily asymmetric divisions that produce numerous differentiating cells (Noctor et al. 2004). Conserved mechanisms of asymmetric division are also present in radial glia. Pioneering work by Chenn and McConnell showed, via time-lapse microscopy in embryonic cortical slices, that cleavage orientation of dividing neural progenitors was predictive of either asymmetric or symmetric daughter cell fate (Chenn and McConnell 1995). Asymmetric inheritance of Numb in dividing radial glia leads to asymmetric daughter cell fate via inhibition of Notch signaling (Shen et al. 2002; Mizutani et al. 2007), and both Par3 and mInsc promote asymmetric divisions via regulation of spindle orientation (Bultje et al. 2009; Postiglione et al. 2011). Additionally, in the developing zebrafish neural tube, asymmetric inheritance of Par3 itself correlates strongly with neuronal fate following the asymmetric division of a neural stem cell (Alexandre et al. 2010); this study remarkably made this observation by continuously visualizing Par3 in dividing radial glia *in vivo*, providing mechanistic backing for the observations of Chenn and McConnell.

Though vertebrate stem cell divisions are influenced by spindle orientation, cellular polarity, and asymmetric segregation of fate determinants, it is clear that asymmetric divisions, if they are present, are rarely the exclusive strategy of a given stem cell population. Indeed, a recent study used the mathematical framework of optimal control theory to predict the most efficient development of the small intestine from a pool of progenitor cells capable of asymmetric and symmetric divisions (Itzkovitz et al. 2012). This approach identified the same mitotic strategy observed in developing skin and brain: early expansion of the stem cell pool via symmetric,

renewing divisions, followed by rapid differentiation via asymmetric divisions. Impressively, *in vivo* analysis of stem versus differentiated cell numbers in developing intestinal crypts over time corresponded with the group's *in silico* solution (Itzkovitz et al. 2012). Similarly, in the developing hematopoietic system, symmetric divisions are more likely to explain periods of rapid stem cell pool expansion (Morrison et al. 1995), even in the absence of *in vivo* data on the outcomes of individual stem cell divisions. For fast-growing vertebrate tissues to develop, then, it may be more efficient for individual stem cell divisions to be dynamically regulated than invariantly predetermined.

Population asymmetry in adult tissues

Compared to the study of asymmetric and symmetric division in developing tissues, mechanistic study of adult stem cell division is relatively young, precluded to a large degree by adult stem cell rarity and quiescence. Nevertheless, technical advancements in lineage tracing, imaging, and molecular characterization of adult stem cells have led to a greatly improved understanding of cycling tissue homeostasis, as well as regeneration (Fuchs and Horsley 2011). Though the concept of population asymmetry dates back to the earliest descriptions of adult stem cell (Till, Mcculloch, and Siminovitch 1964), strong evidence of both heterogeneity amongst stem and progenitor cell populations and also stochasticity in daughter cell fate determination has only recently become available, challenging the long-held dogma regarding strict, hierarchical progression of stem to differentiated cell.

The small intestine exhibits one of the highest rates of cellular turnover of any adult tissue: mature cells persist for only 4-5 days, and must be continuously replaced throughout adulthood (Clevers 2013). However, the identity and behavior of the stem cell type driving the ongoing production of newborn intestinal cells has been the source of much controversy, despite the fact that the intestinal crypt was identified as the source of newborn cells over a century ago (Bizzozero 1893). Cheng and Leblond first postulated that crypt base columnar (CBC) cells were the true intestinal stem cells, based on their uptake of tritiated thymidine (^{3}H) during mitosis and subsequent differentiation into multiple cell types (Cheng and Leblond 1974). A few years later, Potten and colleagues used the same technique to label dividing cells in the crypt, and observed that while CBCs lost their labels after a few days, neighboring cells, dubbed "+4" cells based on their position relative to the crypt base, retained these labels for five days, exhibiting short-term quiescence (C. S. Potten et al. 1978; Christopher S. Potten, Owen, and Booth 2002). Thus, two fundamental characteristics of stem cells (ability to differentiate into multiple lineages or multipotency, and relative quiescence) were confirmed in the intestinal crypt, but in distinct cell types.

The orphan G-protein-coupled receptor Lgr5 labels mitotic CBCs that give rise to all intestinal lineages (Barker et al. 2007). Clonal lineage tracing with Confetti, a modified Brainbow reporter,

has shown that cells arising from parental Lgr5+ CBCs compete with one another before a single clone dominates an entire crypt and associated villus (Ritsma et al. 2015; Snippert et al. 2010). These results are indicative of population asymmetry amongst numerous equipotent, competing CBCs, rather than invariant asymmetry of small numbers of long-lived stem cells, but it remains unclear whether Lgr5+ CBCs are the "true" stem cells of the intestinal crypt, given that they constantly divide.

It increasingly appears that, in the intestine, this distinction is moot. Both newly-differentiated cells and slow-cycling +4 cells can reconstitute Lgr5+ CBCs following injury (van Es et al. 2012; Tian et al. 2013; Tetteh et al. 2016), an example of dedifferentiation that is at odds with canonical models of stem cell hierarchies. Moreover, Paneth cells, which surround dividing CBCs at the crypt base and promote CBC stem-cell character, are themselves descendants of the Lgr5+ lineage, and Paneth cell precursors are capable of de-differentiating back into Lgr5+ CBCs following injury (Buczacki et al. 2014). Interconversion between all constituent cells of the intestinal crypt appears to be a feature of intestinal homeostasis, and even the quiescent reservoir of +4 stem cells is continuously lost and replaced, albeit at a slower rate than CBCs themselves (Clevers 2013).

Plasticity and heterogeneity also exist amongst stem cells of the adult epidermis. In adult tail skin and ear skin (examples of interfollicular epidermis, or IFE), basal stem cells are free to divide either asymmetrically or symmetrically, and the ratio of self-renewal and differentiation is regulated via population asymmetry (Clayton et al. 2007; Doupé et al. 2010). Unlike in intestine, asymmetric divisions in the IFE are common, though not invariant, and cell-type specific Cre drivers have allowed for the tracing of discrete populations of quiescent, reserve stem cells and active, committed progenitors (Mascré et al. 2013). Quiescent and active stem cells can also be discriminated in the adult hair follicle (Greco et al. 2009), but are capable of interconversion following injury (Rompolas et al. 2013), akin to the dedifferentiation of intestinal progenitors into long-lived CBCs. Notably, division orientations here are biased based on a stem cell's position relative to the hair follicle (Rompolas et al. 2013). Thus, skin and intestine exert population-level control over stem cell divisions, while individual stem cell divisions continue to be loosely regulated by conserved mechanisms of fate determination.

Additional examples of plasticity and heterogeneity amongst adult stem cells continue to be uncovered as researchers probe the genetics and clonal dynamics of other cycling tissues, bolstering the notion that flexibility within stem cell populations may be more general than once presumed (Greulich and Simons 2016). Rates of asymmetric and symmetric division are regulated by population asymmetry in the esophagus (Doupé et al. 2012), and clonal tracing of blood progenitors and their progeny using genetic barcoding and PCR recently showed that

numerous long-lived cycling stem cells each contribute minimally to adult hematopoiesis, as opposed to an exclusive minority of quiescent stem cells (Sun et al. 2014).

Nevertheless, it is likely that conserved mechanisms of asymmetric division continue to influence stem cell fate choice in adult tissues, even when population asymmetry ultimately balances self-renewal and differentiation. In the *Drosophila* midgut, asymmetric divisions of intestinal stem cells are guided by apical Par3 and perpendicular spindle orientation, even though symmetric divisions are also observed (Goulas, Conder, and Knoblich 2012). In the mouse intestine, Par3 is stereotypically localized to the apical portion of CBCs, even though these CBCs typically divide symmetrically (Quyn et al. 2010). In sum, adult tissue stem cells are capable of escaping invariant asymmetric divisions, but continue to utilize developmental mechanisms for ensuring asymmetric daughter fates when necessary.

Lastly, the largely quiescent, non-cycling adult nervous system is now appreciated for harboring populations of neural stem cells which persist in producing newborn neurons throughout adulthood. Though adult neural stem cells were first identified fifty years ago (Altman and Das 1965), mainstream scientific acceptance of bona fide adult neurogenesis only emerged in the last twenty years, particularly following confirmation of adult neurogenesis in the human brain (Eriksson et al. 1998; Gage 2000). Neural stem cells are present in both the dentate gyrus of the hippocampus as well as the subventricular zone of the adult brain, but are largely quiescent. Early study of the fate potential of these cells was often limited to *in vitro* experimentation (Ming and Song 2011; Gage et al. 1995; Gensburger, Labourdette, and Sensenbrenner 1987), while lineage tracing of neural precursor cells using cell-specific Cre lines has more recently confirmed the existence of self-renewing, multipotent adult neural progenitors (Suh et al. 2007).

Despite their reduced rate of division compared to stem cells of fast-cycling tissues, adult neural stem cells are capable of numerous types of division, from symmetric and asymmetric self-renewal to symmetric differentiation into multiple classes of glia or neuron (Bonaguidi et al. 2011). However, the mechanisms underlying population asymmetry amongst adult neural stem cells remain poorly understood, thanks in part to the technical limitations of observing rare mitoses deep in the brain, the complexity of cell types that constitute the adult neural stem cell niche, as well as the diversity of adult neural stem cell progeny (Bonaguidi et al. 2016). The morphology of adult neural stem cells, particularly those with apical and/or basal processes, exposes different regions of these cells to a wide variety of both diffusible factors and membrane-bound factors (Fuentealba, Obernier, and Alvarez-Buylla 2012). Some of these factors, like components of the Wnt signaling pathway and BMPs (Bielen and Houart 2014; Choe, Pleasure, and Mira 2015), have well-characterized effects on adult tissue stem cells in addition to neural stem cells, while others, ranging from various neurotransmitters to the local firing activity of nearby neurons, are now recognized for their specific impact on the fates of

adult neural stem cell progeny (Lledo, Alonso, and Grubb 2006; Song et al. 2012; Vivar et al. 2012).

The olfactory epithelium represents an ideal system in which to study the dynamics underlying self-renewal of an epithelial stem cell alongside differentiation into a known neuronal subtype, the olfactory sensory neuron. HBCs reside in the basal compartment of the OE, and their expression of p63, the keratins (K5, K14), ICAM1, and various integrins (Holbrook, Szumowski, and Schwob 1995) is more reminiscent of basal stem cells of the epidermis (Fuchs 2008) than radial glia of the dentate gyrus or the subventricular zone. However, HBC progeny progress through states that resemble stem and progenitor cells of cortical adult neurogenesis, characterized by sequential expression of Sox2, NeuroD, and Lhx2 (Zhao, Deng, and Gage 2008). Investigation of clonal dynamics and regulation of asymmetric division in HBCs can shed light on mechanisms of HBC self-renewal, but understanding the transcriptional regulation of lineage specification in the regenerating OE, or following p63cKO, requires an analysis of gene expression during HBC differentiation. Single-cell sequencing techniques can illuminate subtleties of the transcriptional changes that occur amongst populations of differentiating stem cells, reveal novel cellular subtypes, and aid in the identification of bifurcation points in lineages arising from multipotent stem cells (Wagner, Regev, and Yosef 2016). Thus, this dissertation utilizes both *in vivo* lineage tracing as well as single-cell RNA sequencing to disentangle the dynamics underlying HBC self-renewal and differentiation.

1.3 Single-cell RNA sequencing and statistical deconvolution of cell types in developing lineages

Single-cell RNA sequencing (single-cell RNA-seq) techniques allow for the discrimination of transcriptional states of individual cells within a population, overcoming the weaknesses of relying on bulk RNA sequencing when studying heterogeneous cell populations. Early applications of single-cell RNA-seq to stem cells in development, or following reprogramming, revealed a higher degree of stem cell heterogeneity than expected (Guo et al. 2010; Buganim et al. 2012), illustrating that stem cell behaviors might be obscured by population-level averaging of gene expression incurred by bulk techniques. Considering that adult stem cells are often rare within a population, and that many adult stem cells are heterogeneous as a population and individually plastic (van Es et al. 2012; Greulich and Simons 2016), there is utility in characterizing the transcriptomes of individual cells to better understand, for example, what distinguishes a more long-lived versus a more fate-committed progenitor. Moreover, applying single-cell transcriptional analysis to differentiating lineages can provide insights into how cells transition between stem, progenitor, and differentiated states.

In the last few years, various groups have devised statistical methods for analyzing single-cell gene expression profiles in the pursuit of better classification of diverse cell types as well as delineation of the lineages along which stem cells and their progeny develop. Trapnell and colleagues developed the *Monocle* algorithm to reorder single-cell transcriptomes according to their similarity, in a pairwise fashion, with the goal of defining the developmental relationships between cells independently of the time-point at which those cells were collected during a muscle progenitor differentiation assay (Trapnell et al. 2014). Others have used similar approaches to study differentiation in the human preimplantation embryo (Petropoulos et al. 2016), adult hippocampus (Shin et al. 2015), and adult subventricular zone (Llorens-Bobadilla et al. 2015). Moreover, such frameworks for using single-cell techniques in general to investigate heterogeneous cell populations have provided insights into immune cell development (via single-cell mass cytometry) (Bendall et al. 2014) and intestinal stem cell transcriptional priming prior to division (via single-cell qRT-PCR) (Kim et al. 2016).

Despite the recent wave of interest in using single-cell RNA-seq to analyze differentiation and development, there are few available statistical methods for identifying bifurcating lineages arising from common progenitors, as most published studies have focused on non-branching lineages (Shin et al. 2015; Trapnell et al. 2014). However, a handful of groups have begun to address this methodological gap (Setty et al. 2016; Marco et al. 2014), demonstrating that single-cell RNA-seq is amenable for distinguishing the transcriptional changes that occur as two lineages differentiate simultaneously from a common precursor population. This dissertation leverages a recently developed statistical framework, *Slingshot*, to illuminate the transcriptional changes that define HBC exit from quiescence and bifurcation of olfactory progenitors towards either the neuronal or sustentacular lineages. These data complement *in vivo* clonal analysis of HBC progeny, providing insight into and validation of the processes that regulate HBC self-renewal and differentiation.

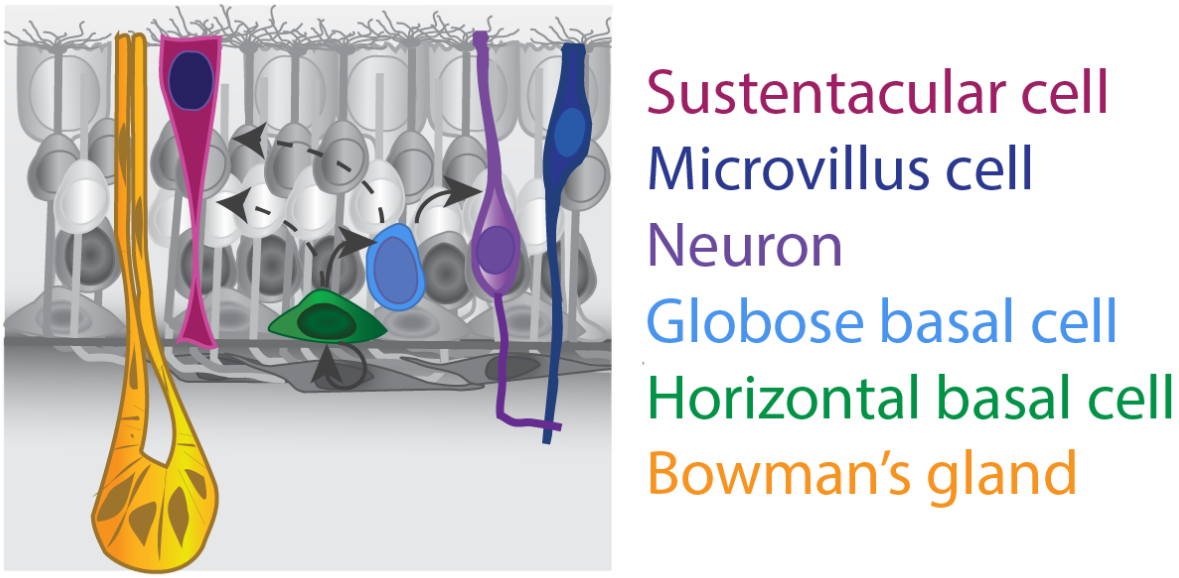

Figure 1.1 Schematic of cell types in the olfactory epithelium
Globose basal cells (GBCs) produce new mature neurons (mOSNs) throughout adulthood via several cellular intermediates, including intermediate neuronal precursors (INPs) and immature olfactory sensory neurons (iOSNs). Microvillus cells are also derived from the neuronal lineage. Following severe injury that ablates all mature olfactory cell types, horizontal basal cells (HBCs) self-renew and give rise to sustentacular cells, Bowman's glands, and cells in the neuronal lineage.

References

Albertson, D. G., and J. N. Thomson. 1993. “Segregation of Holocentric Chromosomes at Meiosis in the Nematode, Caenorhabditis Elegans.” *Chromosome Research: An International Journal on the Molecular, Supramolecular and Evolutionary Aspects of Chromosome Biology* 1 (1): 15–26.

Alexandre, Paula, Alexander M. Reugels, David Barker, Eric Blanc, and Jonathan D. W. Clarke. 2010. “Neurons Derive from the More Apical Daughter in Asymmetric Divisions in the Zebrafish Neural Tube.” *Nature Neuroscience* 13 (6). Nature Publishing Group: 673–79.

Altman, J., and G. D. Das. 1965. “Autoradiographic and Histological Evidence of Postnatal Hippocampal Neurogenesis in Rats.” *The Journal of Comparative Neurology* 124 (3): 319–35.

Barker, Nick, Johan H. van Es, Jeroen Kuipers, Pekka Kujala, Maaike van den Born, Miranda Cozijnsen, Andrea Haegebarth, et al. 2007. “Identification of Stem Cells in Small Intestine and Colon by Marker Gene Lgr5.” *Nature* 449 (7165). Nature Publishing Group: 1003–7.

Bendall, Sean C., Kara L. Davis, El-Ad David Amir, Michelle D. Tadmor, Erin F. Simonds, Tiffany J. Chen, Daniel K. Shenfeld, Garry P. Nolan, and Dana Pe’er. 2014. “Single-Cell Trajectory Detection Uncovers Progression and Regulatory Coordination in Human B Cell Development.” *Cell* 157 (3): 714–25.

Bielen, Holger, and Corinne Houart. 2014. “The Wnt Cries Many: Wnt Regulation of Neurogenesis through Tissue Patterning, Proliferation, and Asymmetric Cell Division.” *Developmental Neurobiology* 74 (8): 772–80.

Bizzozero, G. 1893. “Ueber Die Schlauchförmigen Drüsen Des Magendarmkanals Und Die Beziehungen Ihres Epithels Zu Dem Oberflächenepithel Der Schleimhaut Dritte Mittheilung: Hierzu Tafel VII-X.” *Archiv Für Mikroskopische Anatomie* 42 (1): 82–152.

Bonaguidi, Michael A., Ryan P. Stadel, Daniel A. Berg, Jiaqi Sun, Guo-Li Ming, and Hongjun Song. 2016. “Diversity of Neural Precursors in the Adult Mammalian Brain.” *Cold Spring Harbor Perspectives in Biology* 8 (4): a018838.

Bonaguidi, Michael A., Michael A. Wheeler, Jason S. Shapiro, Ryan P. Stadel, Gerald J. Sun, Guo-Li Ming, and Hongjun Song. 2011. “In Vivo Clonal Analysis Reveals Self-Renewing and Multipotent Adult Neural Stem Cell Characteristics.” *Cell* 145 (7). Elsevier Inc.: 1142–55.

Buczacki, Simon J. A., Heather Ireland Zecchini, Anna M. Nicholson, Roslin Russell, Louis Vermeulen, Richard Kemp, and Douglas J. Winton. 2014. “Intestinal Label-Retaining Cells Are Secretory Precursors Expressing Lgr5.” *Nature* 495 (7439). Nature Publishing Group: 65–69.

Buganim, Yosef, Dina A. Faddah, Albert W. Cheng, Elena Itskovich, Styliani Markoulaki, Kibibi Ganz, Sandy L. Klemm, Alexander van Oudenaarden, and Rudolf Jaenisch. 2012. “Single-Cell Expression Analyses during Cellular Reprogramming Reveal an Early Stochastic and a Late Hierarchic Phase.” *Cell* 150 (6): 1209–22.

Bultje, Ronald S., David R. Castaneda-Castellanos, Lily Yeh Jan, Yuh Nung Jan, Arnold R. Kriegstein, and Song-Hai Shi. 2009. “Mammalian Par3 Regulates Progenitor Cell Asymmetric Division via Notch Signaling in the Developing Neocortex.” *Neuron* 63 (2). Elsevier Inc.: 189–202.

Caggiano, M., J. S. Kauer, and D. D. Hunter. 1994. “Globose Basal Cells Are Neuronal Progenitors in the Olfactory Epithelium: A Lineage Analysis Using a Replication-Incompetent Retrovirus.” *Neuron* 13 (2). Elsevier Inc.: 339–52.

Cheng, H., and C. P. Leblond. 1974. “Origin, Differentiation and Renewal of the Four Main Epithelial Cell Types in the Mouse Small Intestine. V. Unitarian Theory of the Origin of the Four Epithelial Cell Types.” *The American Journal of Anatomy* 141 (4): 537–61.

Chenn, Anjen, and Susan K. McConnell. 1995. “Cleavage Orientation and the Asymmetric Inheritance of Notchl Immunoreactivity in Mammalian Neurogenesis.” *Cell* 82 (4). Elsevier Inc.: 631–41.

Choe, Youngshik, Samuel J. Pleasure, and Helena Mira. 2015. “Control of Adult Neurogenesis by Short-Range Morphogenic-Signaling Molecules.” *Cold Spring Harbor Perspectives in Biology* 8 (3): a018887.

Clayton, Elizabeth, David P. Doupé, Allon M. Klein, Douglas J. Winton, Benjamin D. Simons, and Philip H. Jones. 2007. “A Single Type of Progenitor Cell Maintains Normal Epidermis.” *Nature* 446 (7132). Nature Publishing Group: 185–89.

Clevers, Hans. 2013. “Stem Cells: A Unifying Theory for the Crypt.” *Nature*. Nature Publishing Group. http://eutils.ncbi.nlm.nih.gov/entrez/eutils/elink.fcgi?dbfrom=pubmed&id=23446347&retmode=ref&cmd=prlinks.

Cowan, Carrie R., and Anthony A. Hyman. 2004. “Asymmetric Cell Division in C. Elegans: Cortical Polarity and Spindle Positioning.” *Annual Review of Cell and Developmental Biology* 20: 427–53.

Cuenca, Adrian A., Aaron Schetter, Donato Aceto, Kenneth Kemphues, and Geraldine Seydoux. 2003. “Polarization of the C. Elegans Zygote Proceeds via Distinct Establishment and Maintenance Phases.” *Development* 130 (7): 1255–65.

Doe, C. Q., and B. Bowerman. 2001. “Asymmetric Cell Division: Fly Neuroblast Meets Worm Zygote.” *Current Opinion in Cell Biology* 13 (1). Elsevier Ltd: 68–75.

Doupé, David P., Maria P. Alcolea, Amit Roshan, Gen Zhang, Allon M. Klein, Benjamin D. Simons, and Philip H. Jones. 2012. “A Single Progenitor Population Switches Behavior to Maintain and Repair Esophageal Epithelium.” *Science* 337 (6098): 1091–93.

Doupé, David P., Allon M. Klein, Benjamin D. Simons, and Philip H. Jones. 2010. “The Ordered Architecture of Murine Ear Epidermis Is Maintained by Progenitor Cells with Random Fate.” *DEVCEL* 18 (2). Elsevier: 317–23.

Eriksson, P. S., E. Perfilieva, T. Björk-Eriksson, A. M. Alborn, C. Nordborg, D. A. Peterson, and F. H. Gage. 1998. “Neurogenesis in the Adult Human Hippocampus.” *Nature Medicine* 4 (11): 1313–17.

Es, Johan H. van, Toshiro Sato, Marc van de Wetering, Anna Lyubimova, Annie Ng Yee Nee, Alex Gregorieff, Nobuo Sasaki, et al. 2012. “Dll1+ Secretory Progenitor Cells Revert to Stem Cells upon Crypt Damage.” *Nature Cell Biology* 14 (10). Nature Publishing Group: 1099–1104.

Fletcher, Russell B., Melanie S. Prasol, Jose Estrada, Ariane Baudhuin, Karen Vranizan, Yoon Gi Choi, and John Ngai. 2011. “p63 Regulates Olfactory Stem Cell Self-Renewal and Differentiation.” *Neuron* 72 (5). Elsevier Inc.: 748–59.

Fuchs, Elaine. 2008. “Skin Stem Cells: Rising to the Surface.” *The Journal of Cell Biology* 180 (2): 273–84.

Fuchs, Elaine, and Valerie Horsley. 2011. “Ferreting out Stem Cells from Their Niches.” *Nature Cell Biology* 13 (5). Nature Publishing Group: 513–18.
Fuentealba, Luis C., Kirsten Obernier, and Arturo Alvarez-Buylla. 2012. “Adult Neural Stem Cells Bridge Their Niche.” *Cell Stem Cell* 10 (6): 698–708.
Fuller, Margaret T., and Allan C. Spradling. 2007. “Male and Female Drosophila Germline Stem Cells: Two Versions of Immortality.” *Science* 316 (5823): 402–4.
Gage, F. H. 2000. “Mammalian Neural Stem Cells.” *Science* 287 (5457): 1433–38.
Gage, F. H., P. W. Coates, T. D. Palmer, H. G. Kuhn, L. J. Fisher, J. O. Suhonen, D. A. Peterson, S. T. Suhr, and J. Ray. 1995. “Survival and Differentiation of Adult Neuronal Progenitor Cells Transplanted to the Adult Brain.” *Proceedings of the National Academy of Sciences of the United States of America* 92 (25): 11879–83.
Gensburger, C., G. Labourdette, and M. Sensenbrenner. 1987. “Brain Basic Fibroblast Growth Factor Stimulates the Proliferation of Rat Neuronal Precursor Cells in Vitro.” *FEBS Letters* 217 (1): 1–5.
Goldstein, B., and S. N. Hird. 1996. “Specification of the Anteroposterior Axis in Caenorhabditis Elegans.” *Development* 122 (5): 1467–74.
Gönczy, Pierre, and Lesilee S. Rose. 2005. “Asymmetric Cell Division and Axis Formation in the Embryo.” *WormBook: The Online Review of C. Elegans Biology*, 1–20.
Goulas, Spyros, Ryan Conder, and Juergen A. Knoblich. 2012. “The Par Complex and Integrins Direct Asymmetric Cell Division in Adult Intestinal Stem Cells.” *Cell Stem Cell* 11 (4): 529–40.
Greco, Valentina, Ting Chen, Michael Rendl, Markus Schober, H. Amalia Pasolli, Nicole Stokes, June Dela Cruz-Racelis, and Elaine Fuchs. 2009. “A Two-Step Mechanism for Stem Cell Activation during Hair Regeneration.” *Cell Stem Cell* 4 (2): 155–69.
Greulich, Philip, and Benjamin D. Simons. 2016. “Dynamic Heterogeneity as a Strategy of Stem Cell Self-Renewal.” *Proceedings of the National Academy of Sciences of the United States of America* 113 (27): 7509–14.
Guo, Guoji, Mikael Huss, Guo Qing Tong, Chaoyang Wang, Li Li Sun, Neil D. Clarke, and Paul Robson. 2010. “Resolution of Cell Fate Decisions Revealed by Single-Cell Gene Expression Analysis from Zygote to Blastocyst.” *Developmental Cell* 18 (4): 675–85.
Holbrook, E. H., K. E. Szumowski, and J. E. Schwob. 1995. “An Immunochemical, Ultrastructural, and Developmental Characterization of the Horizontal Basal Cells of Rat Olfactory Epithelium.” *The Journal of Comparative Neurology* 363 (1): 129–46.
Horvitz, H. Robert, and Ira Herskowitz. 1992. “Mechanisms of Asymmetric Cell Division: Two Bs or Not Two Bs, That Is the Question.” *Cell* 68. Elsevier Inc.: 237–55.
Inaba, Mayu, and Yukiko M. Yamashita. 2012. “Asymmetric Stem Cell Division: Precision for Robustness.” *Stem Cells* 11 (4). Elsevier Inc.: 461–69.
Itzkovitz, Shalev, Irene C. Blat, Tyler Jacks, Hans Clevers, and Alexander van Oudenaarden. 2012. “Optimality in the Development of Intestinal Crypts.” *Cell* 148 (3). Elsevier Inc.: 608–19.
Iwai, Naomi, Zhijian Zhou, Dennis R. Roop, and Richard R. Behringer. 2008. “Horizontal Basal Cells Are Multipotent Progenitors in Normal and Injured Adult Olfactory Epithelium.” *Stem Cells* 26 (5): 1298–1306.
Kempermann, G., H. G. Kuhn, and F. H. Gage. 1998. “Experience-Induced Neurogenesis in the Senescent Dentate Gyrus.” *The Journal of Neuroscience: The Official Journal of the Society*

for Neuroscience 18 (9): 3206–12.
Kemphues, K. J., J. R. Priess, D. G. Morton, and N. S. Cheng. 1988. "Identification of Genes Required for Cytoplasmic Localization in Early C. Elegans Embryos." *Cell* 52 (3): 311–20.
Kim, Tae-Hee, Assieh Saadatpour, Guoji Guo, Madhurima Saxena, Alessia Cavazza, Niyati Desai, Unmesh Jadhav, et al. 2016. "Single-Cell Transcript Profiles Reveal Multilineage Priming in Early Progenitors Derived from Lgr5+ Intestinal Stem Cells." *CellReports* 16 (8). The Authors: 2053–60.
Klein, Allon M., Toshinori Nakagawa, Rie Ichikawa, Shosei Yoshida, and Benjamin D. Simons. 2010. "Mouse Germ Line Stem Cells Undergo Rapid and Stochastic Turnover." *Cell Stem Cell* 7 (2): 214–24.
Knoblich, Juergen A. 2008. "Mechanisms of Asymmetric Stem Cell Division." *Cell* 132 (4). Elsevier Inc.: 583–97.
Kriegstein, Arnold, and Arturo Alvarez-Buylla. 2009. "The Glial Nature of Embryonic and Adult Neural Stem Cells." *Annual Review of Neuroscience* 32: 149–84.
Lechler, Terry, and Elaine Fuchs. 2005. "Asymmetric Cell Divisions Promote Stratification and Differentiation of Mammalian Skin." *Nature* 437 (7056). Nature Publishing Group: 275–80.
Leung, Cheuk T., Pierre A. Coulombe, and Randall R. Reed. 2007. "Contribution of Olfactory Neural Stem Cells to Tissue Maintenance and Regeneration." *Nature Neuroscience* 10 (6). Nature Publishing Group: 720–26.
Li, Rong. 2013. "The Art of Choreographing Asymmetric Cell Division." *DEVCEL* 25 (5). Elsevier: 439–50.
Lledo, Pierre-Marie, Mariana Alonso, and Matthew S. Grubb. 2006. "Adult Neurogenesis and Functional Plasticity in Neuronal Circuits." *Nature Reviews. Neuroscience* 7 (3): 179–93.
Llorens-Bobadilla, Enric, Sheng Zhao, Avni Baser, Gonzalo Saiz-Castro, Klara Zwadlo, and Ana Martin-Villalba. 2015. "Single-Cell Transcriptomics Reveals a Population of Dormant Neural Stem Cells That Become Activated upon Brain Injury." *Cell Stem Cell* 17 (3): 329–40.
Lois, C., and A. Alvarez-Buylla. 1993. "Proliferating Subventricular Zone Cells in the Adult Mammalian Forebrain Can Differentiate into Neurons and Glia." *Proceedings of the National Academy of Sciences of the United States of America* 90 (5): 2074–77.
Mackay-Sim, A., and P. Kittel. 1991. "Cell Dynamics in the Adult Mouse Olfactory Epithelium: A Quantitative Autoradiographic Study." *The Journal of Neuroscience: The Official Journal of the Society for Neuroscience* 11 (4): 979–84.
Marco, Eugenio, Robert L. Karp, Guoji Guo, Paul Robson, Adam H. Hart, Lorenzo Trippa, and Guo-Cheng Yuan. 2014. "Bifurcation Analysis of Single-Cell Gene Expression Data Reveals Epigenetic Landscape." *Proceedings of the National Academy of Sciences of the United States of America* 111 (52): E5643–50.
Mascré, Guilhem, Sophie Dekoninck, Benjamin Drogat, Khalil Kass Youssef, Sylvain Broheé, Panagiota A. Sotiropoulou, Benjamin D. Simons, and Cedric Blanpain. 2013. "Distinct Contribution of Stem and Progenitor Cells to Epidermal Maintenance." *Nature* 489 (7415). Nature Publishing Group: 257–62.
Ming, Guo-Li, and Hongjun Song. 2011. "Adult Neurogenesis in the Mammalian Brain: Significant Answers and Significant Questions." *Neuron* 70 (4). Elsevier Inc.: 687–702.
Mizutani, Ken-Ichi, Keejung Yoon, Louis Dang, Akinori Tokunaga, and Nicholas Gaiano. 2007. "Differential Notch Signalling Distinguishes Neural Stem Cells from Intermediate

Progenitors." *Nature* 449 (7160): 351–55.
Morrison, S. J., H. D. Hemmati, A. M. Wandycz, and I. L. Weissman. 1995. "The Purification and Characterization of Fetal Liver Hematopoietic Stem Cells." *Proceedings of the National Academy of Sciences of the United States of America* 92 (22): 10302–6.
Munro, Edwin, Jeremy Nance, and James R. Priess. 2004. "Cortical Flows Powered by Asymmetrical Contraction Transport PAR Proteins to Establish and Maintain Anterior-Posterior Polarity in the Early C. Elegans Embryo." *Developmental Cell* 7 (3): 413–24.
Nipper, Rick W., Karsten H. Siller, Nicholas R. Smith, Chris Q. Doe, and Kenneth E. Prehoda. 2007. "Gαi Generates Multiple Pins Activation States to Link Cortical Polarity and Spindle Orientation in Drosophila Neuroblasts." *Proceedings of the National Academy of Sciences* 104 (36): 14306–11.
Noctor, Stephen C., Verónica Martínez-Cerdeño, Lidija Ivic, and Arnold R. Kriegstein. 2004. "Cortical Neurons Arise in Symmetric and Asymmetric Division Zones and Migrate through Specific Phases." *Nature Neuroscience* 7 (2): 136–44.
Ohshiro, T., T. Yagami, C. Zhang, and F. Matsuzaki. 2000. "Role of Cortical Tumour-Suppressor Proteins in Asymmetric Division of Drosophila Neuroblast." *Nature* 408 (6812): 593–96.
Packard, Adam, Nikolai Schnittke, Rose-Anne Romano, Satrajit Sinha, and James E. Schwob. 2011. "DeltaNp63 Regulates Stem Cell Dynamics in the Mammalian Olfactory Epithelium." *The Journal of Neuroscience: The Official Journal of the Society for Neuroscience* 31 (24): 8748–59.
Peng, C. Y., L. Manning, R. Albertson, and C. Q. Doe. 2000. "The Tumour-Suppressor Genes Lgl and Dlg Regulate Basal Protein Targeting in Drosophila Neuroblasts." *Nature* 408 (6812): 596–600.
Petropoulos, Sophie, Daniel Edsgärd, Björn Reinius, Qiaolin Deng, Sarita Pauliina Panula, Simone Codeluppi, Alvaro Plaza Reyes, Sten Linnarsson, Rickard Sandberg, and Fredrik Lanner. 2016. "Single-Cell RNA-Seq Reveals Lineage and X Chromosome Dynamics in Human Preimplantation Embryos." *Cell* 167 (1): 285.
Postiglione, Maria Pia, Christoph Jüschke, Yunli Xie, Gerald A. Haas, Christoforos Charalambous, and Juergen A. Knoblich. 2011. "Mouse Inscuteable Induces Apical-Basal Spindle Orientation to Facilitate Intermediate Progenitor Generation in the Developing Neocortex." *Neuron* 72 (2). Elsevier Inc.: 269–84.
Potten, Christopher S., Gary Owen, and Dawn Booth. 2002. "Intestinal Stem Cells Protect Their Genome by Selective Segregation of Template DNA Strands." *Journal of Cell Science* 115 (Pt 11): 2381–88.
Potten, C. S. 1974. "The Epidermal Proliferative Unit: The Possible Role of the Central Basal Cell." *Cell and Tissue Kinetics* 7 (1): 77–88.
Potten, C. S., W. J. Hume, P. Reid, and J. Cairns. 1978. "The Segregation of DNA in Epithelial Stem Cells." *Cell* 15 (3): 899–906.
Poulson, Nicholas D., and Terry Lechler. 2010. "Robust Control of Mitotic Spindle Orientation in the Developing Epidermis." *The Journal of Cell Biology* 191 (5): 915–22.
Quyn, Aaron J., Paul L. Appleton, Francis A. Carey, Robert J. C. Steele, Nick Barker, Hans Clevers, Rachel A. Ridgway, Owen J. Sansom, and Inke S. NAthke. 2010. "Spindle Orientation Bias in Gut Epithelial Stem Cell Compartments Is Lost in Precancerous

Tissue." *Stem Cells* 6 (2). Elsevier Inc.: 175–81.
Ritsma, Laila, Saskia I. J. Ellenbroek, Anoek Zomer, Hugo J. Snippert, Frederic J. de Sauvage, Benjamin D. Simons, Hans Clevers, and Jacco van Rheenen. 2015. "Intestinal Crypt Homeostasis Revealed at Single-Stem-Cell Level by in Vivo Live Imaging." *Nature* 507 (7492). Nature Publishing Group: 362–65.
Romano, Rose-Anne, Kirsten Smalley, Caitlin Magraw, Vanida Ann Serna, Takeshi Kurita, Srikala Raghavan, and Satrajit Sinha. 2012. "ΔNp63 Knockout Mice Reveal Its Indispensable Role as a Master Regulator of Epithelial Development and Differentiation." *Development* 139 (4): 772–82.
Rompolas, Panteleimon, Elizabeth R. Deschene, Giovanni Zito, David G. Gonzalez, Ichiko Saotome, Ann M. Haberman, and Valentina Greco. 2013. "Live Imaging of Stem Cell and Progeny Behaviour in Physiological Hair-Follicle Regeneration." *Nature* 487 (7408). Nature Publishing Group: 496–99.
Sarkar, Abby, and Konrad Hochedlinger. 2013. "The Sox Family of Transcription Factors: Versatile Regulators of Stem and Progenitor Cell Fate." *Stem Cells* 12 (1). Elsevier Inc.: 15–30.
Setty, Manu, Michelle D. Tadmor, Shlomit Reich-Zeliger, Omer Angel, Tomer Meir Salame, Pooja Kathail, Kristy Choi, Sean Bendall, Nir Friedman, and Dana Pe'er. 2016. "Wishbone Identifies Bifurcating Developmental Trajectories from Single-Cell Data." *Nature Biotechnology* 34 (6): 637–45.
Shen, Qin, Weimin Zhong, Yuh Nung Jan, and Sally Temple. 2002. "Asymmetric Numb Distribution Is Critical for Asymmetric Cell Division of Mouse Cerebral Cortical Stem Cells and Neuroblasts." *Development* 129 (20): 4843–53.
Shin, Jaehoon, Daniel A. Berg, Yunhua Zhu, Joseph Y. Shin, Juan Song, Michael A. Bonaguidi, Grigori Enikolopov, et al. 2015. "Single-Cell RNA-Seq with Waterfall Reveals Molecular Cascades Underlying Adult Neurogenesis." *Cell Stem Cell* 17 (3): 360–72.
Siminovitch, Louis, Ernest A. McCulloch, and James E. Till. 1963. "The Distribution of Colony-Forming Cells among Spleen Colonies." *Journal of Cellular and Comparative Physiology* 62 (3). Wiley Online Library: 327–36.
Simons, Benjamin D., and Hans Clevers. 2011. "Strategies for Homeostatic Stem Cell Self-Renewal in Adult Tissues." *Cell* 145 (6). Elsevier Inc.: 851–62.
Snippert, Hugo J., Laurens G. van der Flier, Toshiro Sato, Johan H. van Es, Maaike van den Born, Carla Kroon-Veenboer, Nick Barker, et al. 2010. "Intestinal Crypt Homeostasis Results from Neutral Competition between Symmetrically Dividing Lgr5 Stem Cells." *Cell* 143 (1). Elsevier Inc.: 134–44.
Song, Juan, Chun Zhong, Michael A. Bonaguidi, Gerald J. Sun, Derek Hsu, Yan Gu, Konstantinos Meletis, et al. 2012. "Neuronal Circuitry Mechanism Regulating Adult Quiescent Neural Stem-Cell Fate Decision." *Nature* 488 (7414). Nature Publishing Group: 150–54.
Suh, Hoonkyo, Antonella Consiglio, Jasodhara Ray, Toru Sawai, Kevin A. D'Amour, and Fred H. Gage. 2007. "In Vivo Fate Analysis Reveals the Multipotent and Self-Renewal Capacities of Sox2+ Neural Stem Cells in the Adult Hippocampus." *Cell Stem Cell* 1 (5): 515–28.
Sun, Jianlong, Azucena Ramos, Brad Chapman, Jonathan B. Johnnidis, Linda Le, Yu-Jui Ho, Allon Klein, Oliver Hofmann, and Fernando D. Camargo. 2014. "Clonal Dynamics of

Native Haematopoiesis." *Nature* 514 (7522). Nature Publishing Group: 322–27.
Tetteh, Paul W., Onur Basak, Henner F. Farin, Kay Wiebrands, Kai Kretzschmar, Harry Begthel, Maaike van den Born, et al. 2016. "Replacement of Lost Lgr5-Positive Stem Cells through Plasticity of Their Enterocyte-Lineage Daughters." *Stem Cells* 18 (2). Elsevier Inc.: 203–13.
Tetteh, Paul W., Henner F. Farin, and Hans Clevers. 2014. "Plasticity within Stem Cell Hierarchies in Mammalian Epithelia." *Trends in Cell Biology*. Elsevier Ltd, 1–9.
Tian, Hua, Brian Biehs, Søren Warming, Kevin G. Leong, Linda Rangell, Ophir D. Klein, and Frederic J. de Sauvage. 2013. "A Reserve Stem Cell Population in Small Intestine Renders Lgr5-Positive Cells Dispensable." *Nature* 478 (7368). Nature Publishing Group: 255–59.
Till, J. E., and E. A. McCulloch. 1961. "A Direct Measurement of the Radiation Sensitivity of Normal Mouse Bone Marrow Cells." *Radiation Research* 14 (February): 213–22.
Till, J. E., E. A. Mcculloch, and L. Siminovitch. 1964. "A STOCHASTIC MODEL OF STEM CELL PROLIFERATION, BASED ON THE GROWTH OF SPLEEN COLONY-FORMING CELLS." *Proceedings of the National Academy of Sciences of the United States of America* 51: 29–36.
Trapnell, Cole, Davide Cacchiarelli, Jonna Grimsby, Prapti Pokharel, Shuqiang Li, Michael Morse, Niall J. Lennon, Kenneth J. Livak, Tarjei S. Mikkelsen, and John L. Rinn. 2014. "The Dynamics and Regulators of Cell Fate Decisions Are Revealed by Pseudotemporal Ordering of Single Cells." *Nature Biotechnology* 32 (4). Nature Publishing Group: 381–86.
Vivar, Carmen, Michelle C. Potter, Jiwon Choi, Ji-Young Lee, Thomas P. Stringer, Edward M. Callaway, Fred H. Gage, Hoonkyo Suh, and Henriette van Praag. 2012. "Monosynaptic Inputs to New Neurons in the Dentate Gyrus." *Nature Communications* 3: 1107.
Wagner, Allon, Aviv Regev, and Nir Yosef. 2016. "Revealing the Vectors of Cellular Identity with Single-Cell Genomics." *Nature Biotechnology* 34 (11): 1145–60.
Weissman, Irving L. 2011. "50 Years Later: Remembering the Paper." *Radiation Research* 175 (2): 143–44.
Xie, T., and A. C. Spradling. 2000. "A Niche Maintaining Germ Line Stem Cells in the Drosophila Ovary." *Science* 290 (5490): 328–30.
Zhao, Chunmei, Wei Deng, and Fred H. Gage. 2008. "Mechanisms and Functional Implications of Adult Neurogenesis." *Cell* 132 (4). Elsevier Inc.: 645–60.
Zuo, Wei, Ting Zhang, Daniel Zheng'an Wu, Shou Ping Guan, Audrey-Ann Liew, Yusuke Yamamoto, Xia Wang, et al. 2014. "p63+Krt5+ Distal Airway Stem Cells Are Essential for Lung Regeneration." *Nature*. Nature Publishing Group, 1–16.

Chapter 2:
The role of spindle orientation and cell polarity in HBC mitosis during regeneration

Background

The olfactory epithelium (OE) is the only vertebrate sensory organ capable of generating new neurons throughout adulthood, presumably due to the ongoing exposure of sensory neuron dendrites to environmental insults in the nasal cavity. Under homeostatic conditions, these sensory neurons live for a few months before being replaced by newborn neurons derived from pools of progenitor cells residing in the basal compartment of this pseudostratified epithelium (P. P. Graziadei and Graziadei 1979; Mackay-Sim and Kittel 1991). Moreover, the OE replenishes its neuronal population following targeted ablation of the olfactory nerve (G. A. Graziadei and Graziadei 1979) or the olfactory bulb (Carr and Farbman 1992), and regenerates entirely upon severe injury that ablates its structural cells (sustentacular cells) as well as its neurons (Bergman and Brittebo 1999). Though both the stem and differentiated cell types in the OE have been broadly characterized by their expression of well-known markers of epithelial cells and developing neurons, the mechanisms underlying olfactory stem cell self-renewal and differentiation following their exit from quiescence remain unknown.

The horizontal basal cell (HBC) of the OE is the quiescent stem cell responsible for the brunt of olfactory neurogenesis that occurs following severe injury (Leung, Coulombe, and Reed 2007). HBCs are characterized by their expression of known epithelial stem cell markers, including transcription factors (Keratin 5, Keratin 14 and p63), and regulators of stem cell/extracellular matrix interactions, such as the integrins (B1, B4) and ICAM1. These markers are most reminiscent of markers of basal epidermal stem cells, which are long-lived and capable of orchestrating skin regeneration (Lavker and Sun 2000; Lechler and Fuchs 2005). Work in our lab has shown that p63 is a key regulator of HBC quiescence and stem-cell character. HBCs transiently downregulate p63 upon activation following injury, and spontaneously differentiate upon conditional knockout of p63 at steady-state, presumably in conjunction with a loss of HBC self-renewal (Fletcher et al. 2011). To better understand how HBCs exit quiescence following p63 knockout or injury to the OE, however, it is informative to look towards models of epithelial stem cell activation in other contexts.

During development, when stem cells must rapidly multiply to provide differentiated cells for a growing tissue, stem cell divisions are highly regulated to ensure both stem cell self-renewal and robust production of differentiated daughter cells. In the *C. elegans* zygote, this process begins with the establishment of cellular polarity, which is determined by the donated centrosome of a single spermatzoon in the fertilized ovum (Cowan and Hyman 2004; Albertson and Thomson 1993). Recruitment of cellular polarity factors, such as the Par complex, to the apical cortex of

the cell subsequently drives the sequestration of fate-determinants, such as MEX-5 and MEX-6, to either the apical or basal cortices (Kemphues et al. 1988; Schubert et al. 2000), and orients the mitotic spindle such that each daughter cell inherits unique fate-determinants. This type of mitosis is known as an asymmetric division, reflecting the divergent fates of doublets of daughter cells arising from a single parental stem cell; implicit in this definition is the existence of symmetric divisions, which result in the production of daughter cells with identical fates.

Like the early embryonic stem cells of *C. elegans, Drosophila* neural precursor cells (neuroblasts) are polarized by the neuroepithelium, from which they delaminate prior to division (Doe and Bowerman 2001). This results in the asymmetric sequestration of polarity factors, such as the Par complex, at either the apical or basal cortices. The mitotic spindle orients along the now-defined axis of polarity; and division ensures the asymmetric inheritance of fate determinants, such as Numb, that promote differentiation in the basal ganglion mother cell, precursor to neurons and glia, or self-renewal in the apical cell (Matsuzaki 2000).

In the developing mouse embryo, epithelial polarity and spindle orientation play a key role in regulating rates of self-renewal and differentiation at various stages, first by promoting self-renewing, symmetric divisions that occur parallel to the basement membrane, and later by promoting both asymmetric divisions that produce differentiated keratinocytes, as well as a minority of symmetric, renewing divisions (Lechler and Fuchs 2005; Poulson and Lechler 2010). However, in adult mouse tail skin, asymmetric and symmetric divisions both arise from mitoses oriented parallel to the basement membrane, perhaps due to differential exposure of daughter cells to Notch signaling factors independent of spindle orientation (Clayton et al. 2007).

Mixed evidence regarding the role of spindle orientation in driving asymmetric divisions also has been uncovered in the adult intestine as well as in the developing neocortex. While Lgr5-expressing crypt base cells orient their spindles perpendicular to the stem cell niche (Quyn et al. 2010), clonal tracing indicates that symmetric divisions predominate amongst these cells at steady-state (Ritsma et al. 2015; Snippert et al. 2010). Moreover, in developing neocortex, neural progenitor divisions that occur parallel to the growing neuroepithelium often result in symmetric renewing fates for daughter cells, even though asymmetric fates can also result from unequal inheritance of the apical cortex in similarly parallel divisions (Kosodo et al. 2004; Belzil et al. 2014). In sum, the relationship between cell polarity, spindle orientation, and fate determination varies across many contexts, even when the expression of conserved factors required for these phenomena is consistent.

In spite of the OE's tractability as an *in vivo* model of adult neurogenesis, *in vitro* OE slice or culture assays are not available, restricting the observation of the movement of mitotic factors within HBCs to snapshots derived from fixed tissue sections. However, improvements in

single-cell transcriptomics have allowed various groups to probe the transcriptional changes occurring in individual stem cells in different tissues during differentiation, including blood (Sun et al. 2014), intestine (Kim et al. 2016), and brain (Llorens-Bobadilla et al. 2015). In these three cases in particular, differentiated cells arose from heterogeneous classes of stem cells, which stochastically became activated to seed the growth of particular downstream lineages. Thus, even though propensity to undergo asymmetric and symmetric division *per se* can not be teased out of the transcriptional state of single stem cells, these modern techniques allow us to investigate the changes in gene expression that may drive dividing stem cells to adopt differential fates.

To address whether canonical regulators of stem cell division underlie HBC self-renewal during injury, this chapter explores the orientation of the mitotic spindle and localization of Par complex protein Par3 in mitotic HBCs early in regeneration both in the presence of wild-type p63 and in the absence of p63 following Cre-mediated gene knockout.

Methods

Transgenic Mice

Mice bearing transgenic alleles for constitutive tracing of HBCs (Krt5-CrePR; (Zhou et al. 2002)), tamoxifen-inducible tracing of HBCs (Krt5-CreER(T2); (Indra et al. 1999)), conditional knockout of p63 (Trp63loxP/loxP allele; (Mills, Qi, and Bradley 2002)), YFP lineage tracer (Rosa26eYFP; (Srinivas et al. 2001)), and Confetti lineage tracer (Rosa26-Confetti; (Snippert et al. 2010)) were bred and maintained against a mixed B6;129;FVB background. Mice with the following genotypes were used for experiments described in this chapter:

K5CrePR; p63wt/wt; Rosa-YFP (spindle orientation and Par3 experiments; “p63wt”)
K5CrePR; p63fl/wt; Rosa-YFP (spindle orientation and Par3 experiments; “p63het”)
K5CrePR; p63fl/fl; Rosa-YFP (spindle orientation and Par3 experiments; “p63cKO”)

Injury induction and lineage tracing for spindle orientation, Par3 analyses

To determine the angle of the mitotic spindle and localization of cell polarity factor Par3 in HBCs early in regeneration, HBCs were lineage traced using the K5-CrePR driver, which becomes constitutively active in HBCs at postnatal day 5 (P5), in conjunction with the Rosa-YFP reporter. Injury was induced in mice at postnatal day 10 (P10) with an intraperitoneal injection of methimazole (Leung, Coulombe, and Reed 2007), and dividing HBCs were analyzed at 24 hours post injury (hpi), 30hpi, and 39hpi.

Tissue processing

Whole OE tissue was fixed with 4% paraformaldehyde overnight at 4°C, washed with phosphate-buffered saline (PBS), decalcified with 10% ethylenediaminetetraacetic acid in PBS

for 4-5 days at 4°C. Tissue was then washed with distilled H2O for 5 hours at RT, equilibrated in 30% sucrose overnight at 4°C, mounted in tissue-freezing medium (Triangle Biomedical Sciences), and stored at -80°C. Tissue was finally cryosectioned at 12µm thickness and mounted onto Superfrost Plus slides (Fisher Scientific) for immunohistochemical processing.

Immunohistochemistry

Slides were hydrated, washed three times for 20 minutes in PBS with 0.1% Triton-X100 (PBST), and blocked in PBST with 10% donkey serum before being stained overnight at 4°C with primary antibodies diluted in blocking solution. Primary antibody was removed with three five-minute PBST washes, and slides were then stained for 2 hours with secondary antibodies diluted in blocking solution. Processed slides were prepared for imaging using Vectashield hard-set mounting medium (Vector Labs) and coverslips.

To identify dividing HBCs, the YFP lineage tracer was amplified with an anti-GFP antibody (Abcam), and mitotic histones were labeled with anti-phospho-histone-H3 (anti-PH3, Santa Cruz Biotechnology). For spindle orientation assessment, spindle poles were labeled with anti-pericentrin (Covance). For cell polarity assessment, Par3 was labeled with anti-Par3 (Millipore) following antigen retrieval (10 minutes in a 90°C solution of 10mM Tris Base, 1mM EDTA, 0.05% Tween 20). Appropriate Alexa-Fluor secondary antibodies were used to visualize YFP and PH3 at 488 nm and Par3 or pericentrin at 594 nm. YFP and PH3 signals were distinguished in the same channel on the basis of their subcellular localization: YFP lineage tracer was distributed diffusely in the cytoplasm while PH3 localized to discrete, bright puncta corresponding to mitotic histones.

Imaging and Quantitation

Imaging of stained sections was performed via confocal scanning microscopy, and images were processed using ImageJ (NIH) and Photoshop (Adobe) to combine channels and examine z-stacks. For spindle orientation assessment, maximum projections of confocal z-stacks were analyzed. In lineage-traced, PH3-positive basal cells, the angle of the mitotic spindle was measured with respect to the basement membrane by drawing a line approximating the local basal plane.

Results

To assess the orientation of the mitotic spindle in dividing HBCs early in regeneration, injury to the OE was induced in K5CrePR; Rosa-YFP littermate animals bearing zero, one, or two alleles of floxed p63 (p63wt, p63het, p63cKO). Following IHC to label mitotic histones and spindle poles, the angle of the spindle was measured with relation to the basement membrane in basal, lineage-traced, dividing cells only (Fig. 2.1). At 24, 30, and 39 hours post-injury (hpi), spindles

in both wildtype and p63-heterozygous HBCs were predominantly oriented parallel (0°-30°) or perpendicular (60°-90°) to the basement membrane (Fig. 2.2). The paucity of oblique spindles (30°-60°) in these data was confirmed with a statistical test for unimodality, Hartigans' dip test (Hartigan and Hartigan 1985), demonstrating that the distribution of spindles was significantly bimodal at 24 hpi and 39 hpi (24 hpi: $p < 0.0001$; 30 hpi: $p < 0.242$; 39 hpi: $p < 0.004$). In p63-deficient HBCs, however, the mitotic spindle was less likely to orient perpendicular to the basement membrane (Fig. 2.2), and the distribution of spindles was not bimodal at any time point, according to Hartigans' dip test (24 hpi: $p < 0.1$; 30 hpi: $p < 0.766$; 39 hpi: $p < 0.437$).

To determine whether aberrations in cell polarity may underlie the observed deficit of perpendicular spindle orientations in p63-cKO HBCs, tissue from 30 hpi p63wt and p63cKO OE was stained for Par3, a key member of the Par complex, which helps drive the perpendicular orientation of the mitotic spindle during asymmetric division (Siller and Doe 2009). In dividing wild-type HBCs early in regeneration, a crescent of Par3 protein was consistently observed at the apical cortex; in contrast, Par3 not only failed to localize to a discrete, coherent region of the cellular cortex in p63cKO HBCs, but also was distributed around the entirety of the cortex (Fig. 2.3). Thus, loss of cellular polarity in p63cKO HBCs may interfere with the ability of HBCs to orient the spindle perpendicularly to the basement membrane, precluding asymmetric self-renewal during regeneration.

Conclusion/Discussion

Stem cells are tasked with rapidly producing differentiating daughter cells without depleting their own long-lived population during embryonic development, adult homeostasis, and tissue regeneration. In invertebrate development, asymmetric divisions are orchestrated by the coordinated movement of cell polarity factors and the mitotic spindle to ensure that one daughter cell differentiates, while its sibling cell retains the stem-cell characteristics of the parental cell (Doe and Bowerman 2001). Some of these cell polarity factors also ensure asymmetric divisions in vertebrates, particularly in developing skin, but the role of cell polarity and spindle orientation is less clear in cycling adult tissues, where symmetric divisions sometimes predominate without exhausting the stem cell pool (Simons and Clevers 2011) .

In this chapter, I explored whether the long-lived, quiescent olfactory stem cell, the HBC, potentially ensures its own self-renewal via bias in spindle orientation or cell polarization as it approaches its first division during regeneration. Particularly at 24 hpi, but also at 30 hpi and 39 hpi, the HBC mitotic spindle rarely orients at oblique angles to the basement membrane, suggesting that spindle orientation may indeed drive the occurrence of both asymmetric divisions, perpendicular to the basal plane, and symmetric divisions, parallel to the basal plane. HBCs deficient in p63 fail to orient their spindles at high angles, between 60° and 90°, indirectly

implying a relationship between loss of asymmetric divisions and loss of self-renewal during p63cKO. Moreover, cell polarity factor Par3 is sequestered apically in wild type HBCs early in regeneration, while p63cKO HBCs display incoherent and unpolarized localization of Par3 around the cell cortex. These results suggest that HBC self-renewal, and asymmetric cell division, may depend upon both proper apical localization of Par3 and the ability of the mitotic spindle to orient perpendicular to the basement membrane.

In the absence of live-imaging methods for following regenerative HBC divisions, the consequences of a perpendicular spindle or apical Par3 must be inferred by analyzing stained tissue at fixed timepoints later in regeneration, when the fates of clonal daughter cells can be definitively scored, or by analyzing early changes in gene expression occurring as HBCs differentiate. To gain a better understanding of the population and transcriptional dynamics underlying HBC differentiation, a clonal analysis of lineage-traced, differentiating HBC progeny following p63cKO was undertaken, complemented by parallel single-cell RNA sequencing of these progeny during a differentiation time-course, in Chapter 3. In Chapter 4, the issue of population asymmetry and HBC self-renewal is addressed using a more detailed clonal analysis of lineage-traced HBC progeny during regeneration, and is again complemented by parallel single-cell RNA sequencing to gain insight into the transcriptional changes that underlie HBC differentiation into neurons, sustentacular cells, and renewed HBCs.

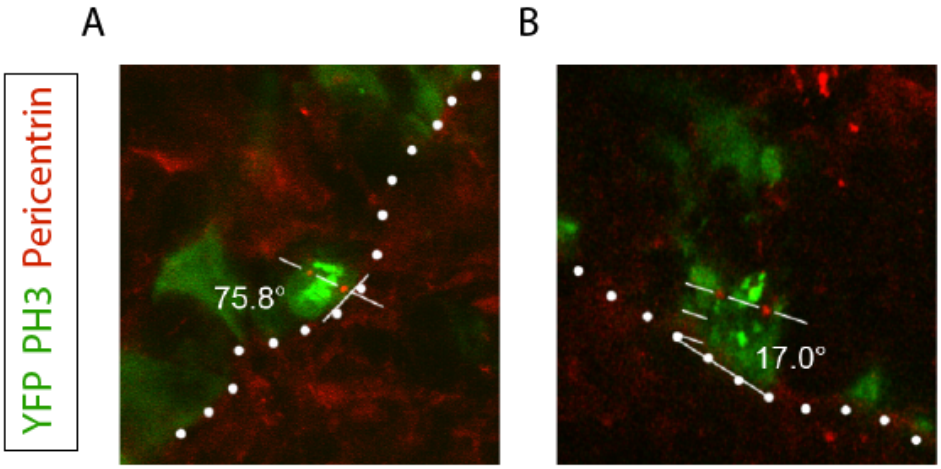

Figure 2.1 Representative measurements of HBC spindle orientation at 30hpi
YFP lineage tracer (cytoplasmic, diffuse) and phospho-histone H3 (PH3) (nuclear, punctate) are discriminated in the green channel on the basis of their subcellular localization and distribution. **(A)** Perpendicular spindle in a dividing HBC. **(B)** Parallel spindle in a dividing HBC. In both images, the basement membrane is indicated by the dotted line.

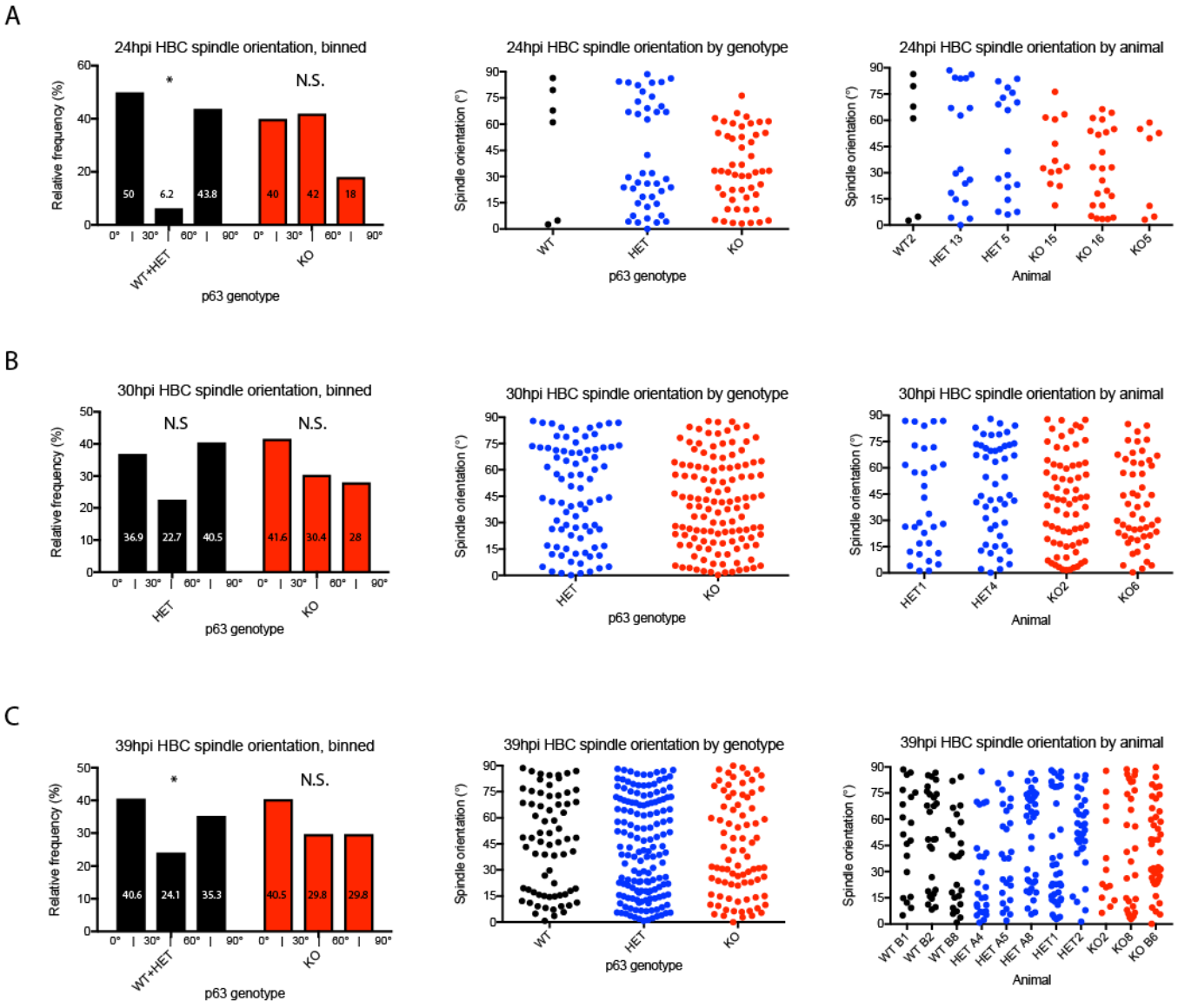

Figure 2.2 Bimodal distributions of wild-type HBC spindle orientation early in regeneration

Binned distributions, spindle angles by genotype, and spindle angles by animal are displayed from left to right for each timepoint. At least two animals were scored for either p63wt+p63het or p63cko. N refers to cells counted. **(A)** At 24hpi, the HBC spindle is heavily biased to orient either parallel or perpendicular to the basement membrane, with spindle angles displaying a bimodal distribution (n = 48; Hartigans' diptest, $p < 0.0001$), while the spindle fails to orient perpendicularly in p63cKO HBCs, leading to a unimodal distribution (n = 50; Hartigans' diptest, $p = 0.1$). **(B)** At 30hpi, spindle orientations appear to distribute bimodally, but the distribution is not significant (n = 84; Hartigans' diptest, $p = 0.24$); p63cKO spindles also do not distribute

bimodally (n = 125; Hartigans' diptest, p = 0.77). **(C)** At 39hpi, the HBC spindle is again biased to orient either parallel or perpendicular to the basement membrane, with angles distributed bimodally (n = 224; Hartigans' diptest, p = 0.004), and p63cKO spindles continue to distribute unimodally (n = 84; Hartigans' diptest, p = 0.437).

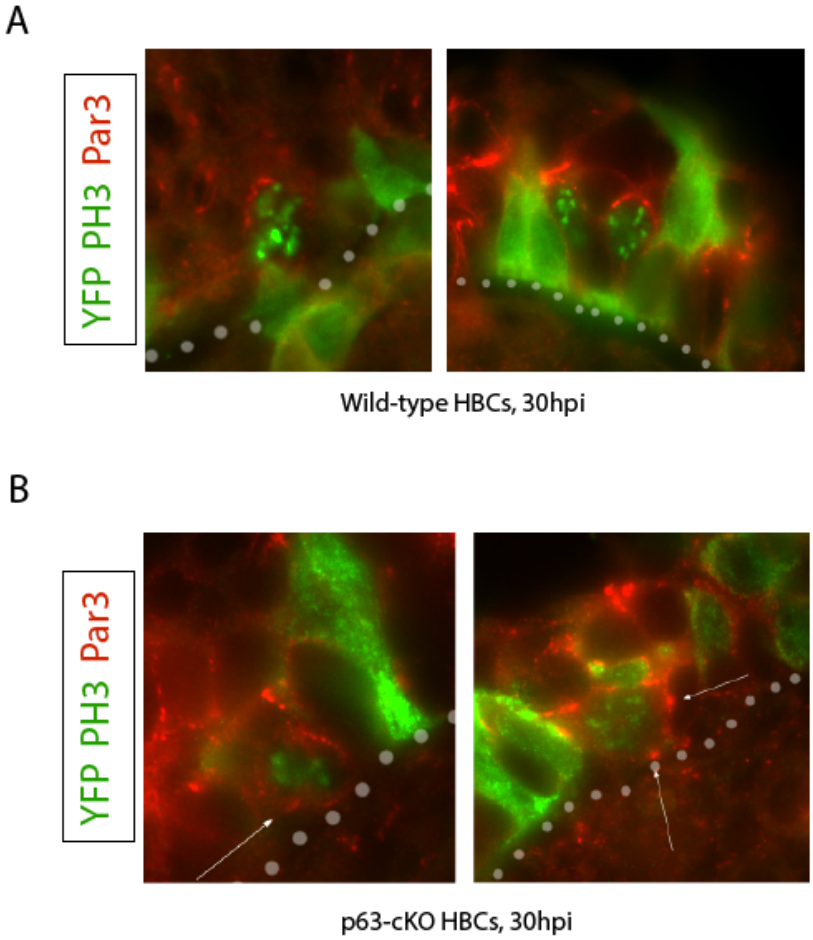

Figure 2.3 Par3 localization in wild-type and p63cKO HBCs during regeneration.
Par3 is restricted to a single crescent at the apical cortex in wild-type HBCs at 30hpi during regeneration **(A)**, while it is less coherently organized throughout the p63cKO HBC cortex at the same timepoint **(B)**. The basement membrane is indicated by the dotted line. In (B), mislocalized Par3 is denoted by white arrows.

References

Albertson, D. G., and J. N. Thomson. 1993. “Segregation of Holocentric Chromosomes at Meiosis in the Nematode, Caenorhabditis Elegans.” *Chromosome Research: An International Journal on the Molecular, Supramolecular and Evolutionary Aspects of Chromosome Biology* 1 (1): 15–26.

Belzil, Camille, Naoyuki Asada, Kei-Ichiro Ishiguro, Takeo Nakaya, Kari Parsons, Valentina Pendolino, Gernot Neumayer, et al. 2014. “p600 Regulates Spindle Orientation in Apical Neural Progenitors and Contributes to Neurogenesis in the Developing Neocortex.” *Biology Open* 3 (6): 475–85.

Bergman, Ulrika, and Eva B. Brittebo. 1999. “Methimazole Toxicity in Rodents: Covalent Binding in the Olfactory Mucosa and Detection of Glial Fibrillary Acidic Protein in the Olfactory Bulb.” *Toxicology and Applied Pharmacology* 155 (2). Elsevier: 190–200.

Carr, V. M., and A. I. Farbman. 1992. “Ablation of the Olfactory Bulb up-Regulates the Rate of Neurogenesis and Induces Precocious Cell Death in Olfactory Epithelium.” *Experimental Neurology* 115 (1): 55–59.

Clayton, Elizabeth, David P. Doupé, Allon M. Klein, Douglas J. Winton, Benjamin D. Simons, and Philip H. Jones. 2007. “A Single Type of Progenitor Cell Maintains Normal Epidermis.” *Nature* 446 (7132). Nature Publishing Group: 185–89.

Cowan, Carrie R., and Anthony A. Hyman. 2004. “Asymmetric Cell Division in C. Elegans: Cortical Polarity and Spindle Positioning.” *Annual Review of Cell and Developmental Biology* 20: 427–53.

Doe, C. Q., and B. Bowerman. 2001. “Asymmetric Cell Division: Fly Neuroblast Meets Worm Zygote.” *Current Opinion in Cell Biology* 13 (1). Elsevier Ltd: 68–75.

Fletcher, Russell B., Melanie S. Prasol, Jose Estrada, Ariane Baudhuin, Karen Vranizan, Yoon Gi Choi, and John Ngai. 2011. “p63 Regulates Olfactory Stem Cell Self-Renewal and Differentiation.” *Neuron* 72 (5). Elsevier Inc.: 748–59.

Graziadei, G. A., and P. P. Graziadei. 1979. “Neurogenesis and Neuron Regeneration in the Olfactory System of Mammals. II. Degeneration and Reconstitution of the Olfactory Sensory Neurons after Axotomy.” *Journal of Neurocytology* 8 (2): 197–213.

Graziadei, P. P., and G. A. Graziadei. 1979. “Neurogenesis and Neuron Regeneration in the Olfactory System of Mammals. I. Morphological Aspects of Differentiation and Structural Organization of the Olfactory Sensory Neurons.” *Journal of Neurocytology* 8 (1): 1–18.

Hartigan, John A., and P. M. Hartigan. 1985. “The Dip Test of Unimodality.” *Annals of Statistics* 13 (1). Institute of Mathematical Statistics: 70–84.

Indra, Arup Kumar, Xavier Warot, Jacques Brocard, Jean-Marc Bornert, Jia-Hao Xiao, Pierre Chambon, and Daniel Metzger. 1999. “Temporally-Controlled Site-Specific Mutagenesis in the Basal Layer of the Epidermis: Comparison of the Recombinase Activity of the Tamoxifen-Inducible Cre-ERT and Cre-ERT2 Recombinases.” *Nucleic Acids Research* 27 (22). Oxford Univ Press: 4324–27.

Kemphues, K. J., J. R. Priess, D. G. Morton, and N. S. Cheng. 1988. “Identification of Genes Required for Cytoplasmic Localization in Early C. Elegans Embryos.” *Cell* 52 (3): 311–20.

Kim, Tae-Hee, Assieh Saadatpour, Guoji Guo, Madhurima Saxena, Alessia Cavazza, Niyati Desai, Unmesh Jadhav, et al. 2016. “Single-Cell Transcript Profiles Reveal Multilineage

Priming in Early Progenitors Derived from Lgr5+ Intestinal Stem Cells." *CellReports* 16 (8). The Authors: 2053–60.
Kosodo, Yoichi, Katja Röper, Wulf Haubensak, Anne-Marie Marzesco, Denis Corbeil, and Wieland B. Huttner. 2004. "Asymmetric Distribution of the Apical Plasma Membrane during Neurogenic Divisions of Mammalian Neuroepithelial Cells." *The EMBO Journal* 23 (11): 2314–24.
Lavker, R. M., and T. T. Sun. 2000. "Epidermal Stem Cells: Properties, Markers, and Location." *Proceedings of the National Academy of Sciences of the United States of America* 97 (25): 13473–75.
Lechler, Terry, and Elaine Fuchs. 2005. "Asymmetric Cell Divisions Promote Stratification and Differentiation of Mammalian Skin." *Nature* 437 (7056). Nature Publishing Group: 275–80.
Leung, Cheuk T., Pierre A. Coulombe, and Randall R. Reed. 2007. "Contribution of Olfactory Neural Stem Cells to Tissue Maintenance and Regeneration." *Nature Neuroscience* 10 (6). Nature Publishing Group: 720–26.
Llorens-Bobadilla, Enric, Sheng Zhao, Avni Baser, Gonzalo Saiz-Castro, Klara Zwadlo, and Ana Martin-Villalba. 2015. "Single-Cell Transcriptomics Reveals a Population of Dormant Neural Stem Cells That Become Activated upon Brain Injury." *Cell Stem Cell* 17 (3): 329–40.
Mackay-Sim, A., and P. Kittel. 1991. "Cell Dynamics in the Adult Mouse Olfactory Epithelium: A Quantitative Autoradiographic Study." *The Journal of Neuroscience: The Official Journal of the Society for Neuroscience* 11 (4): 979–84.
Matsuzaki, F. 2000. "Asymmetric Division of Drosophila Neural Stem Cells: A Basis for Neural Diversity." *Current Opinion in Neurobiology* 10 (1): 38–44.
Mills, Alea A., Yi Qi, and Allan Bradley. 2002. "Conditional Inactivation ofp63 by Cre-Mediated Excision." *Genesis* 32 (2): 138–41.
Poulson, Nicholas D., and Terry Lechler. 2010. "Robust Control of Mitotic Spindle Orientation in the Developing Epidermis." *The Journal of Cell Biology* 191 (5): 915–22.
Quyn, Aaron J., Paul L. Appleton, Francis A. Carey, Robert J. C. Steele, Nick Barker, Hans Clevers, Rachel A. Ridgway, Owen J. Sansom, and Inke S. NAthke. 2010. "Spindle Orientation Bias in Gut Epithelial Stem Cell Compartments Is Lost in Precancerous Tissue." *Stem Cells* 6 (2). Elsevier Inc.: 175–81.
Ritsma, Laila, Saskia I. J. Ellenbroek, Anoek Zomer, Hugo J. Snippert, Frederic J. de Sauvage, Benjamin D. Simons, Hans Clevers, and Jacco van Rheenen. 2015. "Intestinal Crypt Homeostasis Revealed at Single-Stem-Cell Level by in Vivo Live Imaging." *Nature* 507 (7492). Nature Publishing Group: 362–65.
Schubert, C. M., R. Lin, C. J. de Vries, R. H. Plasterk, and J. R. Priess. 2000. "MEX-5 and MEX-6 Function to Establish Soma/germline Asymmetry in Early C. Elegans Embryos." *Molecular Cell* 5 (4): 671–82.
Siller, Karsten H., and Chris Q. Doe. 2009. "Spindle Orientation during Asymmetric Cell Division." *Nature Cell Biology* 11 (4). Nature Publishing Group: 365–74.
Simons, Benjamin D., and Hans Clevers. 2011. "Strategies for Homeostatic Stem Cell Self-Renewal in Adult Tissues." *Cell* 145 (6). Elsevier Inc.: 851–62.
Snippert, Hugo J., Laurens G. van der Flier, Toshiro Sato, Johan H. van Es, Maaike van den Born, Carla Kroon-Veenboer, Nick Barker, et al. 2010. "Intestinal Crypt Homeostasis Results from Neutral Competition between Symmetrically Dividing Lgr5 Stem Cells." *Cell*

143 (1). Elsevier Inc.: 134–44.
Srinivas, S., T. Watanabe, C. S. Lin, C. M. William, Y. Tanabe, T. M. Jessell, and F. Costantini. 2001. “Cre Reporter Strains Produced by Targeted Insertion of EYFP and ECFP into the ROSA26 Locus.” *BMC Developmental Biology* 1 (March): 4.
Sun, Jianlong, Azucena Ramos, Brad Chapman, Jonathan B. Johnnidis, Linda Le, Yu-Jui Ho, Allon Klein, Oliver Hofmann, and Fernando D. Camargo. 2014. “Clonal Dynamics of Native Haematopoiesis.” *Nature* 514 (7522). Nature Publishing Group: 322–27.
Zhou, Zhijian, Dongyan Wang, Xiao-Jing Wang, and Dennis R. Roop. 2002. “In Utero Activation of K5.CrePR1 Induces Gene Deletion.” *Genesis* 32 (2): 191–92.

Chapter 3:
Steady-state dynamics of HBC differentiation following p63 knockout

This chapter, excerpted from a manuscript that is currently under review, represents a collaboration with members of the Ngai Lab (primarily Russell Fletcher and Diya Das) and members of the UC Berkeley Statistics department and Center for Computational Biology. I contributed to the overall experimental design; carried out FACS, single-cell RNA-seq from cells to library preparation for all p63cKO time-points with assistance from Russell Fletcher; clonal analysis methodology, and scoring and analysis at 7 dpi; and editing of the manuscript.

Authors: Russell B. Fletcher[1]*, Diya Das[1]*, Levi Gadye[2], Kelly N. Street[3,8], Ariane Baudhuin[1], Davide Risso[3], Allon Wagner[4,8], Michael B. Cole[5,8], Quetzal Flores[1], Yoon Gi Choi[6], Nir Yosef[4,8], Elizabeth Purdom[7,8], Sandrine Dudoit[3,7,8] and John Ngai[1,2,6]
* These authors contributed equally to this work.
[1] Department of Molecular and Cell Biology
[2] Helen Wills Neuroscience Institute
[3] Division of Biostatistics
[4] Department of Electrical Engineering and Computer Science
[5] Department of Physics
[6] QB3 Functional Genomics Laboratory
[7] Department of Statistics
[8] Center for Computational Biology

Background

The horizontal basal cell (HBC) of the olfactory epithelium is capable of giving rise to all olfactory cell types (Leung et al., 2007; Fletcher et al., 2011). Although some of these cell types can be identified on the basis of marker gene expression, it is unclear how HBC differentiation is regulated either at steady-state, following p63cKO, or during regeneration. In this manuscript, we complemented a clonal analysis of the p63cKO differentiating HBC with single-cell RNA-seq of FACS-sorted HBC progeny. In collaboration with the members of the UC Berkeley Statistics Department, we developed *Slingshot,* a novel statistical approach that allowed for the reordering of single-cell transcriptomes according to their developmental state, independent of the experiment in which they were collected. This provided a fine-grained view of the transcriptional changes that occur as HBC progeny move between cellular states during differentiation. Using these parallel approaches, we were able to identify novel mechanisms of direct fate conversion of HBCs to sustentacular cells, and proliferation of intermediate progenitors in the neuronal lineage following p63cKO, validating the utility of combining *in vivo* lineage tracing with single-cell transcriptional analysis.

Introduction

A fundamental challenge in stem cell biology is to define both the cell fate potential of a given stem cell and where cell fates are specified along a developmental trajectory. Moreover, detailed lineage trajectory maps are necessary for identifying the regulatory networks governing the cell fate transitions underlying tissue maintenance and regeneration, and are essential for designing strategies to manipulate cells for therapeutic applications. Lineage tracing – a technique for permanently labeling the descendants of a targeted cell – is a powerful tool for elucidating the cell fate potential and specification of progenitor cells (Bałakier and Pedersen, 1982; Kimmel and Law, 1985; Moody, 1987; Price et al., 1987; Spemann and Mangold, 1924; Weisblat et al., 1978; 1980; Zinyk et al., 1998). Lineage tracing using transgenic technologies has been applied to genetically defined adult stem cells in regenerative tissues, demonstrating that stem cell multipotency at the population level can reflect a spectrum of differentiation potentials manifested by individual stem cells (Bonaguidi et al., 2011; Clayton et al., 2007; Snippert et al., 2010a; Sun et al., 2014). However, while lineage tracing has greatly advanced our understanding of development and stem cells, this approach alone cannot readily identify all intermediate stages in a lineage or pinpoint when in a branching lineage multiple cell fates arise.

Whole transcriptome profiling of single cells by RNA sequencing (single-cell RNA-seq) has recently emerged as a powerful method for discriminating the heterogeneity of cell types and cell states in a complex population (Deng et al., 2013; Grün et al., 2016; Llorens-Bobadilla et al., 2015; Olsson et al., 2016; Pollen et al., 2015; 2014; Shalek et al., 2014; Treutlein et al., 2014; 2016; Usoskin et al., 2014). New statistical approaches have further enabled the assignment and ordering of cells to discrete stages in developmental lineages based on gradual changes in gene expression detected at the single cell level (Bendall et al., 2014; Haghverdi et al., 2015; Petropoulos et al., 2016; Shin et al., 2015; Trapnell et al., 2014). While powerful, these approaches struggle to overcome the challenge of identifying where lineages diverge in more complex branching trajectories of multipotent progenitors, a problem that is only beginning to be addressed (Setty et al., 2016). Importantly, even the most sophisticated analysis of single-cell RNA-seq data can only provide predictions that require independent experimental validation.

The olfactory epithelium is a sensory neuroepithelium that maintains a steady state population of mature olfactory sensory neurons via continual neurogenesis in the postnatal animal (Graziadei and Graziadei, 1979b; Mackay-Sim and Kittel, 1991). Olfactory neurogenesis is normally sustained through differentiation of globose basal cells (GBCs), which are the actively proliferating neurogenic progenitor cells in the niche (Caggiano et al., 1994; Graziadei and Graziadei, 1979b; Schwob et al., 1994). Upon targeted destruction of the sensory neurons or more severe injury to the entire tissue, the olfactory epithelium can regenerate (Burd, 1993;

Graziadei and Graziadei, 1979a; Matulionis, 1975; 1976; Schultz, 1960; Schwob et al., 1995). Following such injury, the horizontal basal cells (HBCs) – the normally quiescent, reserve stem cells of the niche – become activated to differentiate and reconstitute all major cell types in the epithelium (Iwai et al., 2008; Leung et al., 2007) (Figure 1A).

With its relative simplicity and experimental accessibility, the postnatal olfactory epithelium provides an attractive system for studying the activation and specification events that occur during the differentiation of multiple cell lineages from an adult stem cell. A number of questions relevant to other adult stem cell niches can also be addressed. For example, while lineage tracing suggests that cells arising from HBCs transition through proliferative GBC progenitors to generate olfactory sensory neurons (Leung et al., 2007), it remains unclear whether the epithelium's other cell types arise via a common GBC intermediate. Similarly, characterizing the transitions in gene expression that occur throughout a developing lineage is a prerequisite to disentangling the gene regulatory networks that underlie cell fate decisions. Thus, we sought to determine when and where in the trajectory different sub-lineages diverge, quantify the gene expression changes that accompany these developmental transitions, and define the underlying gene networks that control them.

In the present study, we combined a statistical approach for making branching lineage assignments from single-cell RNA-seq data with in vivo lineage tracing to map the developmental trajectories of the multiple cell lineages arising from the olfactory epithelium's HBC stem cell. The first major bifurcation in the HBC lineage trajectory occurs prior to cell division, producing either sustentacular (support) cells or GBCs. The GBC lineage in turn branches to give rise to microvillous cells and olfactory sensory neurons. Whereas olfactory neurogenesis involves an expansion of the progenitor pool via proliferative GBCs, sustentacular cells instead arise via direct fate conversion of quiescent HBCs, a process that does not require cell division. Moreover, the multipotency of HBCs as a population reflects independent unipotent cell fate decisions made at the single cell level. Our combined approach serves more generally as a model for illuminating and deconstructing branching lineages that arise from multipotent stem cells.

Methods

Transgenic Mice

Mice containing the following transgenes or modified alleles were used in this study: Krt5-CreER(T2) driver (Indra et al., 1999), Trp63lox/lox conditional knockout allele (Mills et al., 2002), Sox2eGFP knock-in reporter allele (Arnold et al., 2011), Rosa26eYFP reporter (Srinivas et al., 2001), and Rosa26Confetti reporter (Snippert et al., 2010a).

Fluorescence-Activated Cell Sorting (FACS)

In the HBC lineage tracing experiments, Krt5-CreER; Rosa26eYFP and Krt5-CreER; Trp63lox/lox; Rosa26eYFP mice were injected with tamoxifen (0.25 mg tamoxifen/g body weight) once at P21-23 days of age and euthanized at the specified times post injection (Figure 1). For all experiments (HBC lineage tracing and Sox2eGFP cells), the OE was surgically removed, and the dorsal, sensory portion was dissected and dissociated. The dissociation protocol was similar to that used previously (Fletcher et al., 2011).

Single-Cell RNA-Seq Cell Capture, Library Preparation, Sequencing

Each FACS collection was considered a biological replicate, and at least two biological replicates were collected for each experimental condition. The Fluidigm C1 system was used to isolate single cells, lyse them, and produce cDNA. Nextera library synthesis was performed using Nextera v2 index oligos. Library size was selected using AMPure XP beads (Beckman Coulter). Indexed, single-cell libraries were sequenced on Illumina Hi-Seq 2000 or HiSeq 2500 sequencers to produce 50 nt single-end reads (with one exception in which paired-end reads were included). Samples were sequenced in multiplex, and each lane typically contained approximately 192 samples.

Single-Cell RNA-Seq Alignment, Pre-processing, Filtering, Normalization, Clustering

Sequencing reads were aligned to the GRCm38.3 (mm10, patch release 3) genome assembly with RefSeq transcript annotations, which were modified to contain sequences of specific transgenic genes used in our analysis (such as CreER and eGFP). We used the adaptive quality metric-based filtering and normalization methods from the open-source R package SCONE, available at https://github.com/YosefLab/scone. We applied a novel Resampling-Based Ensemble Clustering (RSEC) procedure with the aim of obtaining stable and tight clusters. The method is implemented in the open-source Bioconductor R package clusterExperiment, available at http://bioconductor.org/packages/clusterExperiment

Lineage Trajectory and Branching Prediction

A novel method – called Slingshot – was applied to infer lineage trajectories and bifurcations and to order the cells along the trajectory. Slingshot is implemented in an open-source R package available at https://github.com/kstreet13/slingshot.

Clonal Lineage Tracing

Krt5-CreER; Trp63lox/lox; Rosa26Confetti transgenic mice were used for clonal lineage tracing of the HBC lineage. A dose-response was performed to determine an optimal dose of tamoxifen to achieve sparse labeling: 0.025 to 0.05 mg tamoxifen/g body weight administered by intraperitoneal injection. Confocal z-stacks were obtained using a Zeiss LSM 710 or 780 microscope, and images were processed and quantified using ImageJ (NIH). For a breakdown of

clones by animal and reporter, see Figure 3.5.

Immunohistochemisty, RNA In Situ Hybridization, Imaging

Protocols for immunohistochemistry and RNA in situ hybridization were similar to those previously published (Duggan et al., 2008; Fletcher et al., 2011). Fluorescent confocal slices and z-stacks were obtained using Zeiss LSM 710 or 780 microscopes. Brightfield images of RNA in situ hybridization were obtained on a Nikon Microphot compound scope and Leica DFC500 camera. Images were processed with ImageJ (NIH) and Adobe Photoshop and quantified with ImageJ.

Results

We applied single-cell RNA-seq to identify the cell state transitions during differentiation of olfactory HBC stem cells into proliferating progenitors and mature cell types. Two complementary approaches were employed to obtain cells representing different stages in the olfactory lineages. In the first, we used inducible Cre-lox lineage tracing to label HBCs and their progeny. Within postnatal olfactory epithelium, Keratin 5 (Krt5) is expressed exclusively in HBCs (Holbrook et al. 1995). Accordingly, YFP-positive HBCs and their descendants were purified by fluorescence-activated cell sorting (FACS) from olfactory epithelia of Krt5-CreER; Rosa26eYFP mice following activation of Cre recombinase with tamoxifen. In the normal, uninjured olfactory epithelium, most HBCs are quiescent and rarely differentiate (Leung et al. 2007) (Fig. 3.1B). To obtain resting HBCs (controls) we harvested cell samples 72 or 96 hours following tamoxifen-induced Cre activation in three week-old mice (Fig. 3.1C).

The transcription factor Trp63 (also known as p63) is down-regulated upon HBC activation (Fletcher et al. 2011; Packard et al. 2011), and conditional knockout of Trp63 in HBCs leads to their spontaneous differentiation into fully mature olfactory sensory neurons and non-neuronal cells (Fig. 3.1B) (Fletcher et al. 2011). This allowed us to use conditional ablation of Trp63 as a tool to “release” HBCs from their quiescent state and capture differentiating HBCs in large numbers even though HBC differentiation is infrequent in the absence of injury. Thus, we induced the conditional knockout of Trp63 and activated the Rosa26eYFP reporter using tamoxifen. Differentiating YFP-positive lineage-traced cells were harvested and FACS-purified at different time points ranging from 24 hours to 14 days post-tamoxifen (14 dpt; Fig. 3.1C). We isolated a total of 729 YFP lineage-traced cells from both control and Trp63 conditional knockout animals.

In the second approach for isolating olfactory progenitor and neuronal precursor cells, we FACS-purified cells from uninjured olfactory epithelium based on their expression of a Sox2eGFP knock-in reporter gene (Arnold et al. 2011). Sox2 is expressed in the olfactory

epithelium by HBCs, GBCs, microvillous cells, and sustentacular cells (Fig. 3.1 B,D) (Guo et al. 2010). Because of perdurance of the eGFP reporter, the Sox2eGFP transgene also allows for purification of cells later in the neuronal lineage. HBCs express the cell surface marker ICAM1 (Carter et al. 2004), which can be used to deplete the Sox2-eGFP-positive cell population of HBCs by FACS; thus, a preparation containing GBCs (and later differentiating cells from the neuronal lineage), microvillous cells, and sustentacular cells was isolated by sorting for Sox2-eGFP-positive, ICAM-negative cells. Our initial analysis found this preparation to be dominated by sustentacular cells. We therefore identified transcripts for two cell surface markers – Scarb1 and F3 – that are enriched in sustentacular cells. By sorting for Sox2-eGFP-positive, ICAM1-negative, SCARB1/F3-negative cells, we were able to obtain a population of cells that was enriched for GBCs, later neuronal intermediates and microvillous cells over sustentacular cells for a total of 175 cells (Fig. 3.1 D, E).

Single-cell RNA-seq was carried out on FACS-purified cells using the Fluidigm C1 microfluidics cell capture platform followed by Illumina sequencing. Single cell data from YFP lineage tracing experiments and Sox2-eGFP experiments were combined into one data set, a strategy designed to maximize the representation of cell states along the developmental trajectories. RNA-seq data were aligned, filtered to eliminate poor quality samples, and normalized to minimize sources of technical variation and facilitate comparison between single-cell RNA expression profiles. Sequencing data from a total of 687 cells (542 from YFP lineage-traced cells and 145 from Sox2-eGFP-expressing cells) remained after removing doublets, contaminants, and poor quality samples (Fig. 3.1 E).

Clustering of Single-Cell RNA-Seq Data Identifies Distinct Cell Types and Stages of Olfactory Differentiation

To group cells based on their similarities in gene expression profiles, we used our recently developed method RSEC (Resampling-Based Ensemble Clustering) to find stable clusters that are robust over a range of parameters; RSEC found 18 stable clusters. Individual clusters were then manually inspected for the presence of marker genes of known cell types, which were used to make preliminary assignments of cell type identities. Clusters containing fewer than 10 cells (each representing <1.5% of the total population studied) were deemed to be less reliable and therefore set aside to avoid confounding downstream analyses, yielding a final repertoire of 13 clusters.

To visualize cellular heterogeneity, we projected the data onto two dimensions via t-distributed Stochastic Neighbor Embedding (t-SNE; Fig. 3.2 A) (Maaten and Hinton 2008), which confirms that our clustering procedure led to well-defined, distinct groups. Figure 3.2 B shows the cluster medoids in the t-SNE projection, together with preliminary cell type assignments based on the expression of known and/or validated marker genes. For example, we annotated the resting HBC

cluster based on expression of HBC markers Trp63, Krt5, and Krt14 (Fletcher et al. 2011; Holbrook et al. 1995; Suzuki and Takeda 1991). Interestingly, two clusters (ΔHBC1, ΔHBC2) contain cells in which the canonical HBC stem cell markers Trp63, Krt5, and Krt14 appear to be variably down-regulated from cell to cell (Fig. S3.1), suggesting the existence of at least one transition state in which HBCs first begin to differentiate. Cells in the GBC cluster express Kit, Ascl1, and high levels of cell cycle genes, markers of GBC progenitors (Goldstein et al. 2014; Manglapus et al. 2004). Clusters representing immediate neuronal precursors (INP1,2,3) and immature neurons (iOSN) within the olfactory neuronal lineage were also identified based on the expression of genes such as Neurod1, Lhx2, Gap43, and the G protein subunit G8 (Gng8) (Hirota and Mombaerts 2004; Kolterud et al. 2004; Packard et al. 2011; Tirindelli and Ryba 1996; Verhaagen et al. 1989). The mature olfactory sensory neuron cluster (mOSN) was identified by expression of olfactory marker protein (Omp), the main subunit of the cyclic nucleotide-gate channel (Cnga2) and G13 (Gng13), hallmarks of mature olfactory sensory neurons (Huang et al., 1999; Keller and Margolis, 1975; Sautter et al., 1998) . Cells in two clusters (immature and mature sustentacular cells, iSus and mSus, respectively) express increasing levels of Cyp2g1, a marker of sustentacular cells (Gu et al., 1998). We also identified a cluster of microvillous cells (MV2) based on their expression of Ascl3 and Cftr (Pfister et al., 2015). The identity of one small cluster of cells could not be readily classified due to the heterogeneous expression of a few identifying marker genes. Based on the expression of Trpm5, a marker of a subset of microvillous cells (Hansen and Finger, 2008), and Sox9, which we validated as being expressed not only in cells of the Bowman's gland but also in a subset of microvillous cells (not shown), we provisionally assigned this cluster's identity as microvillous cells (MV1), although we cannot exclude the possibility that it contains precursors of Bowman's gland. Thus, clustering of our single-cell RNA-seq data successfully identified three of the major mature HBC-derived cell types in the olfactory epithelium (olfactory sensory neurons, sustentacular cells, microvillous cells) as well as intermediate progenitors and putative transition state stem cells. The absence of cells of the Bowman's gland may reflect their low representation in the overall population and/or their lower survival in our cell isolation procedure.

Assignment of Differentiating Cells to Branching Cell Lineages

Mapping transcriptional changes as cells transition from stem cells to specialized cell types is essential for understanding the mechanisms regulating cell and tissue differentiation. There may not always be clear distinctions between states, however, but rather a series of smooth transitions in which individual cells exist on a continuum between states. In this scenario, cells may undergo gradual transcriptional changes, where the relationship between states can be represented as a continuous lineage dependent on an underlying spatial or temporal variable. This representation, often referred to as pseudotemporal ordering, can provide a basis for understanding how and when cell fate decisions are made (Bendall et al., 2014; Campbell et al., 2015; Haghverdi et al., 2015; Petropoulos et al., 2016; Shin et al., 2015; Trapnell et al., 2014). Here, we seek to identify

the distinct stages through which cells pass as they differentiate from HBC stem cells into mature olfactory cell types, and further to identify when cell type-specific sub-lineages are specified during this process. Does the HBC give rise to a common, multipotent progenitor that in turn generates the different olfactory cell types? Alternatively, do cells adopt different fates during the initial activation of individual HBCs as they transition from a resting state?

The task of assigning and ordering cells in a lineage in the olfactory HBC stem cell niche is complicated by the requirement to accommodate multiple, branching cell fate trajectories that give rise to the multiple cell types of the lineage. To address this problem, we applied Slingshot, a flexible and robust statistical framework for inferring branching lineage assignments and developmental ordering in a continuous differentiation process. Cells were assigned and ordered along multiple olfactory cell lineages and visualized in 3-dimensional PCA plots. Three distinct trajectories were identified, each starting from the resting HBC stage and leading to the three defined mature cell types (Fig. 3.2 C, D). All three trajectories were predicted to pass together through the two transitional HBC stages, at which point the first branching in the lineage occurs. One path leads toward immature and then mature sustentacular cells (magenta). The other path connects transitional HBCs to GBCs, from which the remaining two lineages diverge: one to form microvillous cells (blue) and one to form olfactory sensory neurons (orange). The latter trajectory passes through GBCs, three discrete stages of immediate neuronal precursors (INP1-3), and immature olfactory sensory neurons (iOSN), before concluding in mature olfactory sensory neurons (mOSN).

Developmental Ordering of Cells in the Neuronal and Sustentacular Cell Lineages

We next sought to order all cells and analyze transitions in their transcriptional states as they differentiate to become sustentacular cells and olfactory sensory neurons, the two major mature cell types of the olfactory epithelium. Slingshot inferred three lineage trajectories using principal curves and assigned developmental positions of cells along the lineage trajectory (analogous to the concept of pseudotime (Trapnell et al., 2014) by orthogonal projection of each cell's coordinates in PCA space onto its respective curve. These are displayed as one-dimensional plots in which cells are labeled according to cell cluster (Fig. 3.3 A, C). The linear plots illustrate the developmental distance between cells as captured by dimensionality reduction (via PCA) of the gene expression values. It is evident that the transition from ΔHBC2 to GBCs entails a relatively large jump in gene expression space. Similarly, there is a larger gap between the INP1 and INP2 stages compared to the other transitions following the GBC stage in this lineage. Such jumps in developmental distance represent major transcriptional changes in which distinct networks of genes are turned on or off.

To gain insight into the coordinated patterns of gene expression that underlie the cell fate transitions in the neuronal and sustentacular cell lineages, we identified the most differentially

expressed genes within each lineage (not shown), yielding 2327 genes for the neuronal lineage and 1622 genes for the sustentacular cell lineage. We then clustered these genes using RSEC, identifying 17 clusters of differentially expressed genes in the neuronal lineage and 12 in the sustentacular lineage. The average scaled expression values of the gene clusters in the neuronal and sustentacular cell lineages are displayed in heatmaps in Figure 3.3 B, D, presented in developmental order according to the predictions made by Slingshot. This comparison highlights the dramatic difference in coordinated gene expression through developmental progression in the two lineages. The neuronal lineage contains many modules of genes that are transiently turned on and off, patterns that contrast with the more gradual wave-like changes in gene expression exhibited by the sustentacular lineage. Moreover, there is a longer distance traversed in the neuronal lineage both in terms of the number of distinct cell states and the number of genes showing significant changes at each transition.

Interestingly, transitional HBCs exhibit variable levels of Trp63 mRNA, with some cells exhibiting undetectable levels of Trp63 mRNA and others showing levels comparable to resting HBCs (Fig. S3.1). Expression of mRNAs encoding the cytokeratins Krt5 and Krt14 – established markers of resting HBCs as well as other epithelial stem cells – is also highly variable in transitional HBCs (Fig. S3.1). Pairwise comparisons among Trp63, Krt5, and Krt14 reveal correlated expression of their mRNAs in resting but not transitional HBCs (not shown), suggesting that down-regulation of these genes upon HBC activation reflects a probabilistic process.

Proliferation Is Restricted to the GBC/Neuronal Lineage

Numerous studies have demonstrated that GBCs represent the major proliferative progenitor cell in the steady-state, uninjured olfactory epithelium (Caggiano et al., 1994; Graziadei and Graziadei, 1979b; Schwob et al., 1994). We therefore examined the expression of cell cycle-associated genes (Kowalczyk et al., 2015; Whitfield et al., 2002) in order to determine whether and where expansion occurs in the neuronal and sustentacular cell lineages. As judged by expression of cell proliferation markers, GBCs and INP1 cells comprise the two actively proliferating progenitor cell types in the neuronal lineage (Fig. 3.3 B). In striking contrast, cells progress through the sustentacular cell lineage without a concerted up-regulation of cell proliferation markers (Fig. 3.3 D). Thus, HBCs appear to transdifferentiate into sustentacular cells through a process that does not require cell division.

Lineage Tracing In Vivo Validates Predicted Branch Points in the Olfactory Stem Cell Trajectory

A number of testable predictions can be made from the in silico branching lineage assignments and developmental ordering of differentiating olfactory cells shown in Figures 3.2 and 3.3. First, the initial branching of the sustentacular cell and neuronal lineages at the transitional HBC stage

and in the absence of active cell proliferation suggests that when stimulated to differentiate, each HBC adopts a unique cell fate – i.e., GBC vs. sustentacular cell. In this scenario, the multipotency of the population of HBCs would be driven by independent unipotent differentiation events that occur at the single cell level. To test this prediction, we performed clonal lineage tracing in vivo. HBCs were labeled and stimulated to differentiate by induction of Cre recombinase activity with doses of tamoxifen adjusted to elicit sparse activation of HBCs in Krt5-CreER; Trp63lox/lox; Rosa26Confetti mice. Animals were sacrificed at 7 and 14 days after tamoxifen induction and expression of fluorescent protein reporters encoded by the Rosa26Confetti locus was assessed using an anti-GFP antibody. Representative examples of labeled clones are shown in Figure 3.4 A-D. Consistent with Slingshot's prediction that individual HBCs initially give rise to single lineages, at 14 days of differentiation 91 of 99 scored clones contain cells representing either the combined neuronal/microvillous cell lineage (80, comprising 13 GBCs, 57 neurons, 9 neurons + microvillous cells, and 1 microvillous cell) or sustentacular cells (10), but not cells from both lineages (Fig. 3.4 E). Clones containing a mixture of sustentacular cells and neurons comprise the remaining 9 clones. Labeled Bowman's glands were not detected among the 99 clones scored for this analysis. Similar results were obtained from clones scored at 7 days of differentiation (Fig. 3.5).

A second hypothesis based on our analysis with Slingshot is that sustentacular cells are formed through direct fate conversion from HBCs without cell division, whereas the neuronal lineage expands via proliferation of GBC and INP1 progenitors. Indeed, using our sparse lineage tracing strategy, we observed a marked disparity in the numbers of neurons and sustentacular cells per clone. At 14 days of differentiation, neuron-containing clones contained 13.5 +/- 1.0 neurons (mean +/- SEM) (Fig. 3.4 F), whereas sustentacular cells are present at one to two cells per clone (1.3 +/- 0.1 cells; Fig. 3.4 G). The average number of neurons per clone increases from 7 days (8.8 +/- 1.0 cells/clone) to 14 days, while the number of sustentacular cells per clone remains essentially unchanged over this interval (1.2 +/- 0.1 cells/clone at 7 days; compare Fig. 3.4 F, G to Fig. 3.5). Moreover, most sustentacular cell-containing clones contain only a single cell of this type, confirming the assignment of the first major branch point in the HBC-derived lineage to an early, non-proliferative transitional HBC stage. Complementing the predicted lineage trajectories, these observations provide strong evidence that HBCs differentiate directly into sustentacular cells in the absence of cell division. The presence of two sustentacular cells in a minority fraction of clones may reflect the proliferative capacity of the sustentacular cells themselves (Weiler and Farbman, 1998) and/or the occasional proliferation of resting HBCs (Fletcher et al., 2011) or transitional HBCs. Consistent with these possibilities, rare proliferating cells can be observed in both the HBC and late sustentacular cell stages (Fig. 3.3 D).

The third major prediction of our branching lineage assignment is that microvillous cells and olfactory sensory neurons arise from a common sub-lineage that branches at the GBC stage to

give rise to these two cell types. In support of this prediction, nine of ten clones containing microvillous cells also contain neurons (Fig. 3.4 E). Microvillous cells are rare in comparison to olfactory sensory neurons (Hansen and Finger, 2008; Jia et al., 2013; Ogura et al., 2011; Yamaguchi et al., 2014) (Fig. S3.1); this difference is reflected by the small number of microvillous cell-containing clones detected (13% of neuron-containing clones), as well as the low number of microvillous cells present in any given microvillous-containing clone (1.2 +/- 0.1; Fig. 3.4 H).

Discussion

In the present study, we developed an integrated approach using in silico modeling of single-cell RNA-seq data and in vivo clonal lineage tracing to illuminate the cell fate potentials of individual olfactory stem cells and the locations of branch points in the olfactory lineage trajectory. One sub-lineage gives rise to the niche's proliferative GBCs, which in turn generate olfactory sensory neurons and microvillous cells. The other sub-lineage generates sustentacular cells through a differentiation process characterized by fewer and more gradual transitions that occur in the absence of cell division. The differences in gene expression and cell state transitions in the neuronal and sustentacular cell lineages are likely the result of similarly divergent patterns of coordinated transcription factor expression in the respective lineages. Our approach enabled an analysis of the olfactory HBC stem cell's fate potential and the location of branch points in the lineage at a level of detail not possible by either in vivo lineage tracing or single-cell RNA-seq alone, and serves as a model for elucidating complex lineage trajectories in other stem cell niches.

Multipotency of HBCs at the Population Level Reflects Individual Unipotent Cell Fate Decisions

How do multiple cell types arise from the population of olfactory stem cells? We found that individual HBCs mostly generate clones of cells of a single cell type, with approximately 80% consisting of only cells in the GBC lineage and 10% containing only sustentacular cells (Fig. 3.4). These findings demonstrate a common thread with several other stem cell niches in which individual stem cells adopt singular cell fates that, in aggregate, underlie multipotency at the population level. For example, individual columnar basal cells in the intestine either differentiate or self-renew via symmetric cell divisions to maintain the tissue (Snippert et al., 2010b). The differentiation of HBCs predominantly into neurons is also reminiscent of the behavior of hippocampal stem cells, which usually produce clones exclusively containing neurons (Bonaguidi et al., 2011).

While the majority of individual HBCs appear to restrict their cell fate choices to a single lineage, about 10% of HBC-derived clones contain a single sustentacular cell amid a group of neurons. What can account for the apparent multipotency of individual HBCs in these cases?

One possibility is that GBCs can occasionally give rise to sustentacular cells in addition to neurons and microvillous cells. However, lineage-tracing of GBCs and their descendants using a GBC-specific Ascl1-CreER driver do not support this explanation, since we failed to detect any sustentacular cells out of ~1000 cells lineage-traced under steady state conditions. Alternatively, the occurrence of mixed neuronal/sustentacular cell clones in our analysis could reflect plasticity at the transitional HBC stage, such that a given activated stem cell returns to the resting state and undergoes a self-renewing cell division, leaving its two daughter stem cells free to adopt either cell fate independently. This interpretation dovetails with the suggestion that transitional HBCs are metastable based on their variable expression of Trp63, which plays a critical role in maintaining HBCs in the resting, self-renewing state (Fletcher et al., 2011). It is also possible that the multipotent clones reflect symmetric self-renewing HBC mitoses prior to differentiation. Indeed, we observed elevated expression of cell cycle-associated genes in the occasional resting and transitional HBC (Fig. 3.3), in agreement with our previous observation that about five percent of resting HBCs express the proliferative marker protein Ki67 (Fletcher et al., 2011). Whatever the case, our observations are consistent with the idea that certain cell fate decisions may in fact remain reversible during a limited period early in the trajectory.

Direct Conversion of HBC Stem Cells into Sustentacular Support Cells

Our analysis also reveals direct conversion of quiescent HBCs to sustentacular support cells without cell division, a novel mode of stem cell differentiation. In contrast, olfactory neurogenesis involves an expansion through proliferative GBC and INP intermediates. Thus, HBCs generate cells of the two diverging lineages using dramatically different strategies. Our analysis of gene expression at the single-cell level further indicates that the developmental distance traversed in the sustentacular cell lineage is shorter than the distance covered in the generation of olfactory sensory neurons (Fig. 3.3). In addition to expanding the number of cells in this lineage, proliferation of GBCs and INP1 cells may also activate transcriptional networks by inducing larger scale, cell cycle-associated chromatin remodeling (Ma et al., 2015).

Direct reprogramming of cells to replace damaged or diseased cells in a tissue has enormous therapeutic potential. Transdifferentiation, a process in which one differentiated cell type is converted into another, can be induced in a variety of cell types by expression of exogenous factors in vitro (Davis et al., 1987; Heinrich et al., 2010; Ieda et al., 2010; Vierbuchen et al., 2010; Xie et al., 2004) and in vivo (Banga et al., 2012; Liu et al., 2015; Niu et al., 2013; Qian et al., 2012; Zhou et al., 2008). While HBCs are not differentiated cells per se, unlike many other adult tissue stem cells they are not actively dividing, a characteristic that allowed us to disentangle fate determination of HBC daughter cells from cell division. Moreover, the initiation of HBC differentiation into mature cell types is triggered not by overexpression of a factor but rather by removing one (in this case, Trp63). That removing factors would be an effective strategy for reprogramming is also suggested by the conversion of fibroblasts to

cardiomyocyte-like cells by miRNA expression (Jayawardena et al., 2012) and pancreatic alpha cells to beta-like cells by inhibiting Arx (Courtney et al., 2013). Our findings provide an alternative way to view cell fate transformation in vivo and open up new avenues for inducing transdifferentiation of cells for therapeutic applications.

Conclusion

In this manuscript, we explored how HBCs differentiate into neurons and sustentacular cells following p63cKO using clonal lineage tracing and single-cell RNA-seq, creating a methodological framework for studying adult tissue stem cells more generally. Neurons are produced in large numbers via proliferative intermediate progenitors, entailing large, abrupt changes in gene expression and activation of transcription factor networks, while sustentacular cells develop directly from HBCs in the absence of cell division via a more gradual transcriptional changes. We are now harnessing our transcriptional data to identify novel markers of olfactory cell subtypes, particularly amongst the transitional HBCs, which likely harbor the bifurcation point of the neuronal and sustentacular lineages.

While injury-induced regeneration of the olfactory epithelium by the HBCs shares some features in common with differentiation induced via p63 cKO, regeneration requires that HBC self-renewal be balanced with robust differentiation, placing additional functional requirements on the divisions of activated HBCs. Analysis of spindle orientation and cell polarity in dividing HBCs suggests that population asymmetry may regulate rates of HBC symmetric and/or asymmetric division during regeneration (Chapter 2). In chapter 4, the immediate and long-term outcomes of such regenerative HBC divisions are explored using clonal analysis and single-cell RNA-seq.

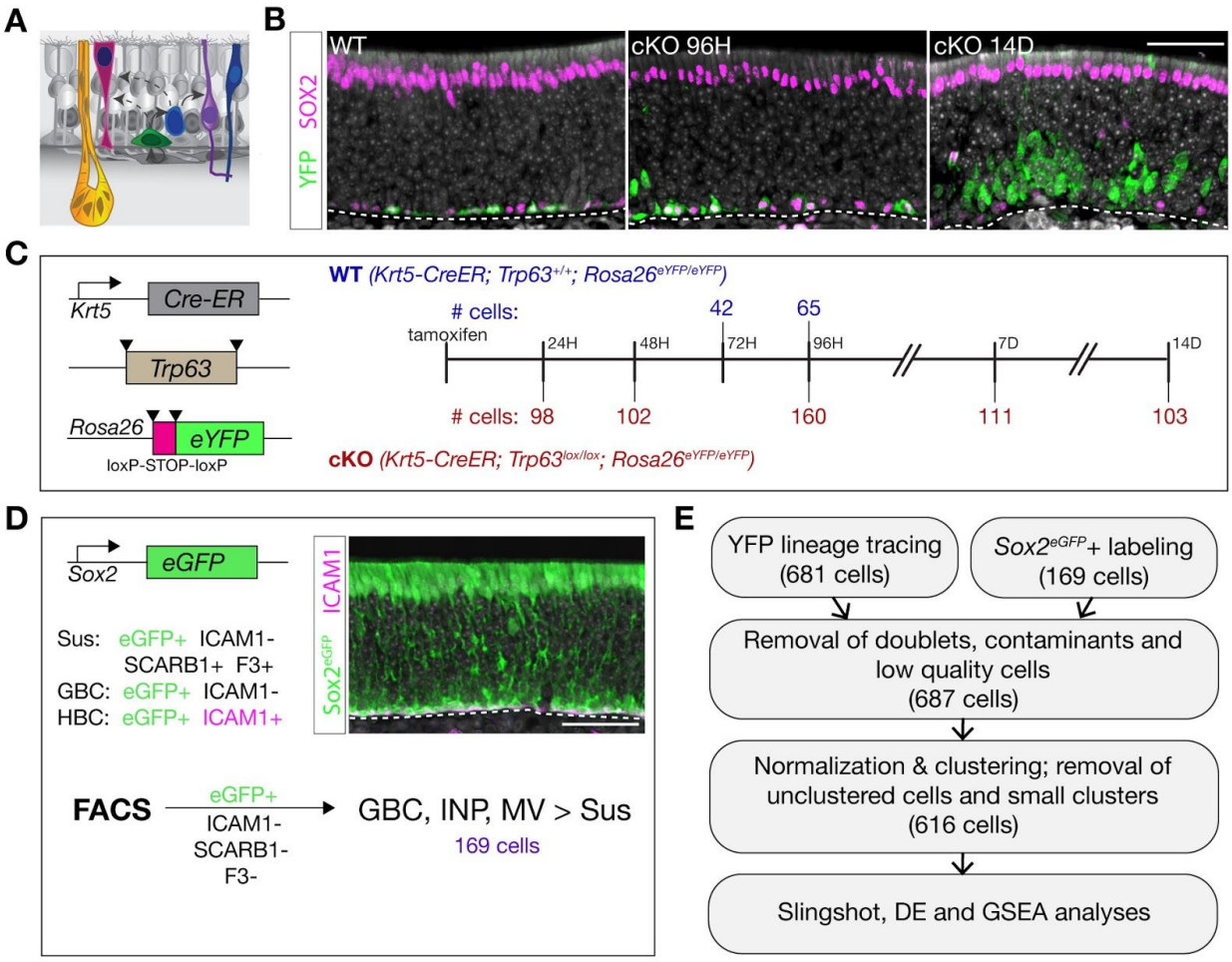

Figure 3.1 Experimental Strategy for Olfactory Stem Cell Lineage Analysis with Single-Cell RNA-Seq

(A) Schematic of the olfactory epithelium describing the constituent cells: horizontal basal cell (HBC, green), globose basal cell (GBC, blue), sustentacular cell (Sus, pink), olfactory sensory neuron (OSN, purple), microvillous cell (MV, dark blue), Bowman's gland (yellow). **(B)** Immunohistochemistry for the HBC lineage tracer YFP (green) and SOX2 (magenta) shows basal resting HBCs in the wild type (WT) background (left panel), and asynchronous differentiation following *Trp63* conditional knockout (cKO) (center, right). **(C)** YFP(+) cells were collected by FACS at the indicated times following tamoxifen administration from mice carrying the *Krt5-CreER; Rosa26*^{eYFP} transgenes and either the *Trp63*$^{+/+}$ (WT) or *Trp63*$^{lox/lox}$ (cKO) alleles. **(D)** Sox2-eGFP(+)/ICAM1(-)/SCARB1(-)/F3(-) cells were collected by FACS; this enriched for the GBC, INP, and MV fates over Sus cells. (E) Data from both experimental designs were combined, filtered, normalized, clustered, and used in downstream analyses. Scale-bars, 50 microns.

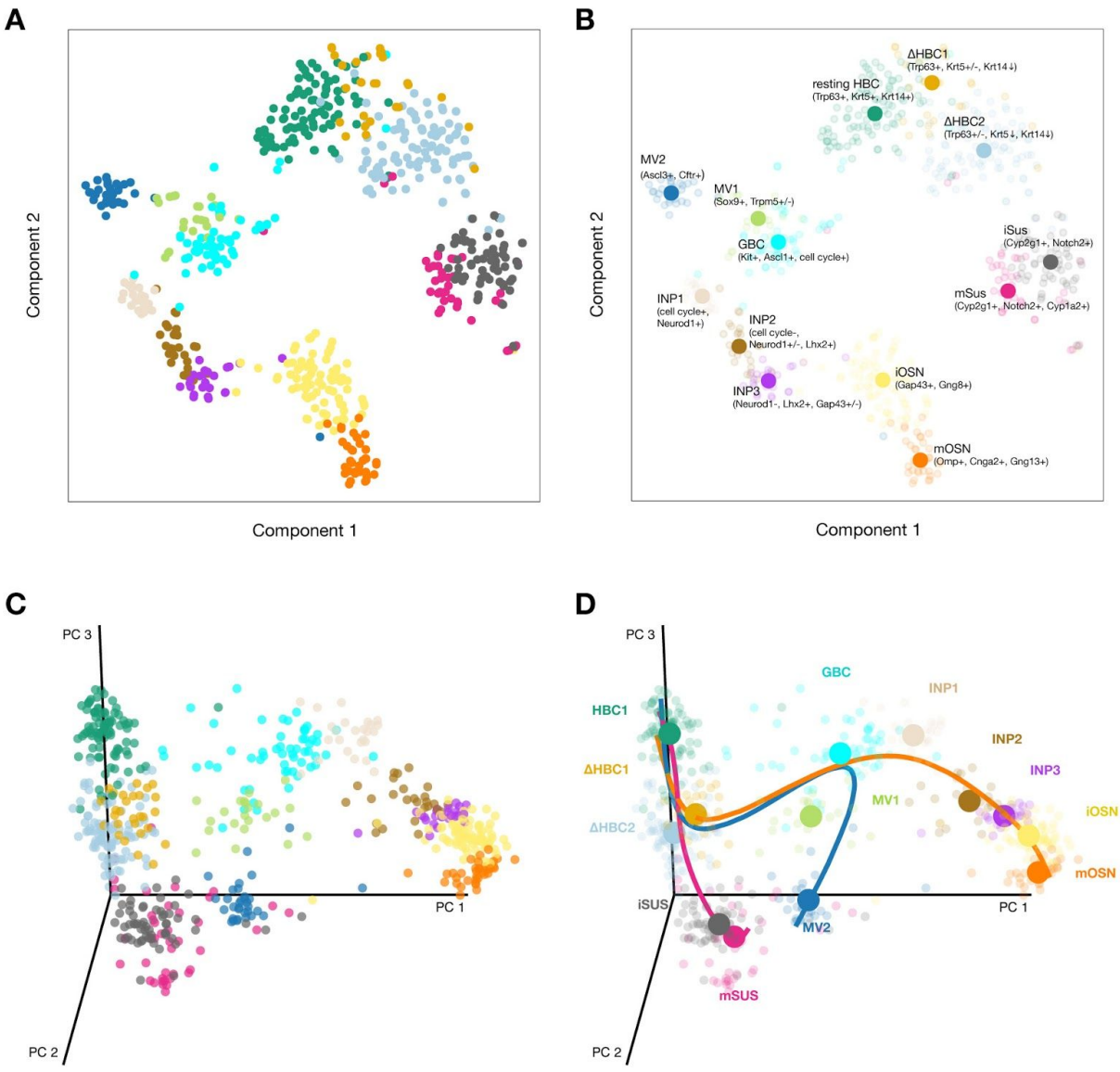

Figure 3.2 Statistical Modeling of Single-Cell RNA-Seq Data Predicts Distinct Cell States and Branch Points in the Olfactory Stem Cell Trajectory

(A, B) t-SNE plot based on the 500 most variable genes shows the separation of the cells into discrete groups congruent with the clustering. Cluster medoids are displayed as larger circles with initial assignments of cluster identity based on the expression of a small number of marker genes (B). **(C, D)** Projection of the cells according to the first three principal components of gene expression data; cells are colored by cluster. *Slingshot* predicts an early bifurcation in the lineage trajectories of the neuronal (orange) and sustentacular cell (magenta) lineages whereas the MV lineage (blue) is predicted to branch later off of the neuronal lineage from the GBCs (D).

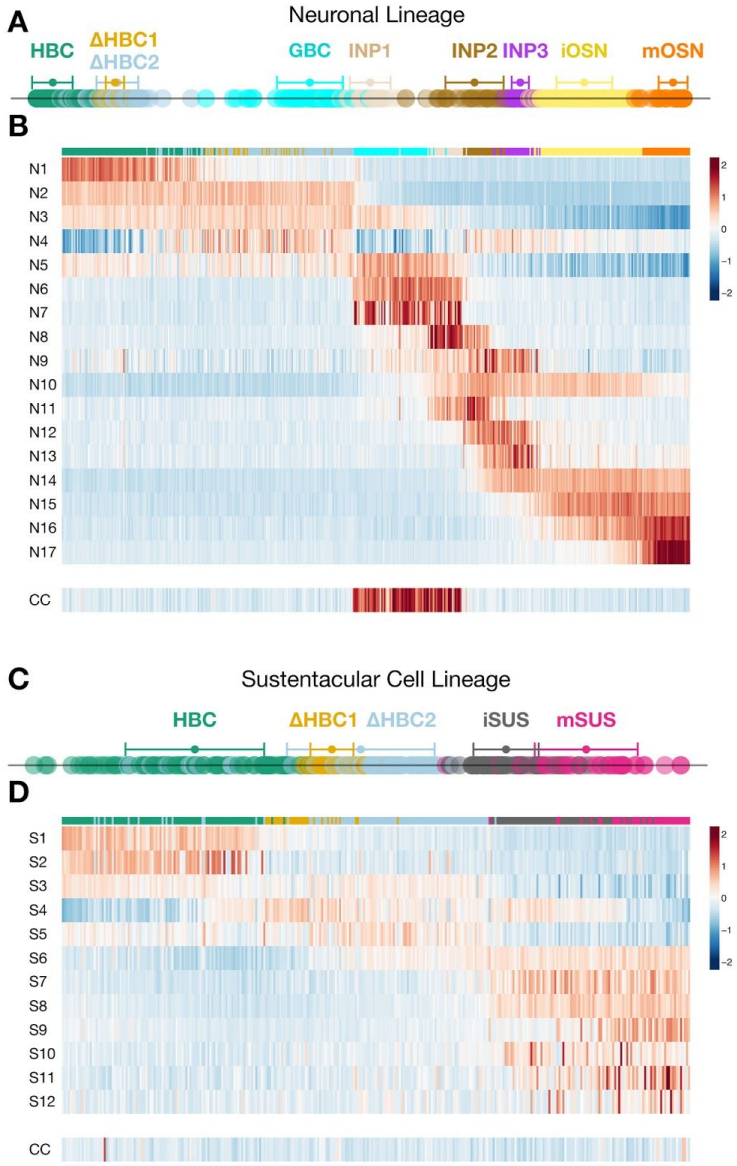

Figure 3.3 Patterns of Coordinated Gene Regulation in the Neuronal and Sustentacular Cell Lineages Reveal Different Strategies for Differentiation

(A, C) Developmental distance derived from the orthogonal projection of cells onto their respective lineage. Mean +/- standard deviation of each cluster position is indicated. (B, D) Heatmaps display the scaled, average expression for each gene cluster (numbered at the left of each row) with cells (columns) ordered in developmental time for the neuronal (B) and sustentacular cell (D) lineages. There are numerous step-like transitions in the neuronal lineage but fewer, wave-like changes in the sustentacular cell lineage. The lower row in each heatmap represents a set of 40 cell cycle (CC) genes.

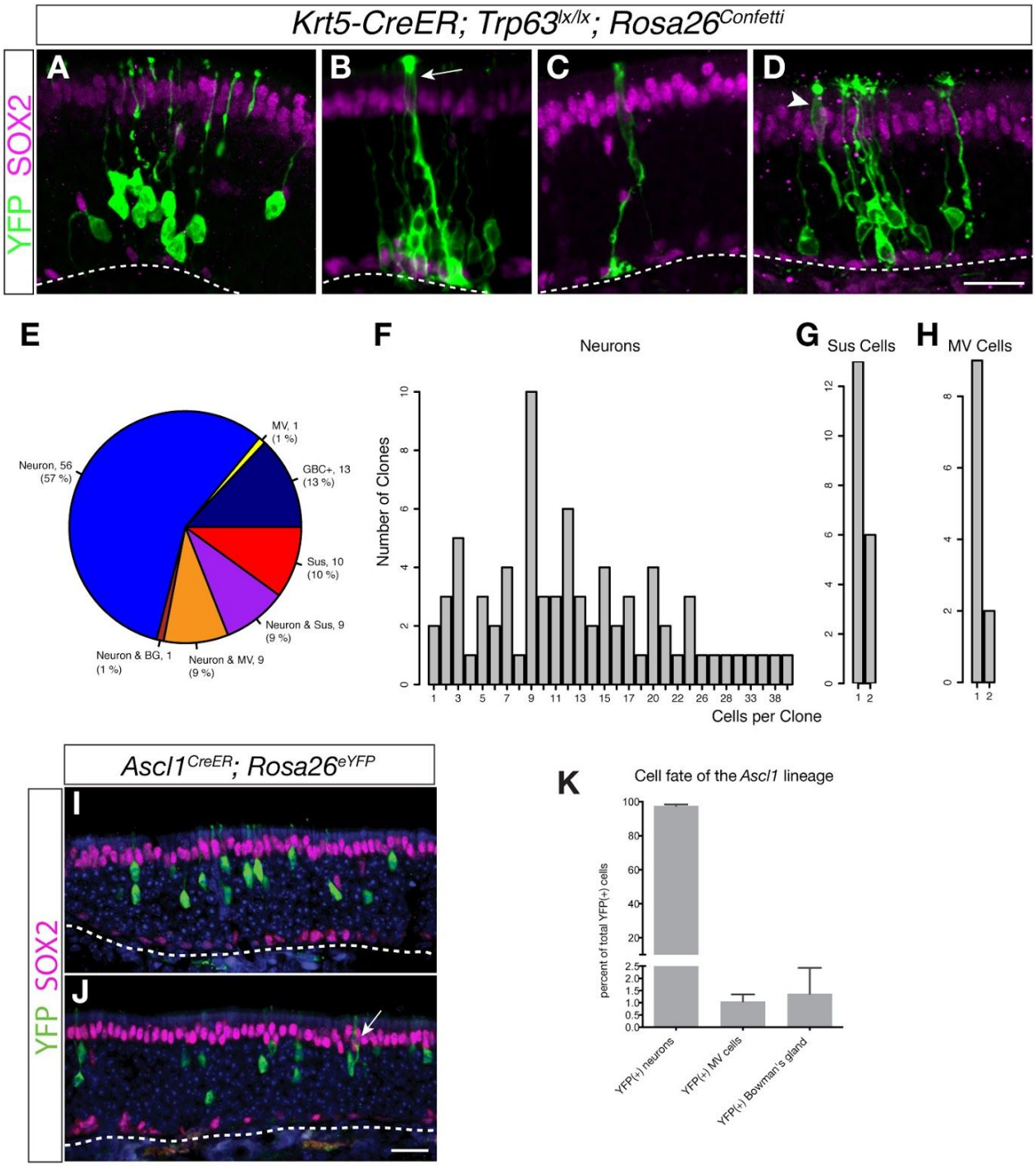

Figure 3.4 Clonal Lineage Tracing In Vivo Validates Branching Lineage Assignment Predictions

(A-D) Example images of clones from *Krt5-CreER; Trp63$^{lox/lox}$; Rosa26^{Confetti}* transgenic animals analyzed 14 days following tamoxifen induction of the CreER driver: neuronal only **(A)**, neuronal and sustentacular **(B)**, sustentacular cell only **(C)**, and neuronal and microvillous cell

(D). **(E)** Most clones represent unipotent differentiation events, supporting the prediction that the lineages bifurcate early: the majority of clones contain only cells in the neuronal lineage, and just over half of all sustentacular cell-containing clones are composed of only sustentacular cells. Almost all microvillous cells are found together with neurons. **(F, G, H)** Clone size distribution. The number of neurons in neuron-containing clones **(F)** is larger, validating that the neuronal lineage contains amplification stages whereas the sustentacular cells are usually present as single cells **(G)**. Microvillous cells are usually found as singlets and typically are found in clones together with neurons. **(I, J, K)** *Ascl1-CreER; Rosa26*^{eYFP} lineage tracing at 21 days following tamoxifen induction shows that although Ascl1-positive GBCs usually form neurons (~ 98%) (I), they occasionally form microvillous cells **(J)**. The percentage of each cell-type formed from lineage-traced cells (three animals and 1072 cells) is summarized in **(K)**. Scale bar, 25 microns. See Figure 3.5.

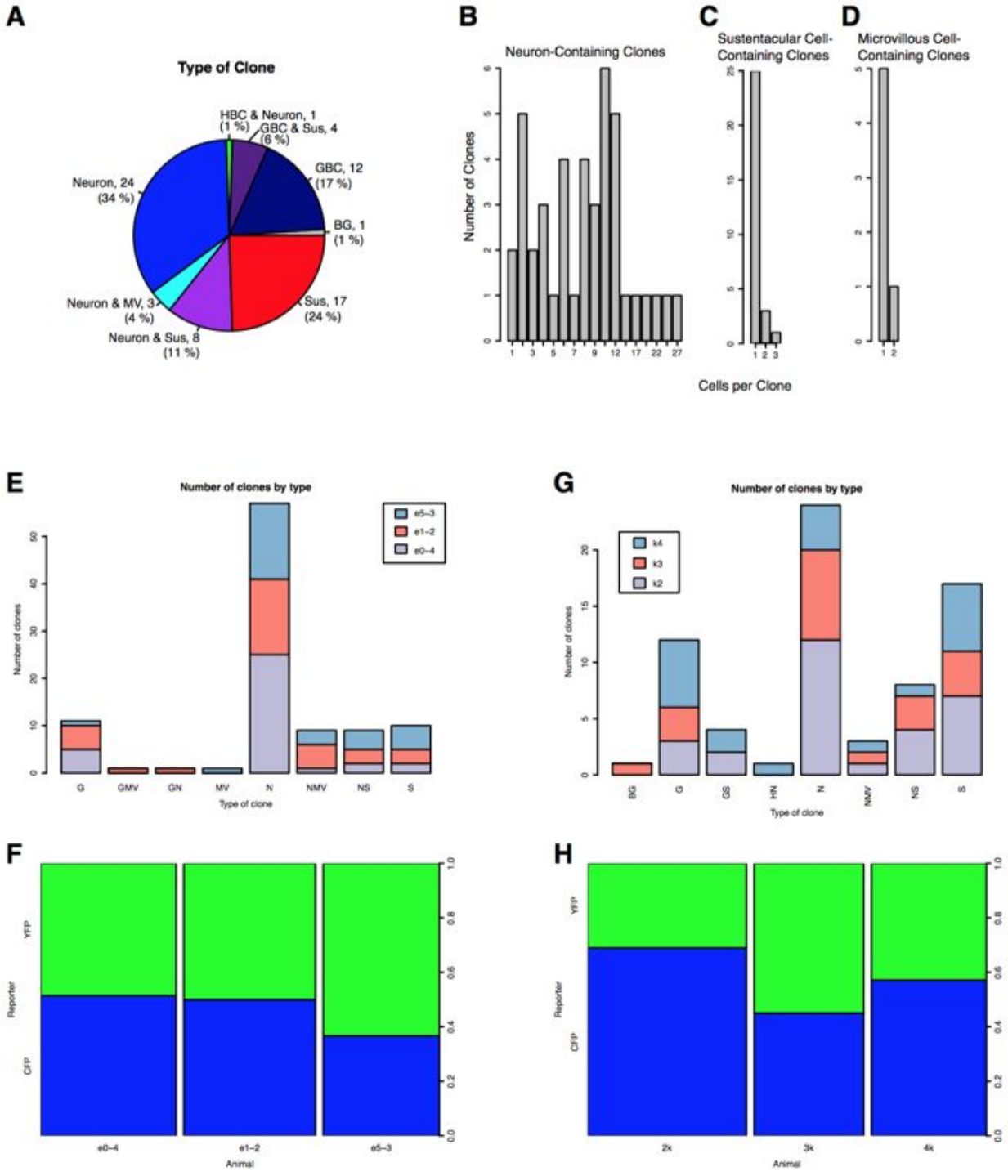

Figure 3.5 Clonal analysis at 7 dpt, and 14 dpt and 7 dpt clone parameters

(A-D) *Krt5-CreER*; *Trp63*$^{lox/lox}$*; Rosa26*^{Confetti} clonal lineage tracing analysis at 7 days post tamoxifen. A summary of the types of clones obtained is presented in (A). Neuron-containing clones nearly always contain more than one neuron (mean = 8.76 +/- 0.96 SEM) whereas sustentacular cells (C) and microvillous cells (D) are almost always limited to one cell of that

type per clone (1.17 +/- 0.09, 1.17 +/- 0.17, respectively). Note that the GBC category in (A) represents all GBC-containing clones that had any type of cell from the neuronal lineage, such as a neuron or microvillous cell. (E-H) Plots relating to the 14 dpt (E,F) or 7 dpt (G,H) clonal lineage tracing. (E, G) The number of clones of each type from each animal in the analysis. (F, H) The proportion of clones that were membrane CFP or cytosolic YFP for each animal. No single animal skewed the results.

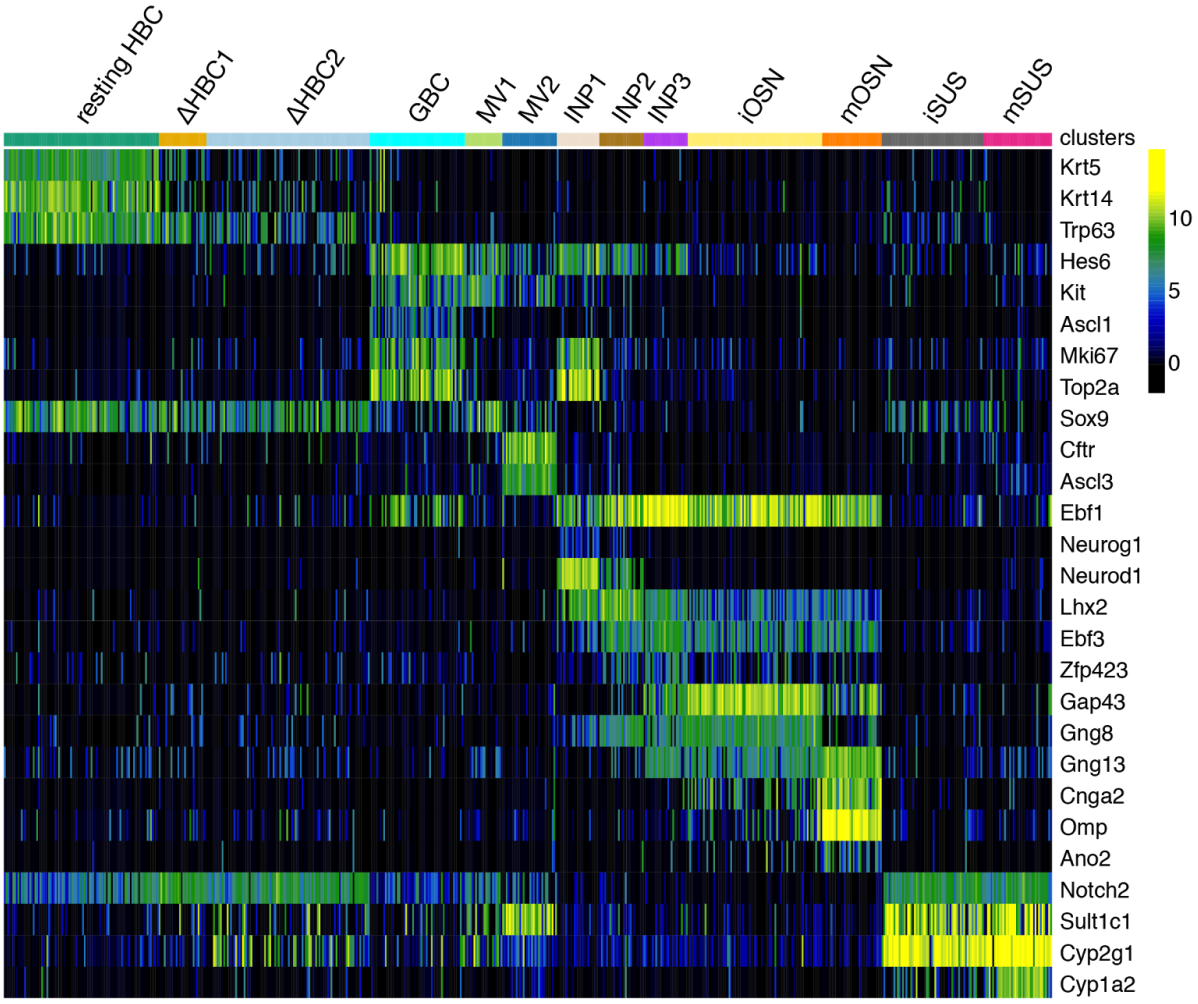

Supplemental Figure 3.1 Heatmap of marker gene expression by cluster

Gene expression, of a curated cohort of OE-specific genes, by cell-type cluster in the p63cKO. ΔHBC1 and ΔHBC2 are transitional HBCs. Microvillus cells (MV1 and MV2), immature neuronal precursors (INP1, INP2, INP3) are separated into sub-clusters. Neurons and sustentacular cells are sub-clustered by immature precursors (iOSN and iSUS) and mature cells (mOSN and mSUS).

References

Arnold, K., Sarkar, A., Yram, M.A., Polo, J.M., Bronson, R., Sengupta, S., Seandel, M., Geijsen, N., and Hochedlinger, K. (2011). Adult Stem and Progenitor Cells Are Important for Tissue Regeneration and Survival of Mice. Stem Cell *9*, 317–329.

Banga, A., Akinci, E., Greder, L.V., Dutton, J.R., and Slack, J.M.W. (2012). In vivo reprogramming of Sox9+ cells in the liver to insulin-secreting ducts. Proceedings of the National Academy of Sciences *109*, 15336–15341.

Bałakier, H., and Pedersen, R.A. (1982). Allocation of cells to inner cell mass and trophectoderm lineages in preimplantation mouse embryos. Developmental Biology *90*, 352–362.

Bendall, S.C., Davis, K.L., Amir, E.-A.D., Tadmor, M.D., Simonds, E.F., Chen, T.J., Shenfeld, D.K., Nolan, G.P., and Pe'er, D. (2014). Single-cell trajectory detection uncovers progression and regulatory coordination in human B cell development. Cell *157*, 714–725.

Bonaguidi, M.A., Wheeler, M.A., Shapiro, J.S., Stadel, R.P., Sun, G.J., Ming, G.-L., and Song, H. (2011). In Vivo Clonal Analysis Reveals Self-Renewing and Multipotent Adult Neural Stem Cell Characteristics. Cell *145*, 1142–1155.

Brault, V., Moore, R., Kutsch, S., Ishibashi, M., Rowitch, D.H., McMahon, A.P., Sommer, L., Boussadia, O., and Kemler, R. (2001). Inactivation of the beta-catenin gene by Wnt1-Cre-mediated deletion results in dramatic brain malformation and failure of craniofacial development. Development *128*, 1253–1264.

Burd, G.D. (1993). Morphological study of the effects of intranasal zinc sulfate irrigation on the mouse olfactory epithelium and olfactory bulb. Microsc. Res. Tech. *24*, 195–213.

Caggiano, M., Kauer, J.S., and Hunter, D.D. (1994). Globose basal cells are neuronal progenitors in the olfactory epithelium: a lineage analysis using a replication-incompetent retrovirus. Neuron *13*, 339–352.

Campbell, K., Ponting, C.P., and Webber, C. (2015). Laplacian eigenmaps and principal curves for high resolution pseudotemporal ordering of single-cell RNA-seq profiles.

Carter, L.A., MacDonald, J.L., and Roskams, A.J. (2004). Olfactory Horizontal Basal Cells Demonstrate a Conserved Multipotent Progenitor Phenotype. Journal of Neuroscience *24*, 5670–5683.

Chen, M., Tian, S., Yang, X., Lane, A.P., Reed, R.R., and Liu, H. (2014). Wnt-responsive lgr5+ globose Basal cells function as multipotent olfactory epithelium progenitor cells. J Neurosci *34*, 8268–8276.

Chen, X., Fang, H., and Schwob, J.E. (2004). Multipotency of purified, transplanted globose basal cells in olfactory epithelium. J. Comp. Neurol. *469*, 457–474.

Choi, Y.S., Zhang, Y., Xu, M., Yang, Y., Ito, M., Peng, T., Cui, Z., Nagy, A., Hadjantonakis, A.-K., Lang, R.A., et al. (2013). Distinct functions for Wnt/β-catenin in hair follicle stem cell proliferation and survival and interfollicular epidermal homeostasis. Cell Stem Cell *13*, 720–733.

Clayton, E., DoupE, D.P., Klein, A.M., Winton, D.J., Simons, B.D., and Jones, P.H. (2007). A single type of progenitor cell maintains normal epidermis. Nature *446*, 185–189.

Clevers, H., Loh, K.M., and Nusse, R. (2014). An integral program for tissue renewal and regeneration: Wnt signaling and stem cell control. Science *346*, 1248012–1248012.

Courtney, M., Gjernes, E., Druelle, N., Ravaud, C., Vieira, A., Ben-Othman, N., Pfeifer, A., Avolio, F., Leuckx, G., Lacas-Gervais, S., et al. (2013). The inactivation of Arx in pancreatic α-cells triggers their neogenesis and conversion into functional β-like cells. PLoS Genet *9*, e1003934.

Davis, R.L., Weintraub, H., and Lassar, A.B. (1987). Expression of a single transfected cDNA converts fibroblasts to myoblasts. Cell *51*, 987–1000.

Deng, Q., Ramskold, D., Reinius, B., and Sandberg, R. (2013). Single-Cell RNA-Seq Reveals Dynamic, Random Monoallelic Gene Expression in Mammalian Cells. Science.

Duggan, C.D., DeMaria, S., Baudhuin, A., Stafford, D., and Ngai, J. (2008). Foxg1 Is Required for Development of the Vertebrate Olfactory System. Journal of Neuroscience *28*, 5229–5239.

Eckert, R.L., Adhikary, G., Young, C.A., Jans, R., Crish, J.F., Xu, W., and Rorke, E.A. (2013). AP1 transcription factors in epidermal differentiation and skin cancer. J Skin Cancer *2013*, 537028–537029.

Fletcher, R.B., Prasol, M.S., Estrada, J., Baudhuin, A., Vranizan, K., Choi, Y.G., and Ngai, J. (2011). p63 regulates olfactory stem cell self-renewal and differentiation. Neuron *72*, 748–759.

Goldstein, B.J., Goss, G.M., Hatzistergos, K.E., Rangel, E.B., Seidler, B., Saur, D., and Hare, J.M. (2014). Adult c-Kit(+) progenitor cells are necessary for maintenance and regeneration of olfactory neurons. J. Comp. Neurol. *523*, 15–31.

Graziadei, G.A., and Graziadei, P.P. (1979a). Neurogenesis and neuron regeneration in the olfactory system of mammals. II. Degeneration and reconstitution of the olfactory sensory neurons after axotomy. J. Neurocytol. *8*, 197–213.

Graziadei, P.P., and Graziadei, G.A. (1979b). Neurogenesis and neuron regeneration in the olfactory system of mammals. I. Morphological aspects of differentiation and structural organization of the olfactory sensory neurons. J. Neurocytol. *8*, 1–18.

Grün, D., Muraro, M.J., Boisset, J.-C., Wiebrands, K., Lyubimova, A., Dharmadhikari, G., van den Born, M., van Es, J., Jansen, E., Clevers, H., et al. (2016). De Novo Prediction of Stem Cell Identity using Single-Cell Transcriptome Data. Cell Stem Cell 1–39.

Gu, J., Zhang, Q.Y., Genter, M.B., Lipinskas, T.W., Negishi, M., Nebert, D.W., and Ding, X. (1998). Purification and characterization of heterologously expressed mouse CYP2A5 and CYP2G1: role in metabolic activation of acetaminophen and 2,6-dichlorobenzonitrile in mouse olfactory mucosal microsomes. J. Pharmacol. Exp. Ther. *285*, 1287–1295.

Guo, Z., Packard, A., Krolewski, R.C., Harris, M.T., Manglapus, G.L., and Schwob, J.E. (2010). Expression of Pax6 and Sox2 in adult olfactory epithelium. J. Comp. Neurol. *518*, 4395–4418.

Haghverdi, L., Buettner, F., and Theis, F.J. (2015). Diffusion maps for high-dimensional single-cell analysis of differentiation data. Bioinformatics *31*, 2989–2998.

Hanchate, N.K., Kondoh, K., Lu, Z., Kuang, D., Ye, X., Qiu, X., Pachter, L., Trapnell, C., and Buck, L.B. (2015). Single-cell transcriptomics reveals receptor transformations during olfactory neurogenesis. Science 1–8.

Hansen, A., and Finger, T.E. (2008). Is TrpM5 a reliable marker for chemosensory cells? Multiple types of microvillous cells in the main olfactory epithelium of mice. BMC Neurosci *9*, 115.

Harada, N., Tamai, Y., Ishikawa, T., Sauer, B., Takaku, K., Oshima, M., and Taketo, M.M. (1999). Intestinal polyposis in mice with a dominant stable mutation of the beta-catenin gene. Embo J. *18*, 5931–5942.

Heinrich, C., Blum, R., Gascón, S., Masserdotti, G., Tripathi, P., Sánchez, R., Tiedt, S., Schroeder, T., Götz, M., and Berninger, B. (2010). Directing astroglia from the cerebral cortex into subtype specific functional neurons. PLoS Biol *8*, e1000373.

Hirota, J., and Mombaerts, P. (2004). The LIM-homeodomain protein Lhx2 is required for complete development of mouse olfactory sensory neurons. Pnas *101*, 8751–8755.

Holbrook, E.H., Szumowski, K.E., and Schwob, J.E. (1995). An immunochemical, ultrastructural, and developmental characterization of the horizontal basal cells of rat olfactory epithelium. J. Comp. Neurol. *363*, 129–146.

Huang, L., Shanker, Y.G., Dubauskaite, J., Zheng, J.Z., Yan, W., Rosenzweig, S., Spielman, A.I., Max, M., and Margolskee, R.F. (1999). Ggamma13 colocalizes with gustducin in taste receptor cells and mediates IP3 responses to bitter denatonium. Nat Neurosci *2*, 1055–1062.

Ieda, M., Fu, J.-D., Delgado-Olguin, P., Vedantham, V., Hayashi, Y., Bruneau, B.G., and Srivastava, D. (2010). Direct reprogramming of fibroblasts into functional cardiomyocytes by defined factors. Cell *142*, 375–386.

Indra, A.K., Warot, X., Brocard, J., Bornert, J.M., Xiao, J.H., Chambon, P., and Metzger, D. (1999). Temporally-controlled site-specific mutagenesis in the basal layer of the epidermis: comparison of the recombinase activity of the tamoxifen-inducible Cre-ER(T) and Cre-ER(T2) recombinases. Nucleic Acids Res. *27*, 4324–4327.

Iwai, N., Zhou, Z., Roop, D.R., and Behringer, R.R. (2008). Horizontal Basal Cells Are Multipotent Progenitors in Normal and Injured Adult Olfactory Epithelium. Stem Cells *26*, 1298–1306.

Jayawardena, T.M., Egemnazarov, B., Finch, E.A., Zhang, L., Payne, J.A., Pandya, K., Zhang, Z., Rosenberg, P., Mirotsou, M., and Dzau, V.J. (2012). MicroRNA-mediated in vitro and in vivo direct reprogramming of cardiac fibroblasts to cardiomyocytes. Circ. Res. *110*, 1465–1473.

Jia, C., Hayoz, S., Hutch, C.R., Iqbal, T.R., Pooley, A.E., and Hegg, C.C. (2013). An IP3R3- and NPY-Expressing Microvillous Cell Mediates Tissue Homeostasis and Regeneration in the Mouse Olfactory Epithelium. PLoS ONE *8*, e58668.

Karin, M., Liu, Z.G., and Zandi, E. (1997). AP-1 function and regulation. Current Opinion in Cell Biology *9*, 240–246.

Kawano, Y., and Kypta, R. (2003). Secreted antagonists of the Wnt signalling pathway. Journal of Cell Science *116*, 2627–2634.

Keller, A., and Margolis, F.L. (1975). Immunological studies of the rat olfactory marker protein. Journal of Neurochemistry *24*, 1101–1106.

Kim, E.J., Ables, J.L., Dickel, L.K., Eisch, A.J., and Johnson, J.E. (2011). Ascl1 (Mash1) Defines Cells with Long-Term Neurogenic Potential in Subgranular and Subventricular Zones in Adult Mouse Brain. PLoS ONE *6*, e18472–e18476.

Kimmel, C.B., and Law, R.D. (1985). Cell lineage of zebrafish blastomeres. III. Clonal analyses of the blastula and gastrula stages. Developmental Biology *108*, 94–101.

Kolterud, A., Alenius, M., Carlsson, L., and Bohm, S. (2004). The Lim homeobox gene Lhx2 is required for olfactory sensory neuron identity. Development *131*, 5319–5326.

Kowalczyk, M.S., Tirosh, I., Heckl, D., Rao, T.N., Dixit, A., Haas, B.J., Schneider, R.K., Wagers, A.J., Ebert, B.L., and Regev, A. (2015). Single-cell RNA-seq reveals changes in cell cycle and differentiation programs upon aging of hematopoietic stem cells. Genome Research *25*, 1860–1872.

Leung, C.T., Coulombe, P.A., and Reed, R.R. (2007). Contribution of olfactory neural stem cells to tissue maintenance and regeneration. Nat Neurosci *10*, 720–726.

Lien, W.-H., Polak, L., Lin, M., Lay, K., Zheng, D., and Fuchs, E. (2014). In vivo transcriptional governance of hair follicle stem cells by canonical Wnt regulators. Nat Cell Biol *16*, 179–190.

Liu, Y., Miao, Q., Yuan, J., Han, S., Zhang, P., Li, S., Rao, Z., Zhao, W., Ye, Q., Geng, J., et al. (2015). Ascl1 Converts Dorsal Midbrain Astrocytes into Functional Neurons In Vivo. J Neurosci *35*, 9336–9355.

Llorens-Bobadilla, E., Zhao, S., Baser, A., Saiz-Castro, G., Zwadlo, K., and Martin-Villalba, A. (2015). Single-Cell Transcriptomics Reveals a Population of Dormant Neural Stem Cells that Become Activated upon Brain Injury. Cell Stem Cell *17*, 329–340.

Ma, Y., Kanakousaki, K., and Buttitta, L. (2015). How the cell cycle impacts chromatin architecture and influences cell fate. Front. Genet. *6*, 19.

Mackay-Sim, A., and Kittel, P. (1991). Cell dynamics in the adult mouse olfactory epithelium: a quantitative autoradiographic study. J Neurosci *11*, 979–984.

Manglapus, G.L., Youngentob, S.L., and Schwob, J.E. (2004). Expression patterns of basic helix-loop-helix transcription factors define subsets of olfactory progenitor cells. J. Comp. Neurol. *479*, 216–233.

Matulionis, D.H. (1975). Ultrastructural study of mouse olfactory epithelium following destruction by ZnSO4 and its subsequent regeneration. Am. J. Anat. *142*, 67–89.

Matulionis, D.H. (1976). Light and electron microscopic study of the degeneration and early regeneration of olfactory epithelium in the mouse. Am. J. Anat. *145*, 79–99.

Mills, A.A., Qi, Y., and Bradley, A. (2002). Conditional inactivation of p63 by Cre-mediated excision. Genesis *32*, 138–141.

Moody, S.A. (1987). Fates of the blastomeres of the 16-cell stage Xenopus embryo. Developmental Biology *119*, 560–578.

Niu, W., Zang, T., Zou, Y., Fang, S., Smith, D.K., Bachoo, R., and Zhang, C.-L. (2013). In vivo reprogramming of astrocytes to neuroblasts in the adult brain. Nat Cell Biol *15*, 1164–1175.

Ogura, T., Szebenyi, S.A., Krosnowski, K., Sathyanesan, A., Jackson, J., and Lin, W. (2011). Cholinergic microvillous cells in the mouse main olfactory epithelium and effect of acetylcholine on olfactory sensory neurons and supporting cells. Journal of Neurophysiology *106*, 1274–1287.

Olsson, A., Venkatasubramanian, M., Chaudhri, V.K., Aronow, B.J., Salomonis, N., Singh, H., and Grimes, H.L. (2016). Single-cell analysis of mixed-lineage states leading to a binary cell fate choice. Nature 1–22.

Packard, A., Schnittke, N., Romano, R.A., Sinha, S., and Schwob, J.E. (2011a). Np63 Regulates Stem Cell Dynamics in the Mammalian Olfactory Epithelium. J Neurosci *31*, 8748–8759.

Packard, A., Giel-Moloney, M., Leiter, A., and Schwob, J.E. (2011b). The progenitor cell capacity of NeuroD1-expressing globose basal cells in the mouse olfactory epithelium. J. Comp. Neurol.

Petropoulos, S., Edsgärd, D., Reinius, B., Deng, Q., Panula, S.P., Codeluppi, S., Plaza Reyes, A., Linnarsson, S., Sandberg, R., and Lanner, F. (2016). Single-Cell RNA-Seq Reveals Lineage and X Chromosome Dynamics in Human Preimplantation Embryos. Cell *165*, 1012–1026.

Pfister, S., Weber, T., Härtig, W., Schwerdel, C., Elsaesser, R., Knuesel, I., and Fritschy, J.-M. (2015). Novel role of cystic fibrosis transmembrane conductance regulator in maintaining adult mouse olfactory neuronal homeostasis. J. Comp. Neurol. *523*, 406–430.

Pollen, A.A., Nowakowski, T.J., Chen, J., Retallack, H., Sandoval-Espinosa, C., Nicholas, C.R., Shuga, J., Liu, S.J., Oldham, M.C., Diaz, A., et al. (2015). Molecular Identity of Human Outer Radial Glia during Cortical Development. Cell *163*, 55–67.

Pollen, A.A., Nowakowski, T.J., Shuga, J., Wang, X., Leyrat, A.A., Lui, J.H., Li, N., Szpankowski, L., Fowler, B., Chen, P., et al. (2014). Low-coverage single-cell mRNA sequencing reveals cellular heterogeneity and activated signaling pathways in developing cerebral cortex. Nature Biotechnology.

Price, J., Turner, D., and Cepko, C. (1987). the vertebrate nervous system. Pnas *84*, 156–160.

Qian, L., Huang, Y., Spencer, C.I., Foley, A., Vedantham, V., Liu, L., Conway, S.J., Fu, J.-D., and Srivastava, D. (2012). In vivo reprogramming of murine cardiac fibroblasts into induced cardiomyocytes. Nature *485*, 593–598.

Ritchie, M.E., Phipson, B., Wu, D., Hu, Y., Law, C.W., Shi, W., and Smyth, G.K. (2015). limma powers differential expression analyses for RNA-sequencing and microarray studies. Nucleic Acids Res. *43*, e47–e47.

Saraiva, L.R., Ibarra-Soria, X., Khan, M., Omura, M., Scialdone, A., Mombaerts, P., Marioni, J.C., and Logan, D.W. (2015). Hierarchical deconstruction of mouse olfactory sensory neurons: from whole mucosa to single-cell RNA-seq. Nature Publishing Group 1–17.

Sautter, A., Zong, X., Hofmann, F., and Biel, M. (1998). An isoform of the rod photoreceptor cyclic nucleotide-gated channel beta subunit expressed in olfactory neurons. Pnas *95*, 4696–4701.

Schnittke, N., Herrick, D.B., Lin, B., Peterson, J., Coleman, J.H., Packard, A.I., Jang, W., and Schwob, J.E. (2015). Transcription factor p63 controls the reserve status but not the stemness of horizontal basal cells in the olfactory epithelium. Proceedings of the National Academy of Sciences *112*, E5068–E5077.

Scholz, P., Kalbe, B., Jansen, F., Altmueller, J., Becker, C., Mohrhardt, J., Schreiner, B., Gisselmann, G., Hatt, H., and Osterloh, S. (2016). Transcriptome Analysis of Murine Olfactory Sensory Neurons during Development Using Single Cell RNA-Seq. Chem. Senses.

Schultz, E.W. (1960). Repair of the Olfactory Mucosa with Special Reference to Regeneration of Olfactory Cells (Sensory Neurons). Am. J. Pathol. *37*, 1–19.

Schwob, J.E., Huard, J.M., Luskin, M.B., and Youngentob, S.L. (1994). Retroviral lineage studies of the rat olfactory epithelium. Chemical Senses *19*, 671–682.

Schwob, J.E., Youngentob, S.L., and Mezza, R.C. (1995). Reconstitution of the rat olfactory epithelium after methyl bromide-induced lesion. J. Comp. Neurol. *359*, 15–37.

Setty, M., Tadmor, M.D., Reich-Zeliger, S., Angel, O., Salame, T.M., Kathail, P., Choi, K., Bendall, S., Friedman, N., and Pe'er, D. (2016). Wishbone identifies bifurcating developmental trajectories from single-cell data. Nature Biotechnology *34*, 637–645.

Shalek, A.K., Satija, R., Shuga, J., Trombetta, J.J., Gennert, D., Lu, D., Chen, P., Gertner, R.S., Gaublomme, J.T., Yosef, N., et al. (2014). Single-cell RNA-seq reveals dynamic paracrine control of cellular variation. Nature.

Shin, J., Berg, D.A., Zhu, Y., Shin, J.Y., Song, J., Bonaguidi, M.A., Enikolopov, G., Nauen, D.W., Christian, K.M., Ming, G.-L., et al. (2015). Single-Cell RNA-Seq with Waterfall Reveals Molecular Cascades underlying Adult Neurogenesis. Cell Stem Cell *17*, 360–372.

Smyth, G.K. (2004). Linear models and empirical bayes methods for assessing differential expression in microarray experiments. Stat Appl Genet Mol Biol *3*, Article3–Article25.

Snippert, H.J., van der Flier, L.G., Sato, T., van Es, J.H., van den Born, M., Kroon-Veenboer, C., Barker, N., Klein, A.M., van Rheenen, J., Simons, B.D., et al. (2010a). Intestinal Crypt Homeostasis Results from Neutral Competition between Symmetrically Dividing Lgr5 Stem Cells. Cell *143*, 134–144.

Snippert, H.J., van der Flier, L.G., Sato, T., van Es, J.H., van den Born, M., Kroon-Veenboer, C., Barker, N., Klein, A.M., van Rheenen, J., Simons, B.D., et al. (2010b). Intestinal Crypt Homeostasis Results from Neutral Competition between Symmetrically Dividing Lgr5 Stem Cells. Cell *143*, 134–144.

Spemann, H., and Mangold, H. (1924). Uber induktion von Embyonalagen durch Implantation Artfremder Organisatoren. Roux Arch. Entw. Mech. 599–638.

Srinivas, S., Watanabe, T., Lin, C.S., William, C.M., Tanabe, Y., Jessell, T.M., and Costantini, F. (2001). Cre reporter strains produced by targeted insertion of EYFP and ECFP into the ROSA26 locus. BMC Dev Biol *1*, 4.

Street, K., Purdom, E., Dudoit, S., and Risso, D. (2016). Slingshot: a robust method for predicting cell lineage trajectories, *in preparation*.

Sun, J., Ramos, A., Chapman, B., Johnnidis, J.B., Le, L., Ho, Y.-J., Klein, A., Hofmann, O., and Camargo, F.D. (2014). Clonal dynamics of native haematopoiesis. Nature *514*, 322–327.

Suzuki, Y., and Takeda, M. (1991). Keratins in the developing olfactory epithelia. Brain Res. Dev. Brain Res. *59*, 171–178.

Tan, L., Li, Q., and Xie, X.S. (2015). Olfactory sensory neurons transiently express multiple olfactory receptors during development. Molecular Systems Biology *11*, 844–844.

Tirindelli, R., and Ryba, N.J. (1996). The G-protein gamma-subunit G gamma 8 is expressed in the developing axons of olfactory and vomeronasal neurons. Eur. J. Neurosci. *8*, 2388–2398.

Trapnell, C., Cacchiarelli, D., Grimsby, J., Pokharel, P., Li, S., Morse, M., Lennon, N.J., Livak, K.J., Mikkelsen, T.S., and Rinn, J.L. (2014). The dynamics and regulators of cell fate decisions are revealed by pseudotemporal ordering of single cells. Nature Biotechnology *32*, 381–386.

Treutlein, B., Brownfield, D.G., Wu, A.R., Neff, N.F., Mantalas, G.L., Espinoza, F.H., Desai, T.J., Krasnow, M.A., and Quake, S.R. (2014). Reconstructing lineage hierarchies of the distal lung epithelium using single-cell RNA-seq. Nature 1–16.

Treutlein, B., Lee, Q.Y., Camp, J.G., Mall, M., Koh, W., Shariati, S.A.M., Sim, S., Neff, N.F., Skotheim, J.M., Wernig, M., et al. (2016). Dissecting direct reprogramming from fibroblast to neuron using single-cell RNA-seq. Nature 1–15.

Usoskin, D., Furlan, A., Islam, S., Abdo, H., nnerberg, P.L.O., Lou, D., Hjerling-Leffler, J., m, J.H.O., Kharchenko, O., Kharchenko, P.V., et al. (2014). Unbiased classification of sensory neuron types by large-scale single-cell RNA sequencing. Nat Neurosci 1–11.

van der Maaten, L., and Hinton, G. (2008). Visualizing Data using t-SNE. Journal of Machine Learning Research *9*, 2579–2605.

Verhaagen, J., Oestreicher, A.B., Gispen, W.H., and Margolis, F.L. (1989). The expression of the growth associated protein B50/GAP43 in the olfactory system of neonatal and adult rats. Journal of Neuroscience *9*, 683–691.

Vierbuchen, T., Ostermeier, A., Pang, Z.P., Kokubu, Y., Südhof, T.C., and Wernig, M. (2010). Direct conversion of fibroblasts to functional neurons by defined factors. Nature *463*, 1035–1041.

Wang, Y.Z., Yamagami, T., Gan, Q., Wang, Y., Zhao, T., Hamad, S., Lott, P., Schnittke, N., Schwob, J.E., and Zhou, C.J. (2011). Canonical Wnt signaling promotes the proliferation and neurogenesis of peripheral olfactory stem cells during postnatal development and adult regeneration. Journal of Cell Science *124*, 1553–1563.

Weiler, E., and Farbman, A.I. (1998). Supporting cell proliferation in the olfactory epithelium decreases postnatally. Glia *22*, 315–328.

Weisblat, D.A., Sawyer, R.T., and Stent, G.S. (1978). Cell lineage analysis by intracellular injection of a tracer enzyme. Science *202*, 1295–1298.

Weisblat, D.A., Zackson, S.L., Blair, S.S., and Young, J.D. (1980). Cell lineage analysis by intracellular injection of fluorescent tracers. Science *209*, 1538–1541.

Whitfield, M.L., Sherlock, G., Saldanha, A.J., Murray, J.I., Ball, C.A., Alexander, K.E., Matese, J.C., Perou, C.M., Hurt, M.M., Brown, P.O., et al. (2002). Identification of genes periodically expressed in the human cell cycle and their expression in tumors. Mol. Biol. Cell *13*, 1977–2000.

Xie, H., Ye, M., Feng, R., and Graf, T. (2004). Stepwise reprogramming of B cells into macrophages. Cell *117*, 663–676.

Yamaguchi, T., Yamashita, J., Ohmoto, M., Aoudé, I., Ogura, T., Luo, W., Bachmanov, A.A., Lin, W., Matsumoto, I., and Hirota, J. (2014). Skn-1a/Pou2f3 is required for the generation of Trpm5-expressing microvillous cells in the mouse main olfactory epithelium. BMC Neurosci *15*, 13.

Zhou, Q., Brown, J., Kanarek, A., Rajagopal, J., and Melton, D.A. (2008). In vivo reprogramming of adult pancreatic exocrine cells to beta-cells. Nature *455*, 627–632.

Zinyk, D.L., Mercer, E.H., Harris, E., Anderson, D.J., and Joyner, A.L. (1998). Fate mapping of the mouse midbrain-hindbrain constriction using a site-specific recombination system. Current Biology *8*, 665–668.

Chapter 4:
Population asymmetry of activated HBCs underlies injury-induced regeneration of the olfactory epithelium

In this chapter, the analysis of single-cell RNA sequencing data represents a collaboration with Russell Fletcher, Diya Das, and members of the UC Berkeley Statistics Department and Center for Computational Biology, and is part of a manuscript that is in preparation.

Background

The regenerating olfactory epithelium presents a unique opportunity for investigating the dynamics underlying adult neural stem cell renewal and differentiation. Globose basal cells (GBCs), which maintain the neuronal population at steady state, also fully reconstitute olfactory neurons upon injury-induced neuronal apoptosis (Graziadei and Graziadei 1979; Carr and Farbman 1992). Moreover, the typically quiescent stem cell of this tissue, the horizontal basal cell (HBC), gives rise to all differentiated cell types of the OE upon severe injury (Bergman and Brittebo 1999). Though lineage-tracing experiments have confirmed that the HBC produces all olfactory cell types during regeneration (Leung, Coulombe, and Reed 2007; Fletcher et al. 2011), it remains unclear how the HBC pool balances self-renewal and differentiation, and how HBCs coordinate the production of diverging lineages during regeneration.

Since the descriptions of adult stem cells in blood, skin, intestine, and brain were first published (Till, Mcculloch, and Siminovitch 1964; Potten 1974; Cheng and Leblond 1974; Altman and Das 1965), various frameworks for understanding the regulation of stem cell renewal and differentiation have been proposed. Asymmetric divisions accomplish simultaneous self-renewal and differentiation with every mitotic event, and in some tissues, stem cells only undergo asymmetric division, a phenomenon known as invariant asymmetry. On the other hand, symmetric divisions, producing either renewed or differentiated daughter cells of equivalent fate, can be balanced within a population to accomplish self-renewal and differentiation; this paradigm is known as population asymmetry, reflecting the maintenance of multiple cell fates at the population, but not necessarily single stem cell, level (Watt and Hogan 2000). Broadly speaking, invariant asymmetry is more common early in development, and in single-celled organisms and invertebrates, while population asymmetry is more common in vertebrate tissues, particularly in adulthood (Simons and Clevers 2011). However, even amongst examples of invariant asymmetry or population asymmetry, the regulation of asymmetric versus symmetric divisions can vary (Siller and Doe 2009; Tetteh, Farin, and Clevers 2014).

In Chapter 2, analysis of spindle orientation in dividing HBCs following injury showed a bias towards mitoses oriented parallel or perpendicular to the basement membrane, and putative

apical sequestration of Par3, a key constituent of the Par complex, which promotes asymmetric divisions in the *C. elegans* embryo, fly neuroblasts, and developing mouse skin (Doe and Bowerman 2001; Lechler and Fuchs 2005). This bias suggests that HBCs may be free to divide both symmetrically and asymmetrically at the onset of regeneration. Furthermore, the loss of perpendicular divisions following conditional knockout of p63 suggests that asymmetric divisions may be required for HBC self-renewal. However, evidence from developing neocortex and adult intestine has shown that spindle orientation, the plane of cell division, and ultimately the fate(s) of stem cell progeny are not always correlated (Quyn et al. 2010; Ritsma et al. 2015; Kosodo et al. 2004; Belzil et al. 2014). Therefore, any relationship between these phenomena in a given stem cell must be empirically validated by tracing the fates of doublets of daughter cells arising from single parental stem cells.

In this chapter, an approach similar to that taken in Chapter 3 was utilized to address whether population asymmetry drives the outcomes of early HBC divisions, and to further probe the population and individual cell level dynamics that underlie the production of differentiated cells throughout regeneration. Sparse lineage tracing of HBCs during regeneration facilitated assessment of the composition and size of clones derived from individual parental cells labeled either prior to injury, or in the days following injury. Additionally, HBCs and their progeny were FACS-sorted at parallel timepoints to the previously described clonal analyses, and individually analyzed for transcriptional changes using single-cell RNA-seq. Lastly, building on previous unpublished work by Michael Sanchez and Russell Fletcher in our lab, sparse lineage tracing and single-cell RNA-seq was applied to better understand differentiation of the neurogenesis-deficient Sox2cKO HBC during regeneration.

Methods

Transgenic mice

Mice bearing transgenic alleles for tamoxifen-inducible tracing of HBCs (Krt5-CreER(T2); (Indra et al. 1999)), conditional knockout of Sox2 (Shaham et al. 2009), YFP lineage tracer (Rosa26eYFP; (Srinivas et al. 2001)), and Confetti lineage tracer (Rosa26-Confetti; (Snippert et al. 2010)) were bred and maintained against a mixed B6;129;FVB background. Mice with the following genotypes were used for experiments described in this chapter:

K5CreER; Rosa-Confetti (clonal analyses during regeneration)
K5CreER; Sox2fl/fl; Rosa-Confetti (Sox2cKO clonal analysis during regeneration)
K5CreER; Rosa-YFP (single-cell RNA-seq, regeneration time course)
K5CreER; Sox2fl/fl; Rosa-YFP (single-cell RNA-seq, Sox2cKO regeneration time course)

Lineage tracing and injury induction

K5-CreER; Rosa-Confetti transgenic mice were used for clonal lineage tracing of HBCs and HBC progeny during regeneration, and K5-CreER; Sox2fl/fl; Rosa-Confetti mice were used for the parallel 14 dpi (days post-injury) Sox2cKO clonal lineage tracing experiment. A dose-response was performed to determine an optimal dose of tamoxifen to achieve sparse HBC labeling with Confetti: 0.025 to 0.05 mg tamoxifen/g body weight administered by intraperitoneal (IP) injection. Tamoxifen was administered to adult (P21) mice three days prior to injury for the 2 dpi, 7 dpi, 14 dpi, and 14 dpi-Sox2cKO experiments, or at 2 dpi or 4 dpi for the two late-tracing experiments (Fig. 4.1). Injury to the OE was induced with IP injection of methimazole for all experiments. For the 2 dpi and 14 dpi clonal analyses, five animals were assayed; for all other clonal analyses, three animals were assayed.

Tissue processing

Tissue samples were collected and processed as described in Chapter 2 Methods, but cryosectioned at 40µm thickness to capture large clones.

Immunohistochemistry

Slides were prepared as described in Chapter 2 Methods, with some modifications. Prior to incubation in primary antibody, mild antigen retrieval (incubation for 30 min in 0.01 M sodium citrate, pH 6.0, as the solution cooled from boiling) was applied to slides to expose the p63 antigen without destroying the thick tissue sections. An antibody to GFP was used to visualize the membrane CFP (mCFP), cytosolic YFP (cYFP), and nuclear GFP (nGFP) reporters in just one channel. Tissue was labeled with an antibody to Sox2 to visualize the stem and progenitor cells, as well as the sustentacular and microvillous cells, and was further labeled with an antibody to p63 to identify renewed HBCs. We independently visualized GFP, SOX2, and p63 immunolabeling with Alexa-488, Alexa-568, and Alexa-647 conjugated secondary antibodies, respectively (Invitrogen).

Imaging and Quantitation

Confocal z-stacks of clones for all lineage-tracing experiments were obtained using a Zeiss LSM 710 confocal microscope, and images were processed and quantified using ImageJ (NIH). Clones located within either 25µm (2 dpi) or 50µm (all other experiments) of another clone expressing the same fluorescent reporter were excluded to minimize the scoring of clusters of cells derived from more than one parental HBC.

We did not visualize the RFP reporter signal: there was no interference because the antigen retrieval necessary for optimal Sox2 and p63 visualization extinguished the RFP signal. We observed very few nGFP clones and could not judge cell morphology with its restricted localization; therefore, we excluded nGFP clones from our analysis. At 2 dpi, tentative fates of

lineage traced cells were assigned on the basis of expression of p63 and Sox2: p63+SOX2+ cells were classified as renewed HBCs (H), p63-SOX2+ cells were classified as differentiating cells (D), and p63-SOX2- cells were classified as unknown (U). At later timepoints, identification of lineage-traced cell types was facilitated by cell morphology and position based on mCFP and cYFP expression. Olfactory sensory neurons were identified by their medially located somata and bipolar morphology, highlighted by a thin apical dendrite often terminating in a singular dendritic knob, and the absence of Sox2 expression. Basal progenitors were identified by position and Sox2 and p63 expression. Microvillous cells were assigned based on the more apical position of their cell bodies, tapered, brush-like apical tufts, and Sox2 expression. Sustentacular cells were identified by their apical localization, branched processes that span the epithelium, columnar apical shape, and Sox2 expression. Cells of the Bowman's gland were identified by their position in bulbous clusters in the subepithelial mesenchyme. See Figure 4.4 for examples of scored clones.

For a summary of clones by animal and reporter, see Supplementary Figures 4.2 and 4.3.

FACS sorting, single cell RNA-seq pipeline
See methods in Chapter 3.

Results

Symmetric divisions drive population asymmetry in HBCs early in regeneration
To assess early strategies of HBC self-renewal and differentiation during regeneration, rare HBCs were lineage traced *in vivo* and analyzed at 2 dpi. Immunohistochemistry for p63, which marks HBCs, and Sox2, which marks both HBCs and GBCs at steady state, was used to tentatively assign the early fates of lineage-traced cells (Fig. 4.2 A, B, C). Of 169 clones analyzed across 5 animals, 129 doublets were identified (Fig. 4.2 E). Pairs of cells arising from putative symmetric and asymmetric divisions of all types were observed (see examples in Fig. 4.2), although symmetric divisions accounted for 83% of all doublets (51% self-renewing, 25% differentiating, 7% unknown; Fig. 4.2 D). Notably, while asymmetric divisions were occasionally observed, they accounted for just 16% of all doublets. Moreover, amongst clones of all sizes, renewed HBCs accounted for 56% of all scored cells at 2 dpi (Fig. 4.2 F). These results suggest that HBCs utilize population asymmetry, accomplished via a balance of primarily symmetric renewing and differentiating divisions, to both self-renew and provide the earliest differentiated progenitor cells for tissue regeneration.

Regeneration of sustentacular cells precedes robust neurogenesis following OE injury
To assess the fate of HBC-derived daughter cells in late regeneration, HBC lineage-traced clones were analyzed at 7 dpi and 14 dpi. Immunohistochemistry for p63 and SOX2, along with

morphology revealed by either the membrane-CFP or cytosolic YFP lineage tracer, allowed for discrimination of all known cell types of the OE (Fig. 4.3).

At 7 dpi, sustentacular cells were the most commonly-traced cell type (46%), followed by renewed HBCs (23%), neurons (17%), and GBCs (11%) (Fig. 4.4 A, top). By 14 dpi, neurons had become the most abundant cell type (51%), followed by sustentacular cells (29%), and both classes of progenitor cell became proportionally depleted (HBC: 12%; GBC: 4%) (Fig. 4.4 B, top). In clones containing neurons, the mean number of neurons per clone increased significantly from 5.42 +/- 1.2 at 7 dpi to 9.4 +/- 0.83 at 14 dpi (mean +/- SEM; $p = 0.04$, unpaired t-test) (Fig. S4.1 A), suggestive of ongoing neural progenitor proliferation and neuronal maturation in the second week of regeneration. In clones containing sustentacular cells, the mean number of sustentacular cells per clone decreased slightly from 5.51 +/- 0.5 at 7 dpi to 4.4 +/- 0.4 at 14 dpi (Fig. S4.1 C), perhaps due to the ongoing generation of small numbers of additional sustentacular cells late in regeneration. In sum, sustentacular cell development precedes olfactory neurogenesis during regeneration, neuronal numbers increase rapidly in the second week of regeneration, and both GBCs and HBCs appear to continue to differentiate as late as one week post-injury.

In light of the observation that the sustentacular cell lineage often arises from the direct fate conversion of transitional HBCs following p63cKO, while the cells in the neuronal lineage proliferate prior to maturation (Chapter 3), the distribution of the number of sustentacular cells and neurons in regenerating clones was examined further. At 7 dpi, 4 of 19 neuron-containing clones possessed a single neuron, and 6 of 51 sustentacular cell-containing clones possessed a single sustentacular cell (Fig. S4.1 A, B; Supp. Table 4.1). At 14 dpi, while single sustentacular cells were still present in 11 of 69 sustentacular cell-containing clones (Fig. S4.1 B) and sometimes in the absence of any clonal siblings (5 of 69 clones), single neurons were rare, occurring in just 1 of 56 neuron-containing clones (Fig. S4.1 A). These data imply that HBCs sometimes produce just one cell in the sustentacular cell lineage during regeneration, perhaps via direct fate conversion, while HBCs typically produce more than one neuron from progeny fated for neurogenesis by 14 dpi.

To assess the potency of individual HBCs during regeneration, the composition of HBC-derived clones was scored for the presence of at least one cell from each of the three primary olfactory lineages (HBCs; GBCs, INPs, MV cells, and neurons in the neuronal lineage; and sustentacular cells in the sustentacular cell lineage). At both timepoints, observed clones reflected the divisions of unipotent, bipotent, and tripotent stem cells. While 61% of 7 dpi clones contained at least one renewed HBC, only 41% of 14 dpi clones contained at least one renewed HBC, implying that a subset of renewed HBCs differentiated in the second week of regeneration (Fig. 4.4, A vs. B, bottom). The percentage of clones possessing at least one neuronal-fated cell or one sustentacular

cell varied little between 7 dpi and 14 dpi (7 dpi: 56% neuronal, 65% sustentacular; 14 dpi: 57% neuronal, 59% sustentacular) (Supp. Table 4.1). However, the composition of clones possessing neuronal-fated cells shifted away from renewing, multipotent clones at 7 dpi towards neuronal-only and bipotent neuronal/sustentacular cell clones at 14 dpi (Fig. 4.4, A vs. B, bottom). Thus, renewed HBCs present in clones at 7 dpi may go on to differentiate into neurons or sustentacular cells late in regeneration, while the balance of differentiating progenitor fates is held constant between 7 dpi and 14 dpi.

Renewed HBCs continue to differentiate days into regeneration

To confirm whether renewed HBCs continue to differentiate throughout regeneration, the Confetti lineage tracer was induced at either 2 or 4 dpi, and clones were analyzed at 14 dpi. 14 dpi clones derived from 2 dpi late-traced HBCs resembled 14 dpi clones derived from HBCs traced prior to injury, both in terms of overall cell type numbers and in terms of clone compositions (Fig. 4.4, B vs C). On the other hand, 14 dpi clones derived from 4 dpi late-traced HBCs exhibited a stronger tendency to produce renewed HBCs than 14 dpi clones derived from 2 dpi late-traced HBCs (27% vs. 13% of all cells, and 54% vs. 41% of clones) (Fig. 4.4 C, D; Supp. Table 4.1). Clones traced from 4 dpi were also less likely to contain either neuronal or sustentacular cells compared to clones traced at 2 dpi (35% vs. 56% neuronal-containing clones; 43% vs. 58% sustentacular cell-containing clones). Renewed HBCs continued to differentiate when traced at either 2 dpi or 4 dpi, although the lineages to which they committed differed.

Renewed HBCs traced at 4 dpi also produced fewer neurons than renewed HBCs traced at 2 dpi. An average of 7.2 +/- 1.8 neurons were present in 14 dpi clones traced at 4 dpi that contained neurons, compared to an average of 9.56 +/- 0.91 neurons in similar 14 dpi clones traced at 2 dpi (Fig. S4.1 A, Supp. Table 4.1). Thus, as early as 4 dpi, olfactory neurogenesis may be throttled to avoid overproduction of neurons by the completion of regeneration. Notably, the average number of sustentacular cells per clone did not vary depending on whether HBCs were traced at 2 dpi or 4 dpi (2.84 +/- 0.28 vs 2.8 +/- 0.4), though sustentacular cell-containing clones traced prior to injury contained, on average, more sustentacular cells (14 dpi, 4.4 +/- 0.3) (Fig. S4.1 B, Supp. Table 4.1). This may reflect early proliferation of progenitors fated for the sustentacular cell lineage, which could ensure that an adequate supraepithelial barrier is in place prior to neurogenesis during regeneration. Alternatively, it is possible that mature sustentacular cells may themselves divide and produce additional sustentacular cells over the two-week time-course.

Conditional knockout of Sox2 in HBCs impedes neurogenesis alone during regeneration

Unpublished work by Michael Sanchez and Russell Fletcher in our lab has demonstrated that *Sox2* is necessary for robust neurogenesis following injury in the OE (Sanchez 2014). These lineage-tracing experiments showed that Sox2cKO strongly impedes regenerative neurogenesis, assayed via population-level cell counts. In collaboration with Russell Fletcher, I supplemented

these findings by tracing sparsely-labeled Sox2cKO HBCs with the Confetti reporter and scoring the compositions of clones at 14 dpi. As expected, neurons were rare, but not absent, from Sox2cKO HBC-derived clones at 14 dpi, accounting for just 7% of all counted cells, compared to 51% in wild-type HBC-derived clones at 14 dpi (Figs. 4.4 B, E, top). Moreover, 46% of all wild-type clones contained at least one neuron, compared to just 10% of Sox2cKO clones, confirming the deficiency of neurogenesis in the Sox2cKO ($p = 0.0021$, Welch's t-test). The few Sox2cKO clones possessing neurons may have escaped Sox2 knockout while being lineage traced, or alternatively reflect a lack of full penetrance of the Sox2cKO phenotype. Renewed HBCs and sustentacular cells were both overabundant in Sox2cKO clones compared to wild-type clones at 14 dpi; in fact, 91% of all clones contained either exclusively HBCs, sustentacular cells, or HBCs and sustentacular cells, in the Sox2cKO experiment (Fig. 4.4 B, E, bottom; Supp. Table 4.1). Thus, at the level of single HBCs, regenerative neurogenesis is impeded in the Sox2cKO, while HBC self-renewal and production of sustentacular cells is retained.

Single-cell RNA sequencing of HBC-derived cells during regeneration

To complement the above analyses of *in vivo* HBC lineage-tracing during regeneration, HBCs from K5CreER; Rosa-YFP animals were FACS sorted at six time points following injury, as well as just prior to injury, and individually characterized on the basis of gene expression using single-cell RNA sequencing. A similar analysis pipeline to that used in Chapter 3 was employed to align, filter, and normalize reads, cluster cells, and reorder cells by developmental state using *Slingshot* (see Chapter 3 Methods). At least 75 cells were analyzed at each time-point, including steady-state, for a total of 672 cells during wild-type regeneration (Fig. 4.5 A).

Following clustering with RSEC and annotation using marker genes of known cell types (see Chapter 3), 11 clusters of cells were identified (Fig. 4.6). The data was projected onto two dimensions via t-distributed Stochastic Neighbor Embedding (Fig. 4.7 A), confirming that clustering led to well-defined, distinct groups. *Slingshot* was applied to this dataset to discern lineage trajectories in the regenerating OE. Cells were assigned and ordered along multiple olfactory cell lineages and visualized in 3-dimensional PCA space (Fig. 4.7 B). Three distinct trajectories were identified, each starting from two novel activated HBC states (HBC*1 [green], HBC*2 [gold]) and leading, respectively, to mature neurons (mOSN [orange]), mature sustentacular cells (SUS [pink]), and renewed HBCs [brown]. The regenerating neuronal lineage resembled the steady-state p63cKO neuronal lineage (Chapter 3), progressing through the GBC/MV [teal], immature neuronal precursors 1-3 (INP1-3 [grey, purple]), and immature neuron (iOSN [yellow]) states before terminating at mOSN. Similarly, the sustentacular lineage progressed directly from the activated HBC states. The renewed HBC lineage, absent in the p63cKO, progressed through two intermediate renewing HBC states [light purple, brown] before terminating at the renewed HBC state.

Finally, to order all cells and analyze transitions in their transcriptional states as they differentiate or renew, *Slingshot* inferred three lineage trajectories using principal curves and assigned developmental positions of cells along the lineage trajectory (analogous to the concept of pseudotime, Trapnell et al., 2014) by orthogonal projection of each cell's coordinates in PCA space onto its respective curve. The three lineages were displayed as one-dimensional plots in which cells are labeled according to cell cluster, illustrating the developmental distance between cells as captured by dimensionality reduction (via PCA) of the gene expression values (Fig. 4.7 C, D, E). The experimental time-point at which each cell was collected is plotted in parallel below the plot showing cell cluster, with lighter colors indicating early time-points and darker colors indicating late time-points (Fig. 4.7 C, D, E).

Preliminary analyses of these results complement earlier observations of steady-state differentiation following p63cKO, as well as some of the findings of the *in vivo* clonal analysis of regeneration. Both the transitional HBCs in the steady-state p63cKO (ΔHBC1 and ΔHBC2) and activated HBCs in regeneration (HBC*1 and HBC*2) lose constitutive expression of p63, with individual cells expressing variable levels of p63 compared to resting HBCs (Figs. S3.1, 4.7). However, unlike transitional HBCs, HBC*1 and HBC*2 continue to express Keratin5 and Keratin14, and begin to express a cohort of wound-response genes, including Sprr1a, Krtdap, and Krt6a (Vermeij and Backendorf 2010; Bazzi et al. 2007) (Fig. 4.7). Furthermore, HBC*2 was uniquely characterized by its expression of cell-cycle genes (Fig. 4.8 B), while neither transitional HBC cluster from steady-state p63cKO entered the cell cycle. These data show that injury and p63cKO induce HBCs to exit quiescence in differential fashions, and suggest that transcriptional wound response programs may spur activated HBCs to proliferate during regeneration as a mechanism of accelerating the production of new cells to repopulate ablated tissue.

As was observed during p63cKO, the developmental distance between the activated HBC clusters and the GBC/MV cluster, evidenced by the relative distance between these clusters in the linear plots in Figure 4.7, is greater than the developmental distance lying between activated HBCs and sustentacular cells, which is relatively small. This difference is indicative of more major changes in transcriptional state that may occur as progenitors progress towards the neuronal lineage compared to the sustentacular cell lineage. Neuronal-fated cells also traverse further distance in developmental space between INP subclusters 1/2 and 3 than between other clusters in this lineage. Thus, the dynamics of the lineages leading from HBCs to both neurons and sustentacular cells in regeneration broadly resemble the same lineage dynamics observed during steady-state p63cKO, both in terms of the magnitude of transcriptional changes and the number of intermediate stages between stem and differentiated cell.

Furthermore, the emergence of each cell-type cluster over the 14 dpi time-course broadly lines up with the emergence of the relevant cell type in the regeneration clonal analysis. By plotting the proportion of cells in each cluster collected at each time point, the developmental timing of each lineage can be qualitatively inferred (Fig. 4.8 A). Clonal analysis shows that the maturation of sustentacular cells precedes the maturation of neurons by a week (Fig. 4.4), and similarly, sustentacular cells represent a large proportion of collected cells at both 4 dpi (96 hpi) and 7 dpi in the single-cell RNA-seq dataset, while mOSNs only become abundant at 14 dpi (Fig. 4.8 A).

The late tracing of HBCs in the regeneration clonal analyses suggests that HBCs continue to differentiate days into regeneration, presumably due to expression of HBC-specific K5-CreER in differentiating HBCs at 2 dpi and 4 dpi (Fig. 4.4 C, D). Both classes of activated HBC (HBC*1, HBC*2) maintain expression of Keratin5 following injury, while p63 expression flickers (Fig. 4.6), implying that tamoxifen administration at 2 dpi and 4 dpi is capable of lineage tracing activated HBCs. Moreover, HBC*2 exhibits high expression of cell-cycle genes (Fig. 4.8 B), suggesting that lineage tracing at late time points may label actively-cycling HBCs as opposed to quiescent HBCs. In support of this interpretation of the late-tracing clonal analysis, HBC*2 is most prominently represented at 48 hpi, and this cluster persists at 96 hpi, 7 dpi, and even 14 dpi (Fig. 4.8 A). Thus, activated HBCs may be responsible for the generation of differentiating clones late in regeneration.

The cycling of HBC*2 cells also may influence the expansion of both neuronal-fated and sustentacular-fated progenitors, explaining the presence of large sustentacular and large neuronal clones in regeneration (Fig. 4.8 B, Fig. S4.1). Notably, transitional HBCs, which arise at steady-state following p63cKO, do not themselves cycle, leading to direct fate conversion of HBCs into sustentacular cells (Chapter 3).

Comparison of wild-type and Sox2cKO regeneration using single-cell RNA-seq

Single-cell RNA-seq was applied to lineage-traced cells following injury in K5CreER; Sox2cKO; Rosa-YFP animals at the same time-points used in the wild-type regeneration single-cell RNA-seq time-course. Single cell transcriptomes from both wild-type and Sox2cKO regeneration were normalized and clustered together in the same manner as described for analysis of wild-type regeneration alone, but in a separate analysis. At least 55 cells were collected in the Sox2cKO at each time point except for 24 hpi (36 cells), resulting in a total of 413 cells analyzed for this genotype; 672 cells were analyzed at the same time points in the wild-type, as previously described. Wild-type and Sox2cKO cells were clustered (Fig. 4.9 A), lineage trajectories were inferred by *Slingshot* (Fig. 4.9 B), and cells were reordered by developmental time and plotted linearly for each predicted lineage (Fig. 4.9 C, D, E), all as previously described. Though Sox2cKO HBCs differentiated into sustentacular cells along the same lineage trajectory as wild-type HBCs, and similarly renewed back into HBCs, they were

unable to progress along the neuronal lineage, stalling at a novel cell type we have termed immature GBC (iGBC, Fig. 4.9 C, D, E). Further analysis of the iGBC cluster will be necessary to determine how loss of Sox2 leads to an interruption of neuronal differentiation, especially given that a subset of wild-type cells are also clustered into this group.

Conclusion/ Discussion

Unlike stem cells of development, adult tissue stem cells often exhibit variability in the outcomes of their mitoses. Even when asymmetric divisions are strongly favored over symmetric divisions, such as in adult epidermis and esophagus (Clayton et al. 2007; Mascré et al. 2013; Doupé et al. 2012), individual stem cells are capable of dividing symmetrically, indicating that overall rates of self-renewal and differentiation are coordinated at the population, rather than individual stem cell, level. Different types of population asymmetry have been documented as well, ranging from neutral competition amongst fast cycling, symmetrically-dividing intestinal crypt base columnar cells (Ritsma et al. 2015; Snippert et al. 2010) to a variety of asymmetric and symmetric divisions that produce a diversity of cell types in the dentate gyrus of the hippocampus (Bonaguidi et al. 2011). The various stem cells underlying these examples of population asymmetry sometimes utilize conserved mechanisms of developmental and invertebrate asymmetric cell division, such as biased spindle orientation and asymmetric localization of cell polarity factors, to generate cellular diversity (Quyn et al. 2010; Clayton et al. 2007); nevertheless, the fates of stem cell progeny are ultimately regulated by the surrounding tissue.

Adult stem cells therefore exhibit more heterogeneity and plasticity in their mitotic behavior than previously appreciated (Simons and Clevers 2011; Greulich and Simons 2016). The olfactory epithelium provides a tractable context in which to study the dynamics of a quiescent, multipotent progenitor, the horizontal basal cell. The HBC population gives rise to all olfactory cell types following severe injury to the OE, and can be induced to differentiate under homeostatic conditions via genetic knockout of the transcription factor, p63 (Fletcher et al. 2011; Leung, Coulombe, and Reed 2007). However, little is known about the either the types of HBC divisions or the dynamics of mature cell production that ensure rapid, controlled regeneration of the OE following injury. In this chapter, *in vivo* clonal analysis was paired with single-cell RNA-seq to address these issues.

In chapter 2, the HBC spindle was biased to orient either perpendicular or parallel to the basement membrane during regeneration, suggestive of a fairly equitable balance of asymmetric and symmetric divisions. However, doublet analysis of HBC progeny using sparse lineage tracing showed that symmetric divisions predominate in the HBC pool during regeneration: 83% of all doublets comprised two daughter cells of equivalent fate (Fig. 4.2 D). Moreover, half of all doublets produced two cells that regained expression of p63, indicative of symmetric self

renewal. Although asymmetric divisions were observed, the high proportion of perpendicular spindles (44%, Fig. 2.2) cannot explain the preponderance of symmetric doublets. Thus, spindle orientation may not be a primary regulator of HBC daughter cell fate during regeneration. This resembles the contradiction documented in the adult intestine in which apical Par3, and perpendicular divisions, cannot account for the preponderance of symmetric divisions that underlie intestinal homeostasis (Quyn et al. 2010; Snippert et al. 2010).

A preliminary comparison of HBC subtypes identified using single-cell RNA-seq in the immediate days following exit from quiescence shows that regeneration creates unique requirements of the surviving HBC pool to quickly enter the cell cycle and proliferate, while steady-state differentiation following p63cKO merely spurs HBCs to exit quiescence. Given that the mitotic spindle of HBCs early in regeneration exhibits a bimodal bias towards perpendicular and parallel, but not oblique, divisions, it is possible that HBC self-renewal during regeneration is contingent on cell-cycle entry and asymmetric division, while HBC activation at steady-state in the p63cKO impedes self-renewal due to failure to divide during differentiation. The loss of perpendicular spindle orientation in the p63cKO following injury may reflect the recruitment of mitotic basal progenitors for regeneration, while self-renewal remains impeded. Further investigation of how basal progenitors manage to perdure, let alone orchestrate regeneration, in the p63cKO is necessary to resolve the necessity of either the cell cycle or asymmetric division during HBC renewal.

At later time-points, sparse lineage tracing of HBCs lent itself to a more detailed analysis of differentiating clones. Sustentacular cells are more numerous than neurons at 7 dpi, but by 14 dpi, neurons constitute approximately half of all counted cells across all clones (Fig. 4.4 A, B). Indeed, single-cell RNA-seq of HBC-derived cells at various time-points during regeneration showed that sustentacular cells form earlier than neurons (Fig. 4.8 A). Both HBCs and GBCs were more abundant at 7 dpi compared to 14 dpi, and it is likely that many of these progenitors differentiated into neurons in the second week of regeneration (Fig. 4.4 A, B).

Additionally, sustentacular cells were occasionally observed in the absence of sibling sustentacular cells, suggesting that, like in the p63cKO, HBCs or their immediate progeny are capable of direct fate conversion to sustentacular cell in the absence of cell division (Supp. Table 4.1, Fig. 3.4). However, most sustentacular cell-containing clones contained numerous sustentacular cells during regeneration (Fig. S4.1 B). Unlike the transitional HBCs that arise just after steady-state p63cKO, one class of activated HBCs that emerges following injury, HBC*2, begins to express cell-cycle genes indicative of mitosis (Fig. 4.7 B), and the sustentacular lineage is derived from these cells. Thus, during regeneration, numerous sustentacular cells are rapidly produced via the proliferation of their HBC*2 progenitors, presumably to establish an epithelial barrier prior to neurogenesis.

Clone compositions at 7 and 14 dpi show that all three lineages can be present in clones derived from a single labeled HBC (Fig. 4.4 A, B). The cycling of the HBC*2 cluster, which defines the early stages of all three lineages, may allow a single parental HBC to produce two HBC*2 progeny, particularly in the first few days of regeneration, a hypothesis that is supported by the large number of symmetric renewing clones at 2 dpi (Fig. 4.2 D) and presence of this cluster at all time-points in the single-cell RNA seq experiment (Fig. 4.8). These renewed progeny might then go on to assume different fates, in spite of renewing after the first division. Are the HBCs truly multipotent?

Late lineage tracing of HBCs during regeneration may shed some light on this question. These experiments show that HBCs continue to differentiate at both 2 dpi and 4 dpi (Fig. 4.4 C, D). At 2 dpi, the cycling HBC*2 cluster makes up the majority of all analyzed cells, and the expression of Keratin5 gives these cells the ability to be lineage-traced via activation of K5-CreER (Figs. 4.6, 4.8 A). At 4 dpi, there are fewer cells in the HBC*2 cluster, but renewed HBCs have now formed (Fig. 4.8A). These renewed HBCs may be able to re-enter the cell cycle due to their inconsistent expression of p63, which must be strongly expressed to maintain HBC quiescence (Chapter 3). Alternatively, activated HBCs may linger before differentiating at 4dpi. Regardless, either of these Keratin5-expressing cell types may be lineage traced with K5-CreER at 4 dpi. Thus it is likely that some of the apparent multipotency observed in HBC-derived clones stems from the unipotent divisions of sibling renewed and/or activated HBCs, though the existence of a "true" multipotent progenitor that produces two types of differentiated progeny after one division cannot be ruled out.

Clonal lineage tracing and single-cell RNA-seq confirms that neurogenesis is all but eliminated in the Sox2cKO. Analysis of Sox2cKO clones at 14 dpi shows that only a small fraction of Sox2cKO HBCs go on to form neurons, and lineage trajectory analysis using Slingshot identifies a novel cell cluster, the immature GBC, as the developmental stage in the neuronal lineage at which Sox2cKO progenitors stall (Fig. 4.4, 4.9). Previous work in our lab has shown that Sox2 is required neurogenesis during OE regeneration at the population level (Sanchez 2014). With the identification of the iGBC cluster, a closer analysis of the impact of Sox2 loss on the transcriptional programs underlying neuronal differentiation in the OE is now possible.

Final Conclusions and Future Directions

This dissertation has explored mechanisms of cellular and transcriptional regulation of HBC self-renewal and differentiation in the OE, both during regeneration and during steady-state p63cKO differentiation, using sparse lineage tracing of HBCs combined with single-cell RNA sequencing of lineage-traced HBC progeny at parallel time-points. The major contributions of

this dissertation are: (1) Population asymmetry amongst primarily symmetrically-dividing HBCs, largely independent of spindle orientation, produces renewed HBCs early in regeneration, some of which likely go on to differentiate later in regeneration; (2) HBC differentiation at steady state in the p63cKO gives rise to a proliferative neuronal lineage, and direct fate conversion into sustentacular cells in the absence of cell division; (3) HBC self-renewal and differentiation during regeneration both entail progression of all quiescent HBCs through a proliferative, activated state prior to fate commitment; and (4) the sustentacular lineage matures prior to the neuronal lineage during regeneration, potentially creating a safe microenvironment for regenerative neurogenesis to subsequently occur. The two-pronged methodology established here provides a model for the study of adult stem cells in other niches, and furthermore lays the groundwork for targeted investigation of novel OE cell types. We are particularly interested in subclasses of activated and transitional HBCs, which may prove to be more amenable to *in vitro* propagation and experimentation.

A more detailed analysis of the transcriptional changes occurring across the renewing, neuronal, and sustentacular lineages during development is ongoing. Our hope is to identify key regulators of the activated HBC state, as well as genes that may prime activated HBCs to adopt committed mature cell fates. Genome editing with CRISPR/Cas9 will allow for more rapid generation of transgenic mice bearing alleles for the lineage tracing of activated HBCs and committed progenitors. Open questions remain relating to mechanisms of gene activation by coordinated changes in transcriptional regulation, particularly in the Sox2cKO, where GBC formation is abrogated.

Stem cells were long considered to sit on top of a strict hierarchy of adult cell development, but the advent of genetic lineage tracing, genomics, and single-cell analyses have increasingly demonstrated that stem cell divisions are sensitive to the real-time needs of given tissues rather than hardwired mitotic strategies. Today, it is appreciated that even hematopoietic stem cells, long assumed to depend on the rare divisions of privileged, long-lived, rarely-dividing stem cells, exist in heterogeneous pools that contribute renewing or differentiating progeny on an as-needed basis (Sun et al. 2014). The resident stem cells of numerous cycling tissues continue to be more-precisely identified and characterized (Doupé et al. 2012; Desai, Brownfield, and Krasnow 2015; Clevers 2013), expanding our understanding of how tissue homeostasis and regeneration is carried out in the adult. Combined with the advent of methods for inducing pluripotency in somatic tissues (Takahashi and Yamanaka 2006) and genome editing (Jinek et al. 2012), these advances are rapidly dovetailing not only with more precise investigation of specific stem cell populations, but also with the development of translational stem cell applications. Regenerating the damaged brain has always been a long shot, but the study of neural regeneration, now a worldwide endeavor, is bringing us closer to that promise than ever before.

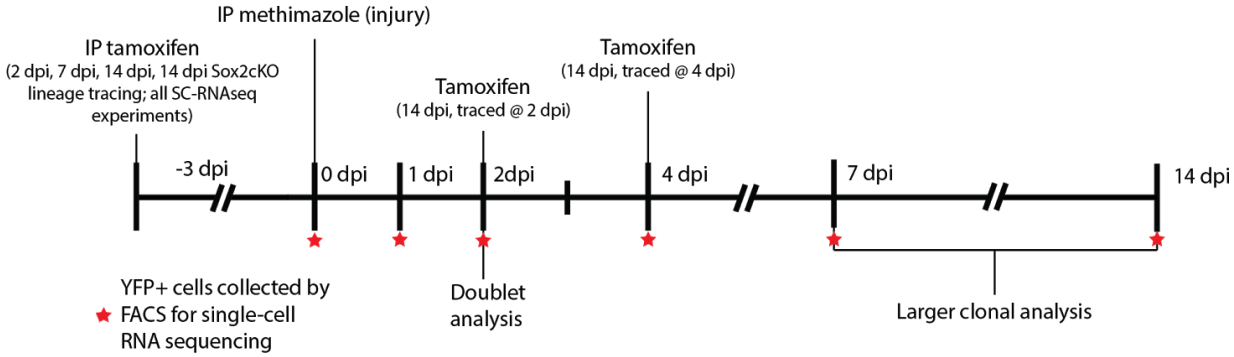

Figure 4.1 Experimental strategy for probing HBC renewal and differentiation following injury

For the 2 dpi, 7 dpi, 14 dpi, and 14 dpi-Sox2cKO clonal lineage tracing experiments, HBCs were sparsely labeled with a low dose of tamoxifen 3 days prior to injury; for all single-cell RNA-seq time points in regeneration, HBCs were labeled with a normal dose of tamoxifen at the same time point prior to injury. For the two late-tracing regeneration experiments, a low dose of tamoxifen was administered at either 2 dpi or 4 dpi. Tissue or cells were collected at the appropriate timepoints for subsequent immunohistochemistry or single-cell RNA-seq, respectively.

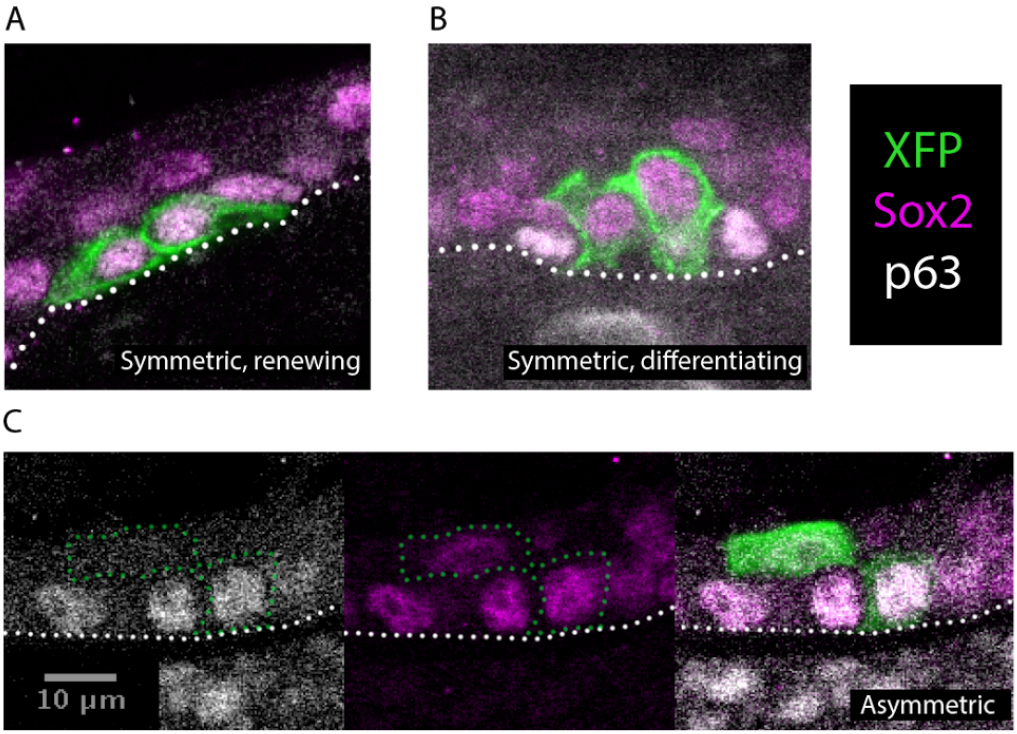

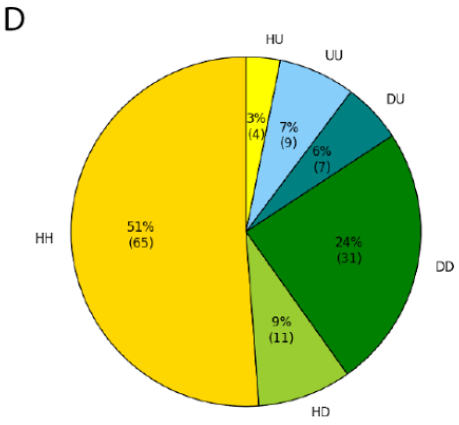

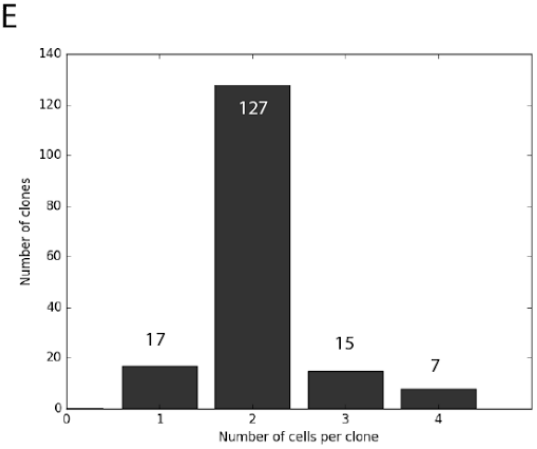

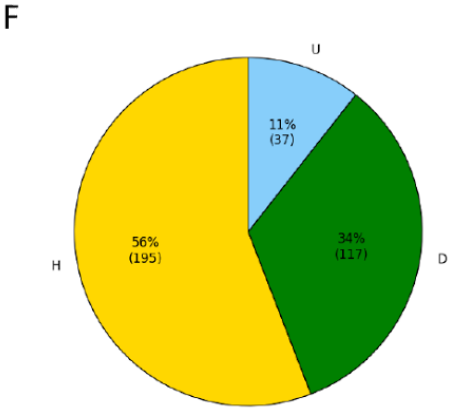

H: HBC-like (p63+ Sox2+)
D: Differentiating progenitor (p63-, Sox2+)
U: Unknown (p63-, Sox2-)

Figure 4.2 Analysis of HBC-derived doublets at 2 dpi

(A, B, C) Example maximum projections of confocal z-stacks of 2 dpi HBC-derived doublets, showing the three most commonly observed doublet compositions (**A**: symmetric renewing; **B**: symmetric differentiating; **C**: asymmetric). P63 and Sox2 were used as proxies for self-renewal (p63+Sox2+) or differentiation into a GBC-like progenitor (p63-Sox2+). Basement membrane, dotted line. **(D)** Doublet composition at 2 dpi. Symmetric divisions producing two renewed HBCs ('HH') were most common, followed by symmetric differentiating divisions ('DD') and asymmetric renewing/differentiating divisions ('HD'). **(E)** Histogram of clone sizes at 2 dpi. The majority of clones assessed at 2 dpi were doublets, containing two cells. **(F)** Total counts of HBCs, differentiating progenitors, and unknown (double negative p63- Sox2-) cells. At 2 dpi, the HBC pool is fully renewed, as more than half of all counted cells have recommenced expression of p63.

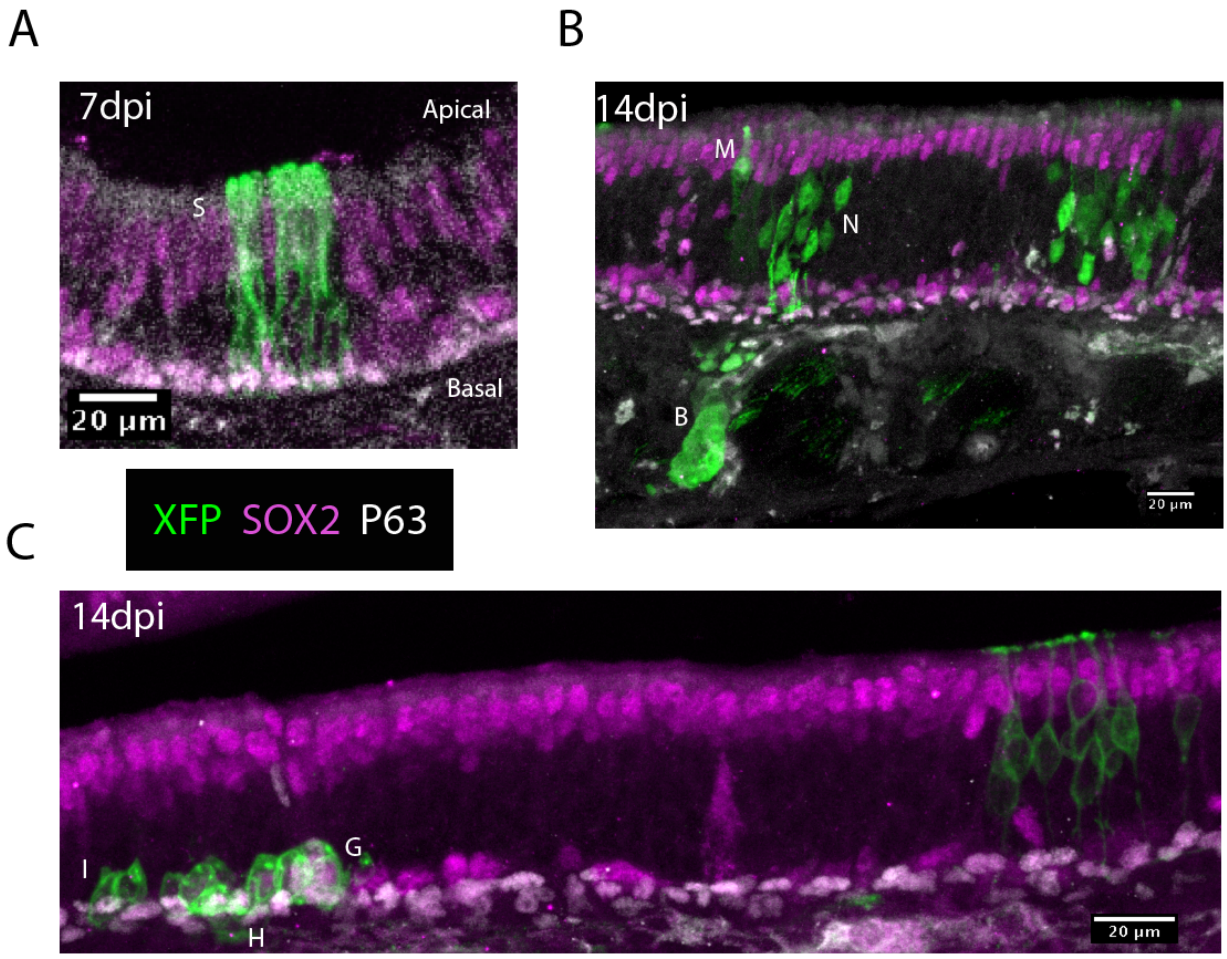

Figure 4.3 Representative morphology and marker expression of OE cell types
Example maximum projections of confocal z-stacks of 7 dpi and 14 dpi HBC-derived clones, illustrating the cell scoring methodology that was applied during clonal analyses late in regeneration. Application of a GFP antibody and Alexa 488 secondary allowed for simultaneous visualization of membrane CFP and cytosolic YFP in the same channel. **(A)** An example clone collected at 7 dpi, consisting exclusively of YFP-labeled sustentacular cells ('S', apical, columnar, Sox2+). **(B)** Example YFP-labeled clones at 14 dpi, highlighting the morphologies of neurons ('N', apical, with dendritic knobs), microvillus cells ('M', apical, with apical process, Sox2+), and Bowman's gland (mesenchymal location, bulbous structure). **(C)** Example CFP-labeled clones at 14 dpi, highlighting HBCs ('H', basal, p63+, Sox2+), GBCs ('G', basal, p63-, Sox2+), and immature neuronal precursors (INP, 'I', basal, p63-, Sox2-) on the left. Also note the neuronal clone on the right.

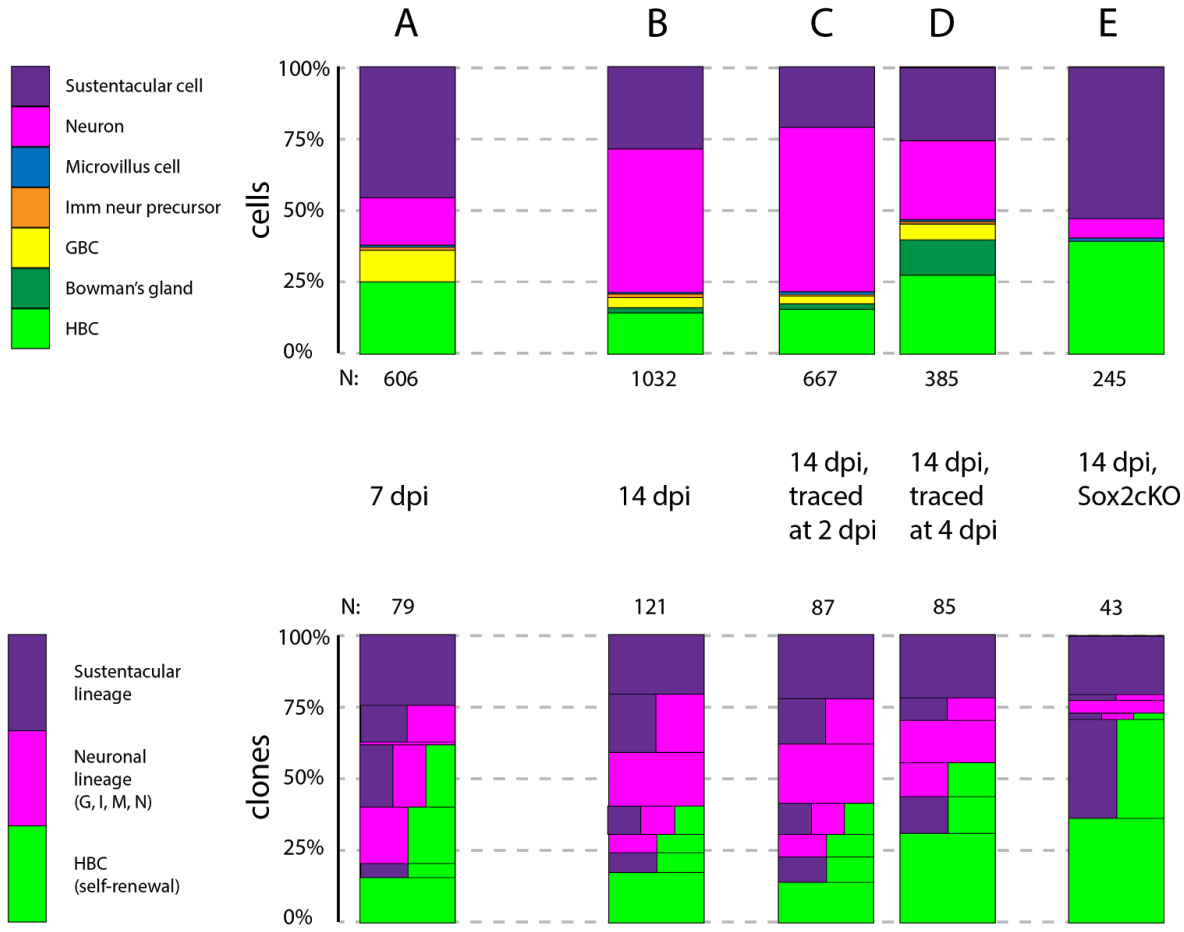

Figure 4.4 Cell type and clone composition breakdowns in clonal analysis experiments. Visualization of cell type distributions (top) and clonal lineage compositions (bottom) from five lineage tracing experiments: 7 dpi **(A)**, 14 dpi **(B)**, 14 dpi, traced at 2 dpi **(C)**, 14 dpi, traced at 4 dpi **(D)**, and 14 dpi, Sox2cKO **(E)**. For cell type distributions, the total number of cells counted for each cell type was summed and compared in each experiment. For clonal lineage compositions, clones were scored on the basis of possessing at least one cell of a given major lineage (HBC, neuronal, sustentacular) and binned to produce the five linear treemaps on the bottom. In each treemap row, columnar divisions indicate the binary presence of a lineage rather than relative abundance of a given cell type. See Supplementary Figure 4.2 for breakdowns of clone compositions by animal.

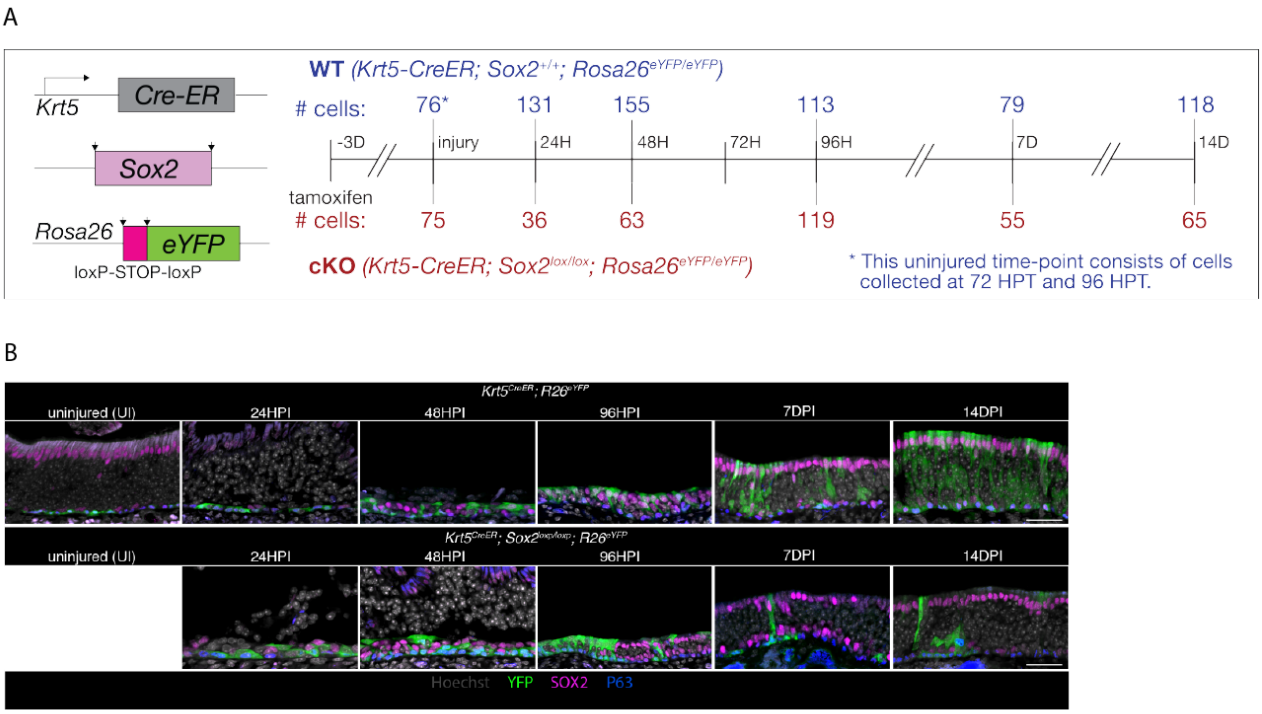

Figure 4.5 Regeneration time-course and collection of lineage-traced cells for single-cell RNA-seq

(A) Schematic of transgenic alleles (left) and regeneration time-course (right) used for single-cell RNA sequencing in both wild-type and Sox2cKO OE, with number of FACS-sorted cells that ultimately contributed transcriptional data to the final analyses.

(B) Representative images of lineage-traced cells at time-points corresponding to the single-cell RNA-seq pipeline for wild-type regeneration (top) and Sox2cKO regeneration (bottom). In the uninjured OE (UI), lineage tracing with K5CreER; RosaYFP labels a monolayer of quiescent HBCs. Following injury, HBCs differentiate into all known OE cell types, from 24 hours post-injury (hpi) to 14 dpi.

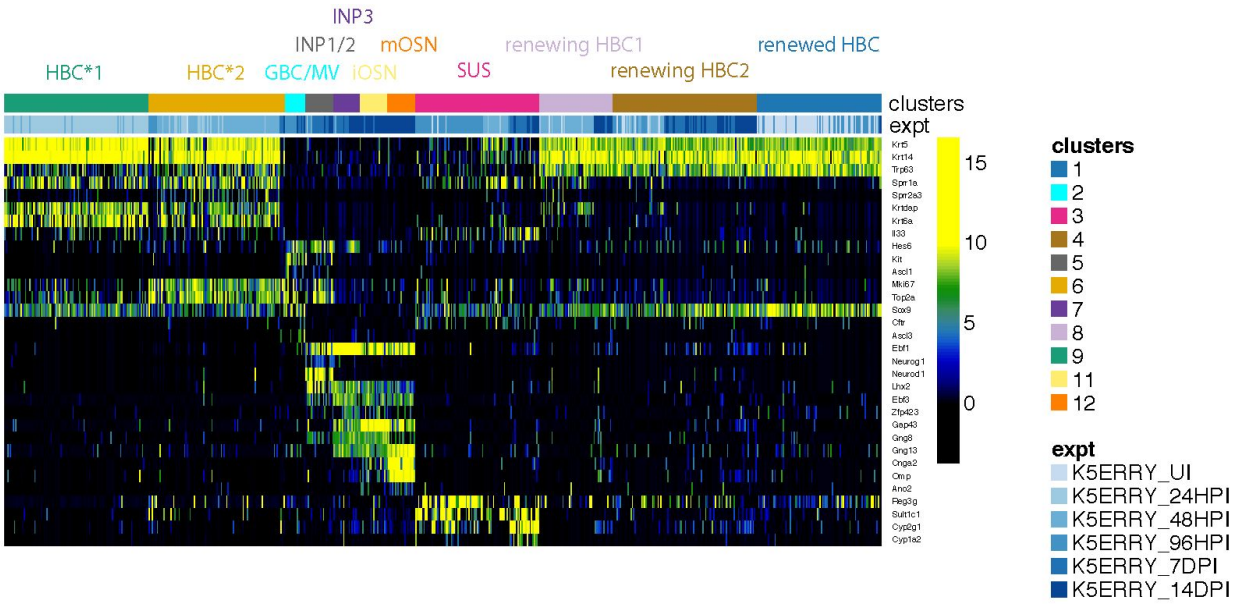

Figure 4.6 Heatmap of single cell gene expression by cluster, using curated OE gene list
Clustering recapitulates known cell identities via expression of canonical OE cell type markers.

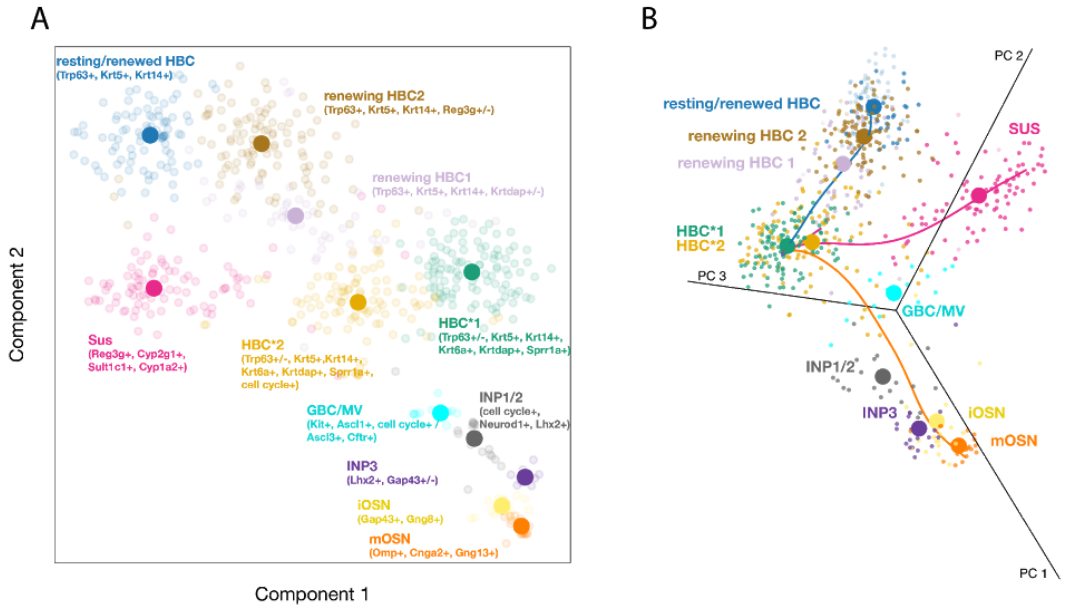
A
resting/renewed HBC
(Trp63+, Krt5+, Krt14+)
renewing HBC2
(Trp63+, Krt5+, Krt14+, Reg3g+/-)
renewing HBC1
(Trp63+, Krt5+, Krt14+, Krtdap+/-)
Sus
(Reg3g+, Cyp2g1+, Sult1c1+, Cyp1a2+)
HBC*2
(Trp63+/-, Krt5+,Krt14+, Krt6a+, Krtdap+, Sprr1a+, cell cycle+)
HBC*1
(Trp63+/-, Krt5+, Krt14+, Krt6a+, Krtdap+, Sprr1a+)
INP1/2
(cell cycle+, Neurod1+, Lhx2+)
GBC/MV
(Kit+, Ascl1+, cell cycle+ / Ascl3+, Cftr+)
INP3
(Lhx2+, Gap43+/-)
iOSN
(Gap43+, Gng8+)
mOSN
(Omp+, Cnga2+, Gng13+)
Component 2
Component 1
B
PC 2
resting/renewed HBC
renewing HBC 2
renewing HBC 1
SUS
HBC*1
HBC*2
PC 3
GBC/MV
INP1/2
INP3
iOSN
mOSN
PC 1
C
HBC lineage
HBC*1
HBC*2
renewing HBC 1
renewing HBC 2
renewed HBC
D
Neuronal lineage
HBC*1
HBC*2
GBC/MV
INP1/2
INP3
iOSN
mOSN
E
Sustentacular lineage
HBC*1
HBC*2
SUS

Figure 4.7 Cell clustering using t-SNE, lineage trajectory prediction with *Slingshot*, and reordering of cells by developmental time during regeneration

(A) Projection of clustered single cells into PCA space using t-distributed stochastic neighbor embedding (t-SNE), based on the 500 most variable genes. Cluster medoids are displayed as larger circles, with initial assignments of cluster identity based on the expression of a small number of marker genes. **(B)** *Slingshot* infers three lineages using principal curves and dimensionality reduction. Cells are projected into 3D PCA space; cluster medoids are indicated with larger circles. Three lineages, all beginning with activated HBCs (HBC*1, HBC*2), diverge to form mature neurons (mOSN), renewed HBCs, and sustentacular cells (SUS). **(C, D, E)** Developmental distance derived from the orthogonal projection of cells onto their respective lineage during regeneration. Mean +/- standard deviation of each cluster position is indicated below cluster assignment. The timepoint at which each ordered cell was collected is indicated on the lower plot of each lineage in blue; lighter shading indicates early time-points, darker shading indicates late time-points.

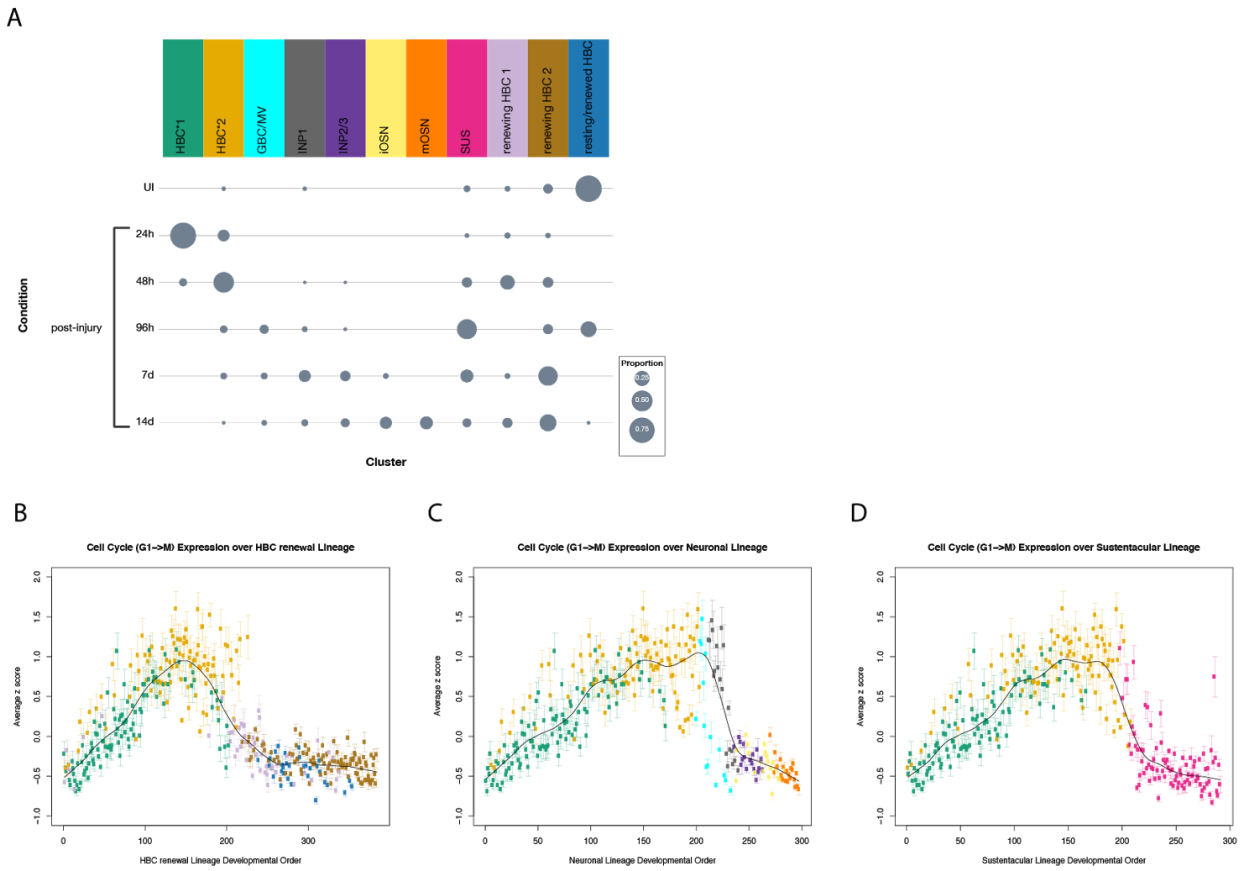

Figure 4.8 Cluster proportions by experiment and cell-cycle gene expression by lineage
(A) Breakdown of proportions of cell clusters collected at each time-point during regeneration. **(B, C, D)** Changes in expression of cell-cycle genes for the three olfactory lineages over developmental time. Scaled expression of 40 cell cycle genes (20 G1/S, 20 G2/M) is plotted across the ordered clusters making up the HBC, neuronal, and sustentacular lineages. HBC*1 and HBC*2 (green, gold) are the only cycling clusters common to the three lineages. GBCs and INPs of the neuronal lineage (teal, grey) are the only clusters of committed cells that exhibit high levels of cycling across the three lineages.

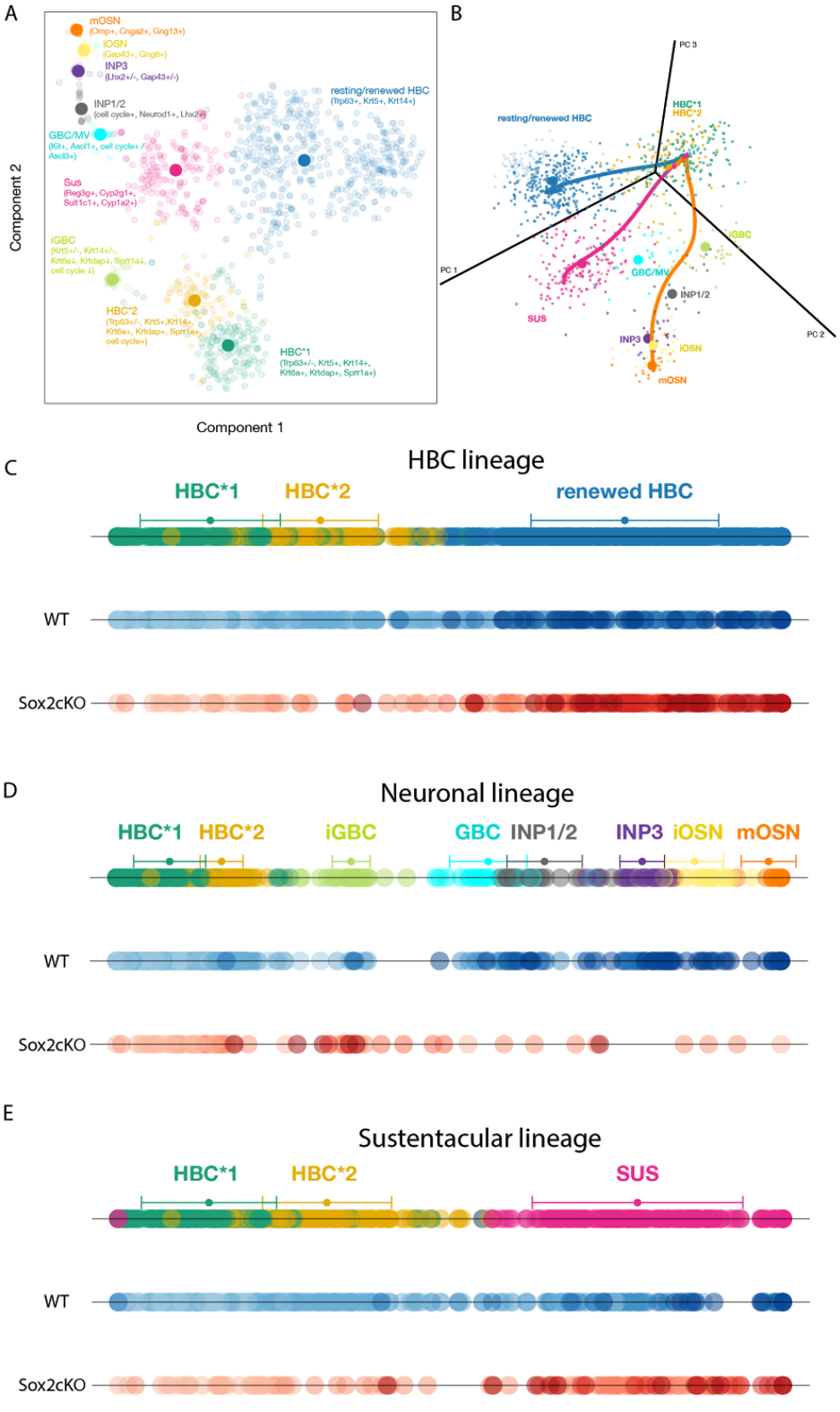
A
mOSN
(Omp+, Cnga2+, Gng13+)
iOSN
(Gap43+, Gng8+)
INP3
(Lhx2+/-, Gap43+/-)
INP1/2
(cell cycle+, Neurod1+, Lhx2+)
GBC/MV
(Kit+, Ascl1+, cell cycle+ / Ascl3+)
Sus
(Reg3g+, Cyp2g1+, Sult1c1+, Cyp1a2+)
iGBC
(Krt5+/-, Krt14+/-, Krt6a+, Krtdap+, Sprr1a+, cell cycle +)
HBC*2
(Trp63+/-, Krt5+,Krt14+, Krt6a+, Krtdap+, Sprr1a+, cell cycle+)
HBC*1
(Trp63+/-, Krt5+, Krt14+, Krt6a+, Krtdap+, Sprr1a+)
resting/renewed HBC
(Trp63+, Krt5+, Krt14+)
Component 2
Component 1
B
PC 3
PC 1
PC 2
resting/renewed HBC
HBC*1
HBC*2
iGBC
GBC/MV
INP1/2
SUS
INP3
iOSN
mOSN
C
HBC lineage
HBC*1
HBC*2
renewed HBC
WT
Sox2cKO
D
Neuronal lineage
HBC*1
HBC*2
iGBC
GBC
INP1/2
INP3
iOSN
mOSN
WT
Sox2cKO
E
Sustentacular lineage
HBC*1
HBC*2
SUS
WT
Sox2cKO

Figure 4.9 Clustering, lineage trajectories, and developmental reordering of cells during regeneration in combined wild-type and Sox2cKO

Wild-type and Sox2cKO single-cell RNA-seq data were analyzed together in this experiment, independently from the previously-described regeneration analysis. **(A)** Projection of clustered single cells into PCA space using t-SNE, as in Figure 4.7. Note the addition of the immature GBC cluster (iGBC, light green) in this dataset. **(B)** *Slingshot* infers three lineages using principal curves and dimensionality reduction, as in Figure 4.7. **(C, D, E)** Developmental distance derived from the orthogonal projection of cells onto their respective lineage during regeneration, as in Figure 4.7. The contribution of each genotype to each cluster is indicated in the two bottom plots for each lineage, with light colors signifying early time points and dark colors signifying late time points. Wild-type cells are plotted in blue and Sox2cKO cells are plotted in red.

A

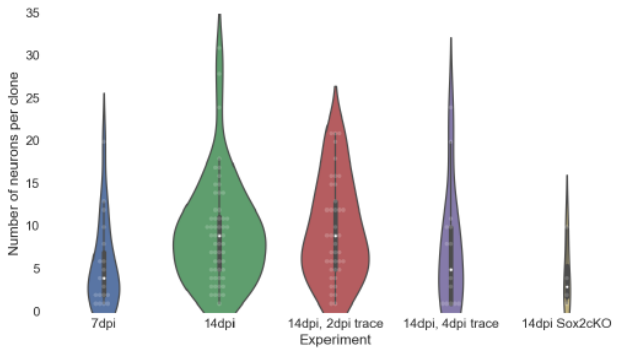
Number of neurons per clone
0
5
10
15
20
25
30
35
7dpi
14dpi
14dpi, 2dpi trace
14dpi, 4dpi trace
14dpi Sox2cKO
Experiment

B

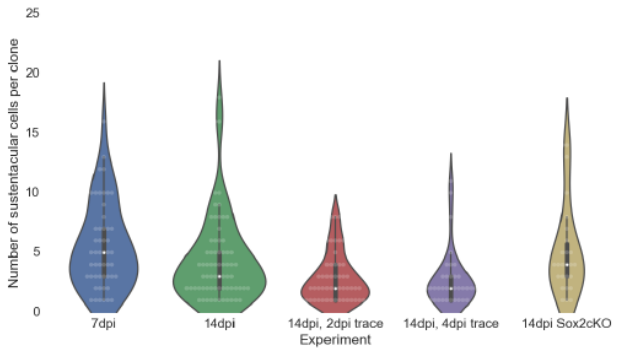
Number of sustentacular cells per clone
0
5
10
15
20
25
7dpi
14dpi
14dpi, 2dpi trace
14dpi, 4dpi trace
14dpi Sox2cKO
Experiment

C

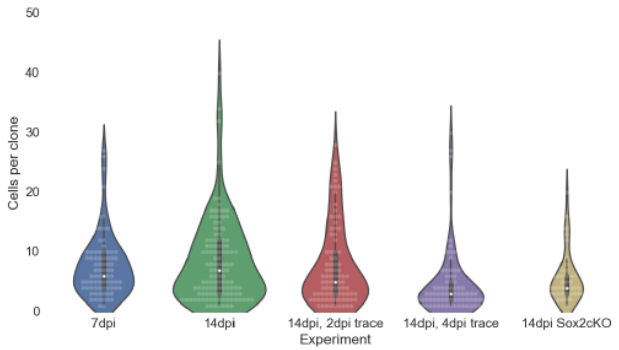
Cells per clone
0
10
20
30
40
50
7dpi
14dpi
14dpi, 2dpi trace
14dpi, 4dpi trace
14dpi Sox2cKO
Experiment

D

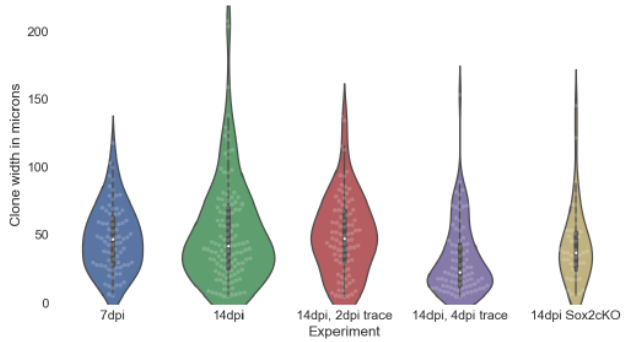
Clone width in microns
0
50
100
150
200
7dpi
14dpi
14dpi, 2dpi trace
14dpi, 4dpi trace
14dpi Sox2cKO
Experiment

Supplemental Figure 4.1 Parameters of clonal analyses

Violin plots of distributions of four clonal parameters across the five lineage tracing experiments carried out late in regeneration. The width of each violin plot is scaled by the number of counts in each experiment. Individual data points are plotted with transparent white points, and a simplified boxplot (minimum, first quartile, median, third quartile, maximum) is overlaid in black, with a white dot signifying the median. **(A)** Distribution of the number of neurons per clone. **(B)** Distribution of the number of sustentacular cells per clone. **(C)** Distribution of the number of cells per clone. **(D)** Distribution of clone widths in microns.

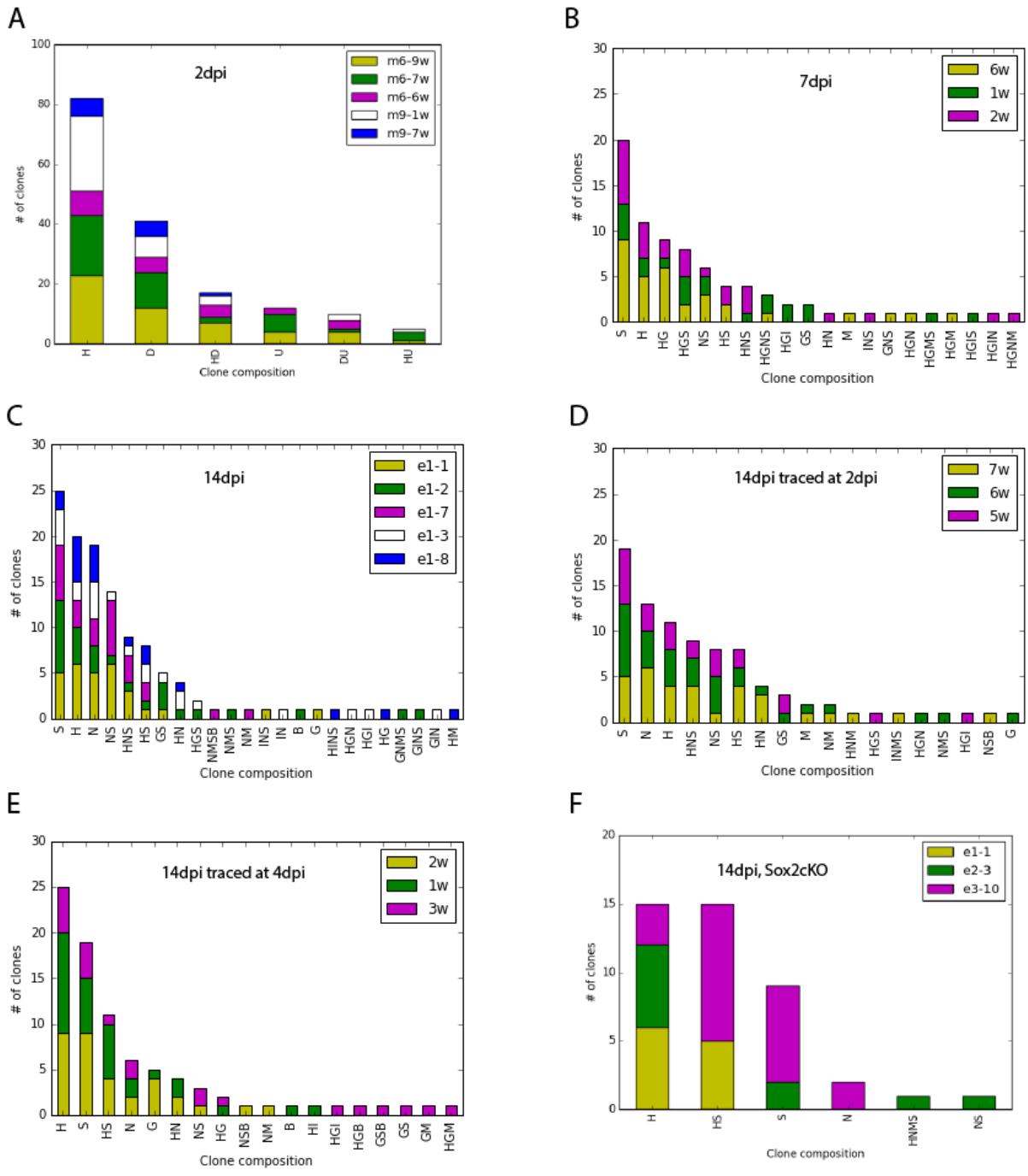

Supplementary Figure 4.2 Clone compositions by animal and experiment

Breakdowns of clone compositions by individual cell type and animal. Clones were scored based on possession of at least one cell of a given cell type. For the 2 dpi experiment **(A)**, when developing cell types are still ambiguous, three tentative fate assignments were used: HBC (H), differentiating progenitor (D), and unknown (U). For all other experiments **(B, C, D, E, F)**, cell

types were scored as follows: HBC (H), GBC (G), immature neuronal precursor (I), microvillus cell (M), neuron (N), sustentacular cell (S), and Bowman's gland (B). Each animal's contribution to a given category of clone is depicted by color. See Figures 4.2 and 4.3 for representative images of the morphology, location, and marker expression of all cell types.

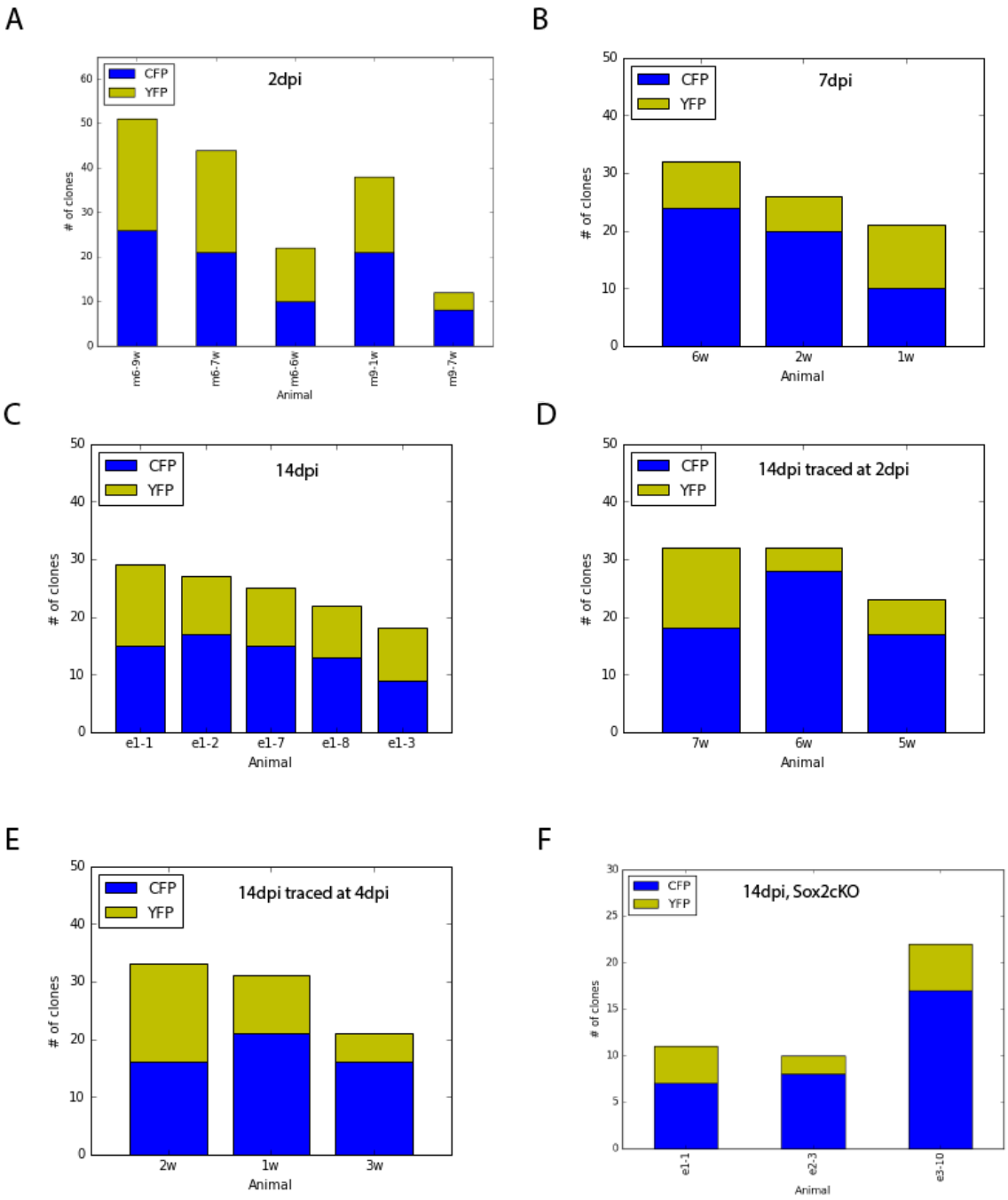

Supplementary Figure 4.3 Confetti reporter representation by animal

Breakdowns of Confetti reporter for each animal. All six lineage tracing experiments are shown **(A, B, C, D, E, F)**. CFP-labeled clones were more common across all experiments compared to YFP-labeled clones. GFP-labeled clones were rare, and were excluded because their nuclear localization precluded assignment of cell type by morphology.

Experiment		7dpi		14dpi		14dpi, traced at 2dpi		14dpi, traced at 4dpi		14dpi, Sox2cKO	
		Number	Percentage	Number	Percentage	Number	Percentage	Number	Percentage	Number	Percentage
Total cell counts											
	H	141	23.3	125	12.1	87	13	102	26.5	93	38
	G	68	11.2	38	3.7	19	2.8	22	5.7	0	0
	I	8	1.3	17	1.6	3	0.4	3	0.8	0	0
	M	5	0.8	7	0.7	8	1.2	3	0.8	3	1.2
	N	103	17	525	50.9	392	58.8	108	28.1	17	6.9
	S	281	46.4	301	29.2	145	21.7	99	25.7	132	53.9
	B	0	0	19	1.8	13	1.9	48	12.5	0	0
	total cells	606		1032		667		385		245	
Lineage composition											
	H	11	14	20	17	11	13	25	29	15	35
	HN	16	20	8	7	7	8	10	12	0	0
	HS	4	5	8	7	8	9	11	13	15	35
	HNS	17	22	12	10	10	11	0	0	1	2
	N	1	1	23	19	18	21	13	15	2	5
	S	20	25	25	21	19	22	19	22	9	21
	NS	10	13	25	21	14	16	7	8	1	2
	total clones	79		121		87		85		43	
	Htot	48	61	48	41	36	41	46	54	31	70
	Ntot	44	56	68	57	49	56	30	35	4	11
	Stot	51	65	70	59	51	58	37	43	26	59
	Uni	32	40	68	57	48	56	57	66	26	64
	Clones (real N)	19	24	56	46	41	47	15	18	4	9
	Clones (1 N)	4		1		2		5		1	
	Clones (real S)	51	65	69	57	51	59	36	42	26	60
	Clones (1 S)	6		11		16		10		3	
	Clones (Solo 1S	1		5		7		4		0	
	Mean N/clone	5.42 +/- 1.18		9.4 +/- 0.83		9.56 +/- 0.91		7.2 +/- 1.8		4.25 +/- 2.02	
	Mean S/clone	5.51 +/- 0.5		4.4 +/- 0.43		2.84 +/- 0.28		2.8 +/- 0.4		5.08 +/- 0.75	
	Mean cell/clone	7.67 +/- 0.6		8.5 +/- 0.67		7.67 +/- 0.73		4.5 +/- 0.6		5.7 +/- 0.64	

Supplementary Table 4.1 Clonal analysis counts, percentages, and statistics
Cell counts, clone composition counts, and percentages for all clonal analyses late in regeneration.

References

Altman, J., and G. D. Das. 1965. “Autoradiographic and Histological Evidence of Postnatal Hippocampal Neurogenesis in Rats.” *The Journal of Comparative Neurology* 124 (3): 319–35.

Bazzi, Hisham, Katherine A. Fantauzzo, Gavin D. Richardson, Colin A. B. Jahoda, and Angela M. Christiano. 2007. “Transcriptional Profiling of Developing Mouse Epidermis Reveals Novel Patterns of Coordinated Gene Expression.” *Developmental Dynamics: An Official Publication of the American Association of Anatomists* 236 (4): 961–70.

Belzil, Camille, Naoyuki Asada, Kei-Ichiro Ishiguro, Takeo Nakaya, Kari Parsons, Valentina Pendolino, Gernot Neumayer, et al. 2014. “p600 Regulates Spindle Orientation in Apical Neural Progenitors and Contributes to Neurogenesis in the Developing Neocortex.” *Biology Open* 3 (6): 475–85.

Bergman, Ulrika, and Eva B. Brittebo. 1999. “Methimazole Toxicity in Rodents: Covalent Binding in the Olfactory Mucosa and Detection of Glial Fibrillary Acidic Protein in the Olfactory Bulb.” *Toxicology and Applied Pharmacology* 155 (2). Elsevier: 190–200.

Bonaguidi, Michael A., Michael A. Wheeler, Jason S. Shapiro, Ryan P. Stadel, Gerald J. Sun, Guo-Li Ming, and Hongjun Song. 2011. “In Vivo Clonal Analysis Reveals Self-Renewing and Multipotent Adult Neural Stem Cell Characteristics.” *Cell* 145 (7). Elsevier Inc.: 1142–55.

Carr, V. M., and A. I. Farbman. 1992. “Ablation of the Olfactory Bulb up-Regulates the Rate of Neurogenesis and Induces Precocious Cell Death in Olfactory Epithelium.” *Experimental Neurology* 115 (1): 55–59.

Cheng, H., and C. P. Leblond. 1974. “Origin, Differentiation and Renewal of the Four Main Epithelial Cell Types in the Mouse Small Intestine. V. Unitarian Theory of the Origin of the Four Epithelial Cell Types.” *The American Journal of Anatomy* 141 (4): 537–61.

Clayton, Elizabeth, David P. Doupé, Allon M. Klein, Douglas J. Winton, Benjamin D. Simons, and Philip H. Jones. 2007. “A Single Type of Progenitor Cell Maintains Normal Epidermis.” *Nature* 446 (7132). Nature Publishing Group: 185–89.

Clevers, Hans. 2013. “The Intestinal Crypt, A Prototype Stem Cell Compartment.” *Cell* 154 (2). Elsevier Inc.: 274–84.

Desai, Tushar J., Douglas G. Brownfield, and Mark A. Krasnow. 2015. “Alveolar Progenitor and Stem Cells in Lung Development, Renewal and Cancer.” *Nature* 507 (7491). Nature Publishing Group: 190–94.

Doe, C. Q., and B. Bowerman. 2001. “Asymmetric Cell Division: Fly Neuroblast Meets Worm Zygote.” *Current Opinion in Cell Biology* 13 (1). Elsevier Ltd: 68–75.

Doupé, David P., Maria P. Alcolea, Amit Roshan, Gen Zhang, Allon M. Klein, Benjamin D. Simons, and Philip H. Jones. 2012. “A Single Progenitor Population Switches Behavior to Maintain and Repair Esophageal Epithelium.” *Science* 337 (6098): 1091–93.

Fletcher, Russell B., Melanie S. Prasol, Jose Estrada, Ariane Baudhuin, Karen Vranizan, Yoon Gi Choi, and John Ngai. 2011. “p63 Regulates Olfactory Stem Cell Self-Renewal and Differentiation.” *Neuron* 72 (5). Elsevier Inc.: 748–59.

Graziadei, G. A., and P. P. Graziadei. 1979. “Neurogenesis and Neuron Regeneration in the Olfactory System of Mammals. II. Degeneration and Reconstitution of the Olfactory Sensory Neurons after Axotomy.” *Journal of Neurocytology* 8 (2): 197–213.

Greulich, Philip, and Benjamin D. Simons. 2016. “Dynamic Heterogeneity as a Strategy of Stem Cell Self-Renewal.” *Proceedings of the National Academy of Sciences of the United States of America* 113 (27): 7509–14.

Indra, Arup Kumar, Xavier Warot, Jacques Brocard, Jean-Marc Bornert, Jia-Hao Xiao, Pierre Chambon, and Daniel Metzger. 1999. “Temporally-Controlled Site-Specific Mutagenesis in the Basal Layer of the Epidermis: Comparison of the Recombinase Activity of the Tamoxifen-Inducible Cre-ERT and Cre-ERT2 Recombinases.” *Nucleic Acids Research* 27 (22). Oxford Univ Press: 4324–27.

Jinek, M., K. Chylinski, I. Fonfara, M. Hauer, J. A. Doudna, and E. Charpentier. 2012. “A Programmable Dual-RNA-Guided DNA Endonuclease in Adaptive Bacterial Immunity.” *Science* 337 (6096): 816–21.

Kosodo, Yoichi, Katja Röper, Wulf Haubensak, Anne-Marie Marzesco, Denis Corbeil, and Wieland B. Huttner. 2004. “Asymmetric Distribution of the Apical Plasma Membrane during Neurogenic Divisions of Mammalian Neuroepithelial Cells.” *The EMBO Journal* 23 (11): 2314–24.

Lechler, Terry, and Elaine Fuchs. 2005. “Asymmetric Cell Divisions Promote Stratification and Differentiation of Mammalian Skin.” *Nature* 437 (7056). Nature Publishing Group: 275–80.

Leung, Cheuk T., Pierre A. Coulombe, and Randall R. Reed. 2007. “Contribution of Olfactory Neural Stem Cells to Tissue Maintenance and Regeneration.” *Nature Neuroscience* 10 (6). Nature Publishing Group: 720–26.

Mascré, Guilhem, Sophie Dekoninck, Benjamin Drogat, Khalil Kass Youssef, Sylvain Broheé, Panagiota A. Sotiropoulou, Benjamin D. Simons, and Cedric Blanpain. 2013. “Distinct Contribution of Stem and Progenitor Cells to Epidermal Maintenance.” *Nature* 489 (7415). Nature Publishing Group: 257–62.

Potten, C. S. 1974. “The Epidermal Proliferative Unit: The Possible Role of the Central Basal Cell.” *Cell and Tissue Kinetics* 7 (1): 77–88.

Quyn, Aaron J., Paul L. Appleton, Francis A. Carey, Robert J. C. Steele, Nick Barker, Hans Clevers, Rachel A. Ridgway, Owen J. Sansom, and Inke S. NAthke. 2010. “Spindle Orientation Bias in Gut Epithelial Stem Cell Compartments Is Lost in Precancerous Tissue.” *Stem Cells* 6 (2). Elsevier Inc.: 175–81.

Ritsma, Laila, Saskia I. J. Ellenbroek, Anoek Zomer, Hugo J. Snippert, Frederic J. de Sauvage, Benjamin D. Simons, Hans Clevers, and Jacco van Rheenen. 2015. “Intestinal Crypt Homeostasis Revealed at Single-Stem-Cell Level by in Vivo Live Imaging.” *Nature* 507 (7492). Nature Publishing Group: 362–65.

Sanchez, Miguel Angel. 2014. “The Roles of Sox2 in Stem and Progenitor Cells of the Mammalian Olfactory Epithelium.” Embargoed doctoral dissertation. UC Berkeley.

Shaham, Ohad, April N. Smith, Michael L. Robinson, Makoto M. Taketo, Richard A. Lang, and Ruth Ashery-Padan. 2009. “Pax6 Is Essential for Lens Fiber Cell Differentiation.” *Development* 136 (15): 2567–78.

Siller, Karsten H., and Chris Q. Doe. 2009. “Spindle Orientation during Asymmetric Cell Division.” *Nature Cell Biology* 11 (4). Nature Publishing Group: 365–74.

Simons, Benjamin D., and Hans Clevers. 2011. “Strategies for Homeostatic Stem Cell Self-Renewal in Adult Tissues.” *Cell* 145 (6). Elsevier Inc.: 851–62.

Snippert, Hugo J., Laurens G. van der Flier, Toshiro Sato, Johan H. van Es, Maaike van den Born, Carla Kroon-Veenboer, Nick Barker, et al. 2010. “Intestinal Crypt Homeostasis

Results from Neutral Competition between Symmetrically Dividing Lgr5 Stem Cells." *Cell* 143 (1). Elsevier Inc.: 134–44.
Srinivas, S., T. Watanabe, C. S. Lin, C. M. William, Y. Tanabe, T. M. Jessell, and F. Costantini. 2001. "Cre Reporter Strains Produced by Targeted Insertion of EYFP and ECFP into the ROSA26 Locus." *BMC Developmental Biology* 1 (March): 4.
Sun, Jianlong, Azucena Ramos, Brad Chapman, Jonathan B. Johnnidis, Linda Le, Yu-Jui Ho, Allon Klein, Oliver Hofmann, and Fernando D. Camargo. 2014. "Clonal Dynamics of Native Haematopoiesis." *Nature* 514 (7522). Nature Publishing Group: 322–27.
Takahashi, Kazutoshi, and Shinya Yamanaka. 2006. "Induction of Pluripotent Stem Cells from Mouse Embryonic and Adult Fibroblast Cultures by Defined Factors." *Cell* 126 (4). Elsevier Inc.: 663–76.
Tetteh, Paul W., Henner F. Farin, and Hans Clevers. 2014. "Plasticity within Stem Cell Hierarchies in Mammalian Epithelia." *Trends in Cell Biology*. Elsevier Ltd, 1–9.
Till, J. E., E. A. Mcculloch, and L. Siminovitch. 1964. "A STOCHASTIC MODEL OF STEM CELL PROLIFERATION, BASED ON THE GROWTH OF SPLEEN COLONY-FORMING CELLS." *Proceedings of the National Academy of Sciences of the United States of America* 51: 29–36.
Vermeij, Wilbert P., and Claude Backendorf. 2010. "Skin Cornification Proteins Provide Global Link between ROS Detoxification and Cell Migration during Wound Healing." *PloS One* 5 (8): e11957.
Watt, Fiona M., and Brigid L. M. Hogan. 2000. "Out of Eden: Stem Cells and Their Niches." *Science* 287 (5457). American Association for the Advancement of Science: 1427–30.